Université de Montréal

Faculté de médecine
Département de neurosciences

Saison
2018-2019

SÉMINAIRE NSC6044

Assistant Professor Jason Shepherd

University of Utah, School of Medicine

Titre: ***" Viral-Like Mechanisms of Intercellular RNA Trafficking in the Nervous System "***

Heure: 12 h

Date: Vendredi, 28 septembre 2018

Lieu: Salle 1120, Pavillon Paul-G.-Desmarais

Université de Montréal

Faculté de médecine
Département de neurosciences

Saison
2018-2019

Biography

Dr. Jason Shepherd is currently an Assistant Professor of Neurobiology and Anatomy at the University of Utah School of Medicine, with adjunct positions in the departments of Biochemistry and Ophthalmology & Visual Sciences. He joined the U in 2013 after obtaining postdoctoral training at the Massachusetts Institute of Technology and his Ph.D. at the Johns Hopkins School of Medicine. Dr. Shepherd's research has garnered recognition worldwide; he is the recipient of the 2010 Gruber International Research Award in Neuroscience from the Society of Neuroscience and the International Society for Neurochemistry Young Investigator Award. He was also a recipient of a K99/R00 pathway to independence award and was recently selected to be a Kavli Fellow by the National Academy of Sciences

Article

Cell

The Neuronal Gene *Arc* Encodes a Repurposed Retrotransposon Gag Protein that Mediates Intercellular RNA Transfer

Graphical Abstract

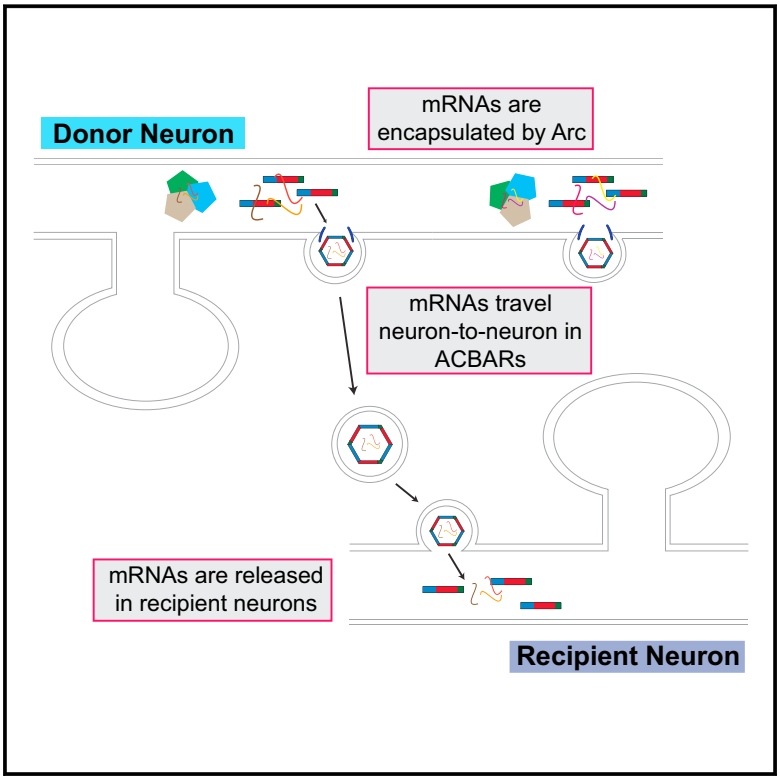

Highlights

- The neuronal gene *Arc* encodes a protein that forms virus-like capsids
- Arc protein exhibits similar biochemical properties as retroviral Gag proteins
- Endogenous Arc protein is released from neurons in extracellular vesicles (EVs)
- Arc EVs and capsids can mediate intercellular transfer of *Arc* mRNA in neurons

Authors

Elissa D. Pastuzyn, Cameron E. Day, Rachel B. Kearns, ..., John A.G. Briggs, Cédric Feschotte, Jason D. Shepherd

Correspondence

jason.shepherd@neuro.utah.edu

In Brief

The neuronal protein Arc is evolutionarily related to retrotransposon Gag proteins and forms virus-like capsid structures that can transfer mRNA between cells in the nervous system.

Pastuzyn et al., 2018, Cell *172*, 275–288
January 11, 2018
https://doi.org/10.1016/j.cell.2017.12.024

CellPress

Arc restores juvenile plasticity in adult mouse visual cortex

Kyle R. Jenks[a,1], Taekeun Kim[b,1], Elissa D. Pastuzyn[a,1], Hiroyuki Okuno[c,d], Andrew V. Taibi[a], Haruhiko Bito[d], Mark F. Bear[b,2], and Jason D. Shepherd[a,2]

[a]Department of Neurobiology and Anatomy, University of Utah, Salt Lake City, UT 84112; [b]The Picower Institute for Learning and Memory, Massachusetts Institute of Technology, Cambridge, MA 02139; [c]Medical Innovation Center, Kyoto University Graduate School of Medicine, Sakyo-ku, Kyoto 606-8507, Japan; and [d]Department of Neurochemistry, Graduate School of Medicine, The University of Tokyo, Hongo 7-3-1, Bunkyo-ku, Tokyo 113-0033, Japan

Edited by Carla J. Shatz, Stanford University, Stanford, CA, and approved July 17, 2017 (received for review January 17, 2017)

The molecular basis for the decline in experience-dependent neural plasticity over age remains poorly understood. In visual cortex, the robust plasticity induced in juvenile mice by brief monocular deprivation during the critical period is abrogated by genetic deletion of Arc, an activity-dependent regulator of excitatory synaptic modification. Here, we report that augmenting Arc expression in adult mice prolongs juvenile-like plasticity in visual cortex, as assessed by recordings of ocular dominance (OD) plasticity in vivo. A distinguishing characteristic of juvenile OD plasticity is the weakening of deprived-eye responses, believed to be accounted for by the mechanisms of homosynaptic long-term depression (LTD). Accordingly, we also found increased LTD in visual cortex of adult mice with augmented Arc expression and impaired LTD in visual cortex of juvenile mice that lack Arc or have been treated in vivo with a protein synthesis inhibitor. Further, we found that although activity-dependent expression of *Arc* mRNA does not change with age, expression of Arc protein is maximal during the critical period and declines in adulthood. Finally, we show that acute augmentation of Arc expression in wild-type adult mouse visual cortex is sufficient to restore juvenile-like plasticity. Together, our findings suggest a unifying molecular explanation for the age- and activity-dependent modulation of synaptic sensitivity to deprivation.

Arc | synaptic plasticity | visual cortex | ocular dominance | critical period

A defining feature of early postnatal brain development is the activity-dependent winnowing of synaptic connections. This process is readily demonstrated by the response of visual cortical circuits to temporary monocular deprivation (MD) during early life. When MD is initiated during an early critical period, the synapses serving the deprived eye in visual cortex lose strength and are eliminated. Deprived-eye depression diminishes with age such that by the onset of adolescence, circuits are less vulnerable to the effects of deprivation. Understanding the molecular mechanisms that underlie the effect of age on this type of ocular dominance (OD) plasticity is considered one of the great challenges in neuroscience (1).

It is now well established that OD plasticity after MD occurs through synaptic plasticity of excitatory transmission, using mechanisms that include homosynaptic long-term depression (LTD), metaplasticity, and homeostatic scaling of AMPA-type glutamate receptors (2, 3). Clues to the molecular basis for the decline in juvenile plasticity have come from several diverse experimental treatments that can restore or prolong sensitivity to MD in adult animals. These include genetic manipulations that slow the maturation of cortical inhibition (4, 5), enrichment of animal housing conditions (6), increased exposure to visual stimulation (7), and enhanced modulatory neurotransmission (8). It has been suggested that a common thread connecting these varied treatments might be an increase in the ratio of excitation to inhibition (9, 10). However, it is completely unknown how, at the molecular level, general increases in cortical activity can facilitate deprivation-induced synaptic plasticity in adult visual cortex. Since the immediate early gene Arc is exquisitely sensitive to changes in cortical activity, and is essential for both OD plasticity and modification of excitatory synaptic transmission (11–13), we set out to determine whether availability of Arc limits or changes the qualities of plasticity in adults and whether up-regulating Arc levels in adult animals can restore juvenile synaptic plasticity.

Results

Augmentation of Arc Expression in Adult Mouse Visual Cortex Extends the Critical Period of Juvenile OD Plasticity. In young mice [≤ postnatal day (P) 40], the main consequence of short (3–4 d) MD is the robust loss of cortical responsiveness to stimulation of the deprived eye. A compensatory potentiation of responses to the nondeprived eye may also occur, and is typically observed with longer periods of MD (5–7 d) (14). Importantly, although open-eye potentiation after long-duration MD is common in adult rodents, deprived-eye depression typically is only observed during the juvenile critical period in animals housed under standard laboratory conditions (15, 16). We predicted that augmenting Arc levels would prolong juvenile plasticity, as defined by closed-eye depression, past the conventional critical period in mouse visual cortex. To test this hypothesis, we used a transgenic (Tg) mouse line that expresses an additional allele of *Arc* tagged with mCherry that is driven by the activity-dependent *Arc* promoter in a similar manner to the previously characterized Arc-GFP Tg mouse line (17, 18) (Fig. S1).

We compared the qualities of OD plasticity after short (3–4 d) MD in Arc-Tg mice and wild-type (WT) littermate controls at P30 (juvenile) and P180 (adult) using chronic recordings of

Significance

Neuronal plasticity peaks early in life during critical periods and normally declines with age, but the molecular changes that underlie this decline are not fully understood. Using the mouse visual cortex as a model, we found that activity-dependent expression of the neuronal protein Arc peaks early in life, and that loss of activity-dependent Arc expression parallels loss of synaptic plasticity in the visual cortex. Genetic overexpression of Arc prolongs the critical period of visual cortex plasticity, and acute viral expression of Arc in adult mice can restore juvenile-like plasticity. These findings provide a mechanism for the loss of excitatory plasticity with age, and suggest that Arc may be an exciting therapeutic target for modulation of the malleability of neuronal circuits.

Author contributions: M.F.B. and J.D.S. designed research; K.R.J., T.K., E.D.P., H.O., A.V.T., and J.D.S. performed research; H.O. and H.B. contributed new reagents/analytic tools; K.R.J., T.K., E.D.P., H.O., A.V.T., and J.D.S. analyzed data; and K.R.J., M.F.B., and J.D.S. wrote the paper.

The authors declare no conflict of interest.

This article is a PNAS Direct Submission.

[1]K.R.J., T.K., and E.D.P. contributed equally to this work.

[2]To whom correspondence may be addressed. Email: mbear@mit.edu or jason.shepherd@neuro.utah.edu.

This article contains supporting information online at www.pnas.org/lookup/suppl/doi:10.1073/pnas.1700866114/-/DCSupplemental.

visually evoked potentials (VEPs) from binocular visual cortex contralateral (contra) to the deprived eye (Fig. 1*A*) as previously described (11). There was no significant difference between P30 WT and Arc-Tg VEPs before MD, and following MD, both WT and Arc-Tg P30 mice exhibited a significant decrease in contra (closed-eye) VEP amplitudes (WT: $n = 7$, baseline = 251 ± 28 μV, post-MD = 166 ± 12 μV, $P = 0.03$; Arc-Tg: $n = 10$, baseline = 227 ± 21 μV, post-MD = 159 ± 22 μV, $P = 0.01$ by paired t test; Fig. 1*B*). As expected, adult P180 WT mice did not exhibit depression of contra VEP amplitude after MD, reflecting the loss of juvenile plasticity. In sharp contrast, P180 Arc-Tg mice still exhibited a significant decrease in contra VEPs (WT: $n = 7$, baseline = 184 ± 19 μV, post-MD = 183 ± 20 μV, $P = 0.9$; Arc-Tg: $n = 6$, baseline = 208 ± 26 μV, post-MD = 136 ± 20 μV, $P = 0.02$ by paired t test; Fig. 1*C*), comparable to the decrease observed in WT juveniles. There was a significant treatment by genotype interaction, indicating that OD plasticity differs in Arc-Tg mice compared with WT mice ($P = 0.0092$, repeated measures ANOVA).

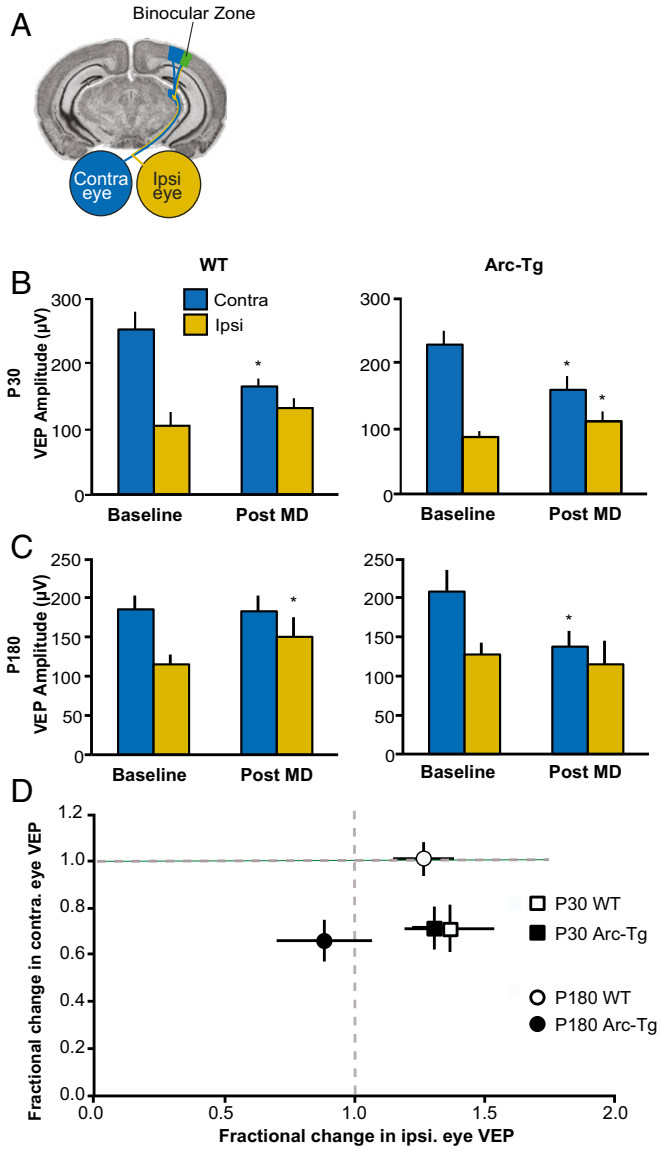

Fig. 1. Arc-Tg mice exhibit juvenile-like OD plasticity well past the conventional critical period. (*A*) Schematic of recording site for VEPs in layer IV of binocular visual cortex. (*B*) At P30, both WT and Arc-Tg mice show a significant decrease in contra (closed-eye) VEP amplitude following MD (WT: $n = 7$, $^*P = 0.03$; Arc-Tg: $n = 10$, $^*P = 0.01$). Additionally, Arc-Tg mice exhibited a small but significant increase in ipsi (open-eye) VEPs (Arc-Tg: $^*P = 0.008$). There is no significant difference between WT and Arc-Tg animals before or after MD. (*C*) At P180, only Arc-Tg mice exhibit a significant decrease in contra VEPs (Arc-Tg: $n = 6$, $^*P = 0.02$). (*D*) Plot of the fractional change in ipsi (*x* axis) and contra (*y* axis) eye VEPs following MD (same data as in *B* and *C*). At P30, there is no significant difference between WT and Arc-Tg mice. However, at P180, there is a significant difference between the fractional change of WT and Arc-Tg mice following MD ($P = 0.03$). Data are represented as mean ± SEM.

Because the chronic VEP method enables measurements of response strength in the same mouse before and after MD, we can also analyze the qualities of the OD shift by plotting the fractional changes in response magnitude to stimulation of the deprived contra eye and the nondeprived ipsilateral (ipsi) eye (19, 20). This analysis confirms that at P30, both WT and Arc-Tg mice exhibit robust and comparable levels of contra eye depression and a variable potentiation of the nondeprived ipsi eye [Fig. 1*D*, squares; WT: contra depression = 0.7 ± 0.1, ipsi potentiation = 1.4 ± 0.2; Arc-Tg: contra depression = 0.7 ± 0.1, ipsi potentiation = 1.3 ± 0.1; $P = 0.9$, multivariate ANOVA (MANOVA)]. There was, however, a significant difference in the qualities of OD plasticity in WT and Arc-Tg adult mice (Fig. 1*D*, circles). In WT mice, the OD shift was accounted for entirely by ipsi eye potentiation (Fig. 1*D*, open circles), whereas the shift in Arc-Tg mice (Fig. 1*D*, filled circles) was solely due to contra eye depression (WT: contra depression = 1.0 ± 0.01, ipsi potentiation = 1.3 ± 0.1; Arc-Tg: contra depression = 0.7 ± 0.1, ipsi potentiation = 0.9 ± 0.2; $P = 0.03$, MANOVA; Fig. 1*D*).

These data show that augmenting Arc levels in adult mice prolongs juvenile-like OD plasticity, as evidenced by deprivation-induced synaptic depression well past the conventional critical period in mice.

Activity-Dependent Arc Protein Expression Is High During the Critical Period and Low in Adulthood. We reasoned that if availability of Arc influences the qualities of OD plasticity, Arc expression might decline as the animal ages. In mouse visual cortex, Arc is first detected after eye-opening (~P14) and expression steadily increases until ~P30, corresponding to the age of peak sensitivity to MD (21). To determine whether Arc levels decline with age, WT or Arc-Tg mice were killed at P30 or P180. Basal Arc expression in visual cortex is highly variable under standard housing conditions (21); therefore, we housed mice in the dark for 24 h and then either killed them immediately ("dark" condition) or exposed them to light for 2 h ("light" condition) before euthanasia ($n = 6$ per group) (22). The brain was fixed and sectioned at 30 μm on a cryostat, and immunohistochemistry (IHC) was performed for Arc protein using a custom-made Arc antibody (Fig. S2) on sections of brain containing primary visual cortex. The integrated density of Arc-expressing cells in layer IV of visual cortex, where VEPs and LTD were recorded, was measured with the experimenter blinded to genotype and age (Fig. 2*A*). A three-way ANOVA comparing genotype (WT or Arc-Tg), age (P30 or P180), and condition (dark or light) revealed a main effect of genotype ($P < 0.0001$), age ($P = 0.02$), and condition ($P < 0.0001$), as well as a genotype × condition interaction ($P = 0.02$). Post hoc Student's t tests showed that in P30 mice, light significantly induced Arc expression in both WT and Arc-Tg mice (WT: light > dark; light: 4.5 ± 1.3, dark: 1 ± 0.6, $P = 0.02$; Arc-Tg: light > dark; light: 8.2 ± 1, dark: 2.7 ± 2.7, $P = 0.002$). However, Arc-Tg mice expressed significantly more Arc after light exposure than WT mice ($P = 0.008$). At P180, WT mice no longer exhibited detectable Arc expression, even after light exposure. Arc-Tg mice, on the other hand, exhibited significant Arc expression after light exposure (light: 7.1 ± 0.8, dark: 1.8 ± 1.2; $P = 0.001$). Furthermore, levels of light-induced Arc in P180 Arc-Tg mice were not significantly different from P30 Arc-Tg mice ($P > 0.05$), suggesting that activity-dependent expression of Arc in Arc-Tg mice does not decline with

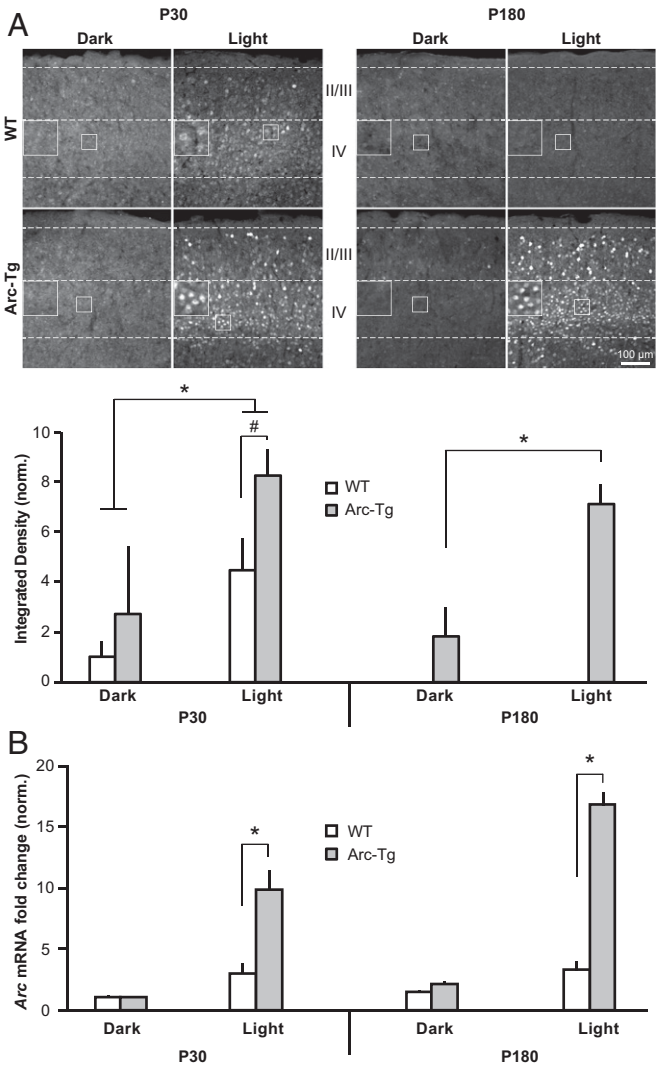

Fig. 2. Activity-dependent Arc protein, but not mRNA expression, declines with age in WT mouse visual cortex, but not in Arc-Tg mice. (*A*) IHC for Arc expression in layers I–IV of visual cortex after 24 h of being housed in the dark or 24 h of dark housing followed by 2 h of light exposure. Layer IV Arc expression is quantified in the graphs ($n = 6$ per group). Light increased Arc expression in both WT and Arc-Tg mice at P30 (WT: $^{*}P = 0.02$, Arc-Tg: $^{*}P = 0.002$), but Arc levels were higher in Arc-Tg mice ($^{\#}P = 0.008$). At P180, WT mice did not express Arc after light exposure, while Arc-Tg mice exhibited the same light-induced increase in Arc observed at P30 ($^{*}P = 0.001$). (Scale bar: 100 μm.) (*B*) WT and Arc-Tg mice were dark-housed for 24 h and then either killed in the dark (dark condition) or exposed to light for 2 h before euthanasia (light condition). qRT-PCR was run on dissected visual cortex to quantify *Arc* mRNA expression. All values were first normalized to GAPDH to control for total RNA levels. Light-induced *Arc* mRNA expression was higher in Arc-Tg mice than WT mice at both P30 and P180 (P30: $^{*}P < 0.0001$, P180: $^{*}P < 0.0001$). However, light-induced mRNA expression did not decrease with age in WT mice. Plotted data are normalized to P30 WT dark ($n = 5$ for WT light, $n = 4$ for Arc-Tg light, and $n = 3$ for all dark groups). Data are represented as mean ± SEM.

age. These data show that activity-dependent Arc protein expression significantly declines with age in WT but not Arc-Tg mice. This loss of endogenous Arc protein over age correlates with the decline of deprived-eye depression following MD.

Arc transcription and translation are exquisitely regulated in the brain and are finely tuned to experience and neuronal activity (12). Of particular interest, transcription and translation of Arc can be independently regulated by activity (23). We therefore sought to determine whether endogenous activity-dependent *Arc* mRNA expression also declines with age. Mice underwent dark and light exposure as described above ($n = 3$–5 per group). The visual cortex was dissected and qRT-PCR, the most sensitive and quantitative method of RNA detection, was performed on lysates (Fig. 2*B*). A three-way ANOVA revealed a main effect of genotype ($P = 0.002$) and condition ($P = 0.0002$), but not age. Post hoc *t* tests showed that light-induced *Arc* mRNA expression was higher in Arc-Tg than WT mice (P30 WT: 2.9 ± 0.9, P30 Arc-Tg: 9.8 ± 1.6, $P < 0.0001$; P180 WT: 3.3 ± 0.7, P180 Arc-Tg: 16.7 ± 1.1, $P < 0.0001$). Interestingly, however, levels of activity-induced *Arc* mRNA expression did not differ with age in either genotype ($P > 0.05$). Although we cannot rule out the possibility that analysis of layer IV alone would reveal an age effect, we note that Arc protein cannot be detected in any layer of V1 in adult WT mice. These data suggest that availability of endogenous *Arc* mRNA alone cannot fully explain the differences in Arc protein expression across the lifespan of WT mice and point to the possibility of a decrease in either activity-dependent translation or stability of endogenous Arc protein in adult visual cortex. Nevertheless, the increased expression of *Arc* mRNA in the active visual cortex of Arc-Tg mice is paralleled by a proportional increase in protein.

Augmenting Arc Expression Restores LTD in Adult Visual Cortex. Deprived-eye depression occurs via mechanisms shared with LTD (3), which also diminishes with age (24). In addition to the profound deficit in OD plasticity (11), juvenile (P20–25) Arc knockout (KO) mice exhibit impaired layer IV LTD in visual cortex, induced in slices with low-frequency stimulation (LFS) of the white matter, compared with WT mice, which showed robust LFS LTD (WT: $n = 7$ slices from four mice, 67.5 ± 5.7%; Arc KO: $n = 7$ slices from five mice, 90.6 ± 4.6%; $P < 0.001$, *t* test; Fig. 3*A*). We therefore hypothesized that the persistence of juvenile OD plasticity in adult Arc-Tg mice was accompanied (and perhaps accounted for) by continued expression of juvenile-like LTD. To ensure expression of Arc protein in the slices, mice were exposed briefly (30 min) to an enriched environment before euthanasia as described previously (23). We first measured LTD in juvenile mice when both WT and Arc-Tg animals show comparable OD plasticity, characterized by robust deprived-eye depression after MD. Over the age range examined, between P26 and P41, LTD in WT and Arc-Tg mice was also comparable (WT: $n = 9$ slices from seven mice, 75.4 ± 11.6%; Arc-Tg: $n = 7$ slices from six mice, 81.3 ± 7.1%; $P > 0.5$, *t* test; Fig. 3*B*). Subgroup analysis of this juvenile cohort revealed no difference in LTD in animals of either genotype at P26–33 or P34–41 (Fig. 3*B*, circles and inverted triangles, respectively). However, in adult mice (P180–200), we observed significant LTD in Arc-Tg slices but not in WT littermate slices (WT: $n = 11$ slices from six mice, 102.8% ± 8.7; Arc-Tg: $n = 12$ slices from six mice, 74.5 ± 7.9%; Fig. 3*C*). The difference between genotypes was significant ($P = 0.04$, *t* test). Thus, augmented expression of Arc in adult visual cortex restores or maintains two features of juvenile plasticity: LTD in vitro (Fig. 3*C*) and deprived-eye depression following MD in vivo (Fig. 1*C*).

Inhibition of Protein Synthesis in Vivo Impairs LTD in Juvenile Visual Cortex. The apparent requirement of Arc translation for deprived-eye depression may offer a partial explanation for why juvenile OD plasticity following brief MD is impaired when the visual cortex is infused locally with the protein synthesis inhibitor cycloheximide (CHX) (25). If this explanation is correct, and the mechanisms of LTD are used for deprived-eye depression following MD, we would also expect to observe reduced LTD ex vivo following microinfusion of CHX into visual cortex. To test this prediction, WT visual cortex was infused in vivo via an osmotic minipump with CHX for 4 d as described (25), and slices were then prepared to conduct LTD experiments. Similar to our observations in the Arc KO visual cortex, there was no LTD in juvenile visual cortex after chronic inhibition

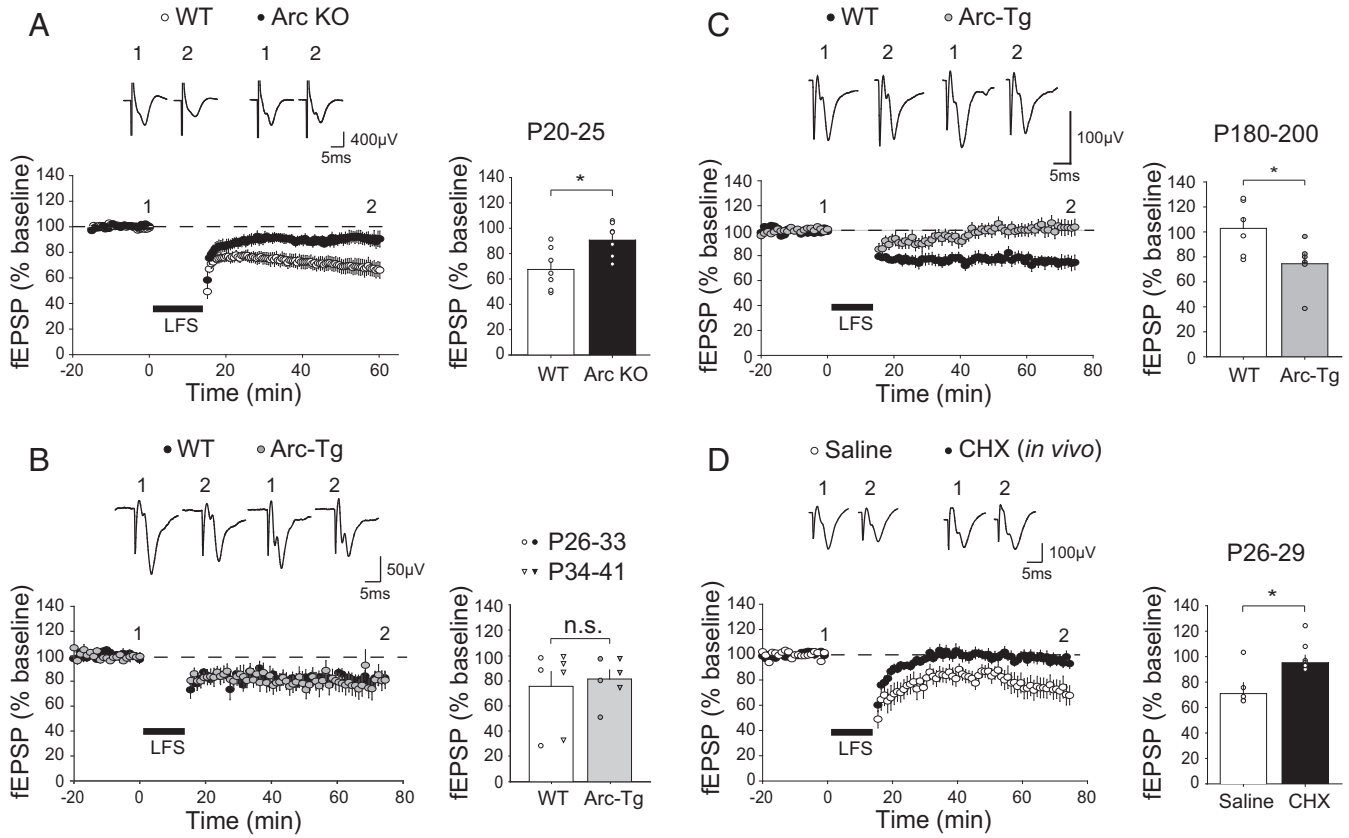

Fig. 3. Arc and protein translation are required for LTD in layer IV of visual cortex. (*A*) LFS (900 stimuli at 1 Hz) induces robust LTD in juvenile (P20–25) WT, but not Arc-KO, slices (average of last 5 min of recordings normalized to the baseline; WT: $n = 4$ mice, KO: $n = 5$; $^*P < 0.001$). (*B*) LFS induces LTD to the same degree in young (P26–41) WT and Arc-Tg slices (WT: $n = 7$, Arc-Tg: $n = 6$; $P > 0.5$). The LTD amplitudes of field excitatory postsynaptic potential (fEPSP) of the youngest animals in this group (P26–33, circles) and the older animals (P34–41, inverted triangles) do not show any significant difference ($P > 0.5$, *t* test), and were therefore combined. (*C*) LFS induces robust LTD in adult (P180–200) Arc-Tg slices, but not WT slices (WT: $n = 11$, Arc-Tg: $n = 6$; $^*P = 0.04$). (*D*) LFS induced LTD in juvenile (P25–30) visual cortex previously infused with saline, but not in visual cortex infused with CHX (saline: $n = 5$, CHX: $n = 5$; $^*P = 0.02$). Data are represented as mean ± SEM.

of protein synthesis (saline: $n = 5$ slices from five mice, 72.4 ± 8.6%; CHX: $n = 7$ slices from five mice, 96.2 ± 5.9%; $P = 0.02$, *t* test; Fig. 3*D*). Together, these findings are consistent with the hypothesis that translation of Arc gates the mechanism of deprivation-induced synaptic depression in visual cortex.

Acute Expression of Arc in Adult Mouse Visual Cortex Is Sufficient to Reopen the Critical Period of Juvenile OD Plasticity. Augmenting the availability of Arc protein throughout development and into adulthood prolongs the critical period for juvenile OD plasticity (Fig. 1). However, this does not address whether restoring Arc protein expression is sufficient to reopen the critical period of OD plasticity once it has closed. To determine whether acutely increasing Arc protein in adult visual cortex is sufficient to restore juvenile-like plasticity, we expressed Arc using a lentivirus injected into visual cortex of P180 WT mice, which robustly increased Arc levels (Fig. 4*A* and Fig. S3). Lentivirus containing GFP-Arc or GFP was injected into layer IV of visual cortex, and baseline VEP recordings were conducted 1 wk after virus injection. Unlike the case in Arc-Tg mice, viral Arc overexpression is constitutively driven and not activity-dependent. Based on previous studies (26, 27), we predicted that VEP amplitude might be depressed by constitutive Arc expression since the VEP is mainly a synaptic population response that correlates with surface AMPA receptor expression (11). Indeed, a significant decrease in overall binocular VEP amplitude was observed compared with GFP-injected mice (GFP-injected mice: 197 ± 30 μV, GFP-Arc–injected mice: 75 ± 21 μV; $P = 0.005$; Fig. 4*B*). No deprived-eye depression was observed in GFP-injected mice following short (3–4 d) MD (GFP: normalized to baseline contra values: $n = 11$; contra baseline = 1 ± 0.2, post-MD = 0.9 ± 0.2; $P = 0.4$, paired *t* test; Fig. 4*C*). However, despite a reduction in baseline VEP magnitude, contra VEP responses were further reduced after MD in GFP-Arc–injected mice (GFP-Arc: normalized to baseline contra values: $n = 5$, contra baseline = 1 ± 0.2, post-MD = 0.6 ± 0.2; $P = 0.02$; Fig. 4*D*). Further, when comparing the fractional change in contra eye and ipsi eye visual responses following MD, there was a significant difference between GFP- vs. GFP-Arc–injected mice (GFP: contra depression = 0.9 ± 0.1, ipsi potentiation = 1.4 ± 0.1; GFP-Arc: contra depression = 0.5 ± 0.1, ipsi potentiation = 1.0 ± 0.1; $P = 0.01$, MANOVA; Fig. 4*E*). Critically, the fractional OD shift in the P180 GFP-injected mice was the same as in noninjected WT P180 mice ($P = 0.3$, MANOVA), indicating virus injection had no effect on cortical responses or OD plasticity. Additionally, the fractional OD shift in P180 WT mice injected with GFP-Arc did not significantly differ from age-matched Arc-Tg mice, indicating that acute viral expression of Arc can restore OD plasticity to a degree similar to that achieved by Tg augmentation of Arc throughout life ($P = 0.6$, MANOVA; Fig. 4*E*). Intriguingly, not only was contra eye depression observed in Arc-Tg and GFP-Arc–injected mice but a lack of ipsi eye potentiation was also observed, further suggesting that Arc protein levels control the qualitative aspects of OD plasticity.

These data show that acutely increasing Arc protein expression in visual cortex is sufficient to restore juvenile OD plasticity

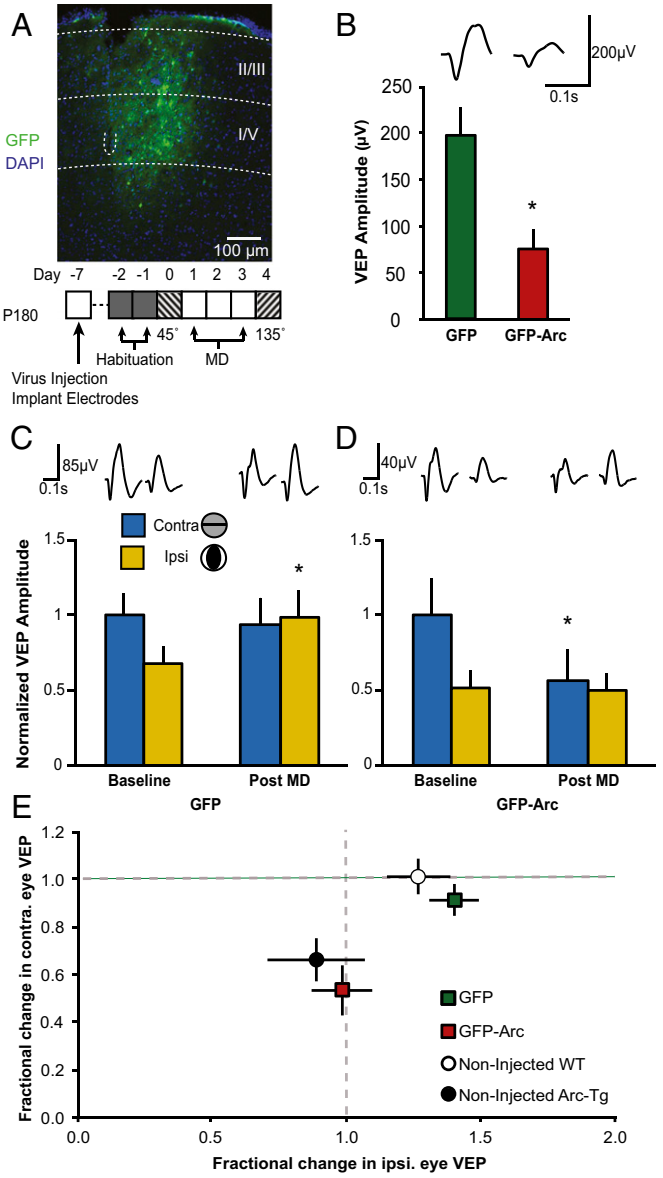

Fig. 4. Acute Arc expression in adult mouse visual cortex is sufficient to restore juvenile OD plasticity. P180 WT mice were injected unilaterally in the visual cortex with lentivirus expressing either GFP alone or GFP-Arc. (*A*) Representative image of virally driven GFP expression in binocular visual cortex and time line of the experiment. The white dashed lines demarcate the cortical layers, as well as the position of the tip of the recording electrode. (*B*) GFP- and GFP-Arc–injected P180 mice were visually stimulated before MD with both eyes open to record binocular baseline VEPs. GFP-Arc–injected mice had significantly smaller VEPs than GFP-injected mice (GFP: $n = 11$, GFP-Arc: $n = 5$; $^*P = 0.005$). Traces represent average VEPs for GFP- and GFP-Arc–injected mice. (*C*) Data were normalized to baseline contra values. There was no significant change in contra VEP amplitudes following MD in GFP-injected animals ($P > 0.05$); however, there was a significant ipsi increase ($^*P = 0.003$). (*D*) Data were normalized to baseline contra values. GFP-Arc–injected mice exhibited significant contra depression following MD ($^*P = 0.016$) and no change in ipsi responses. Averaged VEP traces are presented above the graphs. (*E*) Plot of the fractional change in ipsi (*x* axis) and contra (*y* axis) eye VEPs following MD (same data as in *C* and *D*, noninjected WT and Arc-Tg data are from Fig. 1*B*). There is a significant difference between the fractional change in visual responses between GFP- and GFP-Arc–injected mice ($P < 0.01$). GFP-injected mice exhibit the same lack of change as noninjected P180 WT mice ($P = 0.3$), while GFP-Arc–injected mice exhibit the same degree of change as noninjected P180 Arc-Tg mice ($P = 0.6$). Data are represented as mean ± SEM.

in adult visual cortex, suggesting the increased availability of Arc protein is sufficient to allow deprivation-induced synaptic depression in adult visual cortex.

Discussion

Here, we show that acute or chronic up-regulation of Arc protein in adult mice renders visual cortical synapses sensitive to deprived-eye depression following MD, recapitulating juvenile critical period OD plasticity. In agreement with the prevailing hypothesis that LTD mechanisms mediate deprived-eye depression (3), overexpression of Arc also prolongs juvenile-like LTD in adult visual cortex. Conversely, elimination of Arc expression or inhibition of mRNA translation in juvenile visual cortex prevents deprived-eye depression after MD in vivo (11, 25) and LTD ex vivo. Together, these data indicate that availability of Arc is critical for the expression of juvenile plasticity in visual cortex.

Considering the key role for Arc in determining the qualities of OD plasticity in visual cortex of juvenile animals, we predicted that the loss of deprived-eye depression after MD in adult visual cortex correlates with a lack of activity-dependent Arc expression. Indeed, we found that endogenous Arc protein expression in the active visual cortex declines with age, coincident with the loss of juvenile plasticity. Surprisingly, however, we found that activity-dependent *Arc* mRNA expression is comparable in juvenile (~P30) and adult (~P180) WT mouse visual cortex. This finding implies that the normal decline in Arc protein expression in active visual cortex results from a decrease in experience-dependent *Arc* translation, which can occur via mechanisms that are distinct from those regulating activity-dependent transcription (12, 23). The lack of decline in activity-dependent Arc expression in Arc-Tg mice could be due to the increase in *Arc* mRNA levels. Alternatively or in addition, the extra *Arc* allele in the Arc-Tg line does not contain an intron in the 3′ UTR region, which may result in an increase in mRNA stability in dendrites due to a lack of nonsense-mediated decay (28), and would thus potentially have a longer half-life than endogenous *Arc* mRNA. Restoration of juvenile plasticity in adult mice injected with GFP-Arc suggests that the presence of Arc protein in visual cortex is sufficient for juvenile OD plasticity.

Deprived-eye depression after MD is believed to occur via mechanisms revealed by the study of LTD in layer IV. LTD in this layer is triggered by NMDA receptor activation and expressed by internalization of AMPA receptors (29). Although NMDA receptor-dependent LTD is not affected by acute (in vitro) inhibition of protein synthesis (30), we discovered that chronic inhibition of protein synthesis by in vivo microinfusion of CHX, which has been shown to prevent deprived-eye depression (25), impairs layer IV LTD ex vivo. These findings are reminiscent of the recent observation that chronic, but not acute, inhibition of metabotropic glutamate receptor 5 (mGluR5) can disrupt both deprived-eye depression after MD and LTD in layer IV (19). Activity-dependent synthesis of Arc protein occurs downstream of mGluR5 activation (12, 23). Thus, a simple explanation for this constellation of findings is that NMDA receptor-dependent LTD and deprived-eye depression require Arc protein as a necessary cofactor, and are inhibited by chronic block of either mGluR5 or protein synthesis. Decreased availability of Arc, and a consequent down-regulation of the mechanisms of LTD, also offers a simple molecular explanation for the age-dependent loss of synaptic sensitivity to visual deprivation.

Inhibition develops later than excitatory transmission in the cortex, and it has been suggested that the consequent decrease in the ratio of excitation to inhibition brings the critical period for juvenile plasticity to a close (10). We propose that decreasing the excitability of the visual cortex ultimately affects OD plasticity by preventing the activity-dependent expression of key activity-regulated plasticity proteins at the synapse that are important mediators of excitatory synaptic modification, such as Arc (Fig. S4).

Indeed, in addition to manipulations of inhibition, OD plasticity can be restored in adult rodents exposed to an enriched visual environment (6, 7), treated chronically with fluoxetine (8), or genetically engineered to express constitutively active CREB (31), manipulations that also increase Arc protein levels (32). The precise regulation of Arc expression during development therefore provides a potential mechanistic link between the maturation of inhibition and changes in the qualities of excitatory synaptic modification over the lifespan.

Materials and Methods

Animals. Tg mouse lines harboring the Arc-promoter mCherry-Arc transgene (mCherry-Arc/Arc) were generated as previously described (18). Further details can be found in *SI Materials and Methods*. Requests for mice should be directly addressed to H.B. or H.O. Arc KO mice were obtained from Kuan Wang, NIH, Bethesda, and were previously described (22). Both male and female mice were used, and the experimenter was blinded to genotype in all experiments. Male C57BL/6 mice (Charles River Laboratories) at the age of P22–25 were used for the Alzet pump implantation experiments. Male C57BL/6 mice (The Jackson Laboratory) at the age of P180 were used for lentiviral VEP experiments. All procedures were approved by the Institutional Animal Care and Use Committees of the Massachusetts Institute of Technology, the University of Utah, and The University of Tokyo Graduate School of Medicine, in conjunction with NIH guidelines.

Virus Production/Injection.

Virus production. Kimberly Huber, University of Texas Southwestern Medical Center, Dallas, generously donated FUGW lentiviral plasmids for ubiquitin (Ubq)-GFP and Ubq-GFP-Arc. Injections were carried out as previously described (33).

VEP recordings, slice electrophysiology, and IHC. VEP recordings, slice electrophysiology, and IHC were carried out as previously described (11, 19). Detailed methods on IHC, qRT-PCR, VEP recordings, and slice electrophysiology can be found in *SI Materials and Methods*.

Statistics. ANOVA/MANOVA tests and post hoc Student's *t* tests were performed using JMP Pro software (v12; SAS Institute). For slice electrophysiology experiments, post hoc paired *t* tests were performed to determine the significance of changes before and after LFS and unpaired *t* tests were performed to test the differences between groups after LFS.

ACKNOWLEDGMENTS. We thank the late Dr. Roger Y. Tsien (University of California, San Diego) for the gift of the mCherry plasmid. We thank Dr. Kimberly Huber (University of Texas Southwestern Medical Center) for the FUGW GFP and Arc-GFP plasmids and Dr. Kuan Wang (NIH) for the Arc KO mouse line. K.R.J. was supported by the University of Utah Neuroscience Training Program (Grant 5T32NS076067) and by NIH National Research Service Award F31 (Grant MH112326). E.D.P. was supported by a developmental biology training grant at the University of Utah (Grant 5T32HD00749117). This work was funded by the Japan Agency for Medical Research and Development–Core Research for Evolutional Science and Technology grant (H.B.), KAKENHI Grants 15H02358, 15H04258, 16H01268 from the Japan Society for the Promotion of Science (to H.O. and H.B.), a grant-in-aid from the Ministry of Health, Labour, and Welfare of Japan (to H.O. and H.B), the NIH (Grants R00-NS076364 and R01-MH112766 to J.D.S.), the E. Matilda Ziegler Foundation (J.D.S.), the Howard Hughes Medical Institute, and The Picower Institute Innovation Fund (M.F.B.).

1. Hübener M, Bonhoeffer T (2014) Neuronal plasticity: Beyond the critical period. *Cell* 159:727–737.
2. Espinosa JS, Stryker MP (2012) Development and plasticity of the primary visual cortex. *Neuron* 75:230–249.
3. Cooke SF, Bear MF (2013) How the mechanisms of long-term synaptic potentiation and depression serve experience-dependent plasticity in primary visual cortex. *Philos Trans R Soc Lond B Biol Sci* 369:20130284.
4. Hensch TK, et al. (1998) Local GABA circuit control of experience-dependent plasticity in developing visual cortex. *Science* 282:1504–1508.
5. Choi SY, Morales B, Lee HK, Kirkwood A (2002) Absence of long-term depression in the visual cortex of glutamic acid decarboxylase-65 knock-out mice. *J Neurosci* 22: 5271–5276.
6. Greifzu F, et al. (2014) Environmental enrichment extends ocular dominance plasticity into adulthood and protects from stroke-induced impairments of plasticity. *Proc Natl Acad Sci USA* 111:1150–1155.
7. Matthies U, Balog J, Lehmann K (2013) Temporally coherent visual stimuli boost ocular dominance plasticity. *J Neurosci* 33:11774–11778.
8. Maya Vetencourt JF, et al. (2008) The antidepressant fluoxetine restores plasticity in the adult visual cortex. *Science* 320:385–388.
9. Hensch TK, Fagiolini M (2005) Excitatory-inhibitory balance and critical period plasticity in developing visual cortex. *Prog Brain Res* 147:115–124.
10. Jiang B, Huang ZJ, Morales B, Kirkwood A (2005) Maturation of GABAergic transmission and the timing of plasticity in visual cortex. *Brain Res Brain Res Rev* 50: 126–133.
11. McCurry CL, et al. (2010) Loss of Arc renders the visual cortex impervious to the effects of sensory experience or deprivation. *Nat Neurosci* 13:450–457.
12. Shepherd JD, Bear MF (2011) New views of Arc, a master regulator of synaptic plasticity. *Nat Neurosci* 14:279–284.
13. Shepherd JD, et al. (2006) Arc/Arg3.1 mediates homeostatic synaptic scaling of AMPA receptors. *Neuron* 52:475–484.
14. Frenkel MY, Bear MF (2004) How monocular deprivation shifts ocular dominance in visual cortex of young mice. *Neuron* 44:917–923.
15. Sawtell NB, et al. (2003) NMDA receptor-dependent ocular dominance plasticity in adult visual cortex. *Neuron* 38:977–985.
16. Sato M, Stryker MP (2008) Distinctive features of adult ocular dominance plasticity. *J Neurosci* 28:10278–10286.
17. Kawashima T, et al. (2009) Synaptic activity-responsive element in the Arc/Arg3.1 promoter essential for synapse-to-nucleus signaling in activated neurons. *Proc Natl Acad Sci USA* 106:316–321.
18. Okuno H, et al. (2012) Inverse synaptic tagging of inactive synapses via dynamic interaction of Arc/Arg3.1 with CaMKIIβ. *Cell* 149:886–898.
19. Sidorov MS, Kaplan ES, Osterweil EK, Lindemann L, Bear MF (2015) Metabotropic glutamate receptor signaling is required for NMDA receptor-dependent ocular dominance plasticity and LTD in visual cortex. *Proc Natl Acad Sci USA* 112: 12852–12857.
20. Dölen G, et al. (2007) Correction of fragile X syndrome in mice. *Neuron* 56:955–962.
21. Tagawa Y, Kanold PO, Majdan M, Shatz CJ (2005) Multiple periods of functional ocular dominance plasticity in mouse visual cortex. *Nat Neurosci* 8:380–388.
22. Wang KH, et al. (2006) In vivo two-photon imaging reveals a role of arc in enhancing orientation specificity in visual cortex. *Cell* 126:389–402.
23. Jakkamsetti V, et al. (2013) Experience-induced Arc/Arg3.1 primes CA1 pyramidal neurons for metabotropic glutamate receptor-dependent long-term synaptic depression. *Neuron* 80:72–79.
24. Dudek SM, Friedlander MJ (1996) Developmental down-regulation of LTD in cortical layer IV and its independence of modulation by inhibition. *Neuron* 16:1097–1106.
25. Taha S, Stryker MP (2002) Rapid ocular dominance plasticity requires cortical but not geniculate protein synthesis. *Neuron* 34:425–436.
26. Rial Verde EM, Lee-Osbourne J, Worley PF, Malinow R, Cline HT (2006) Increased expression of the immediate-early gene arc/arg3.1 reduces AMPA receptor-mediated synaptic transmission. *Neuron* 52:461–474.
27. Chowdhury S, et al. (2006) Arc/Arg3.1 interacts with the endocytic machinery to regulate AMPA receptor trafficking. *Neuron* 52:445–459.
28. Giorgi C, et al. (2007) The EJC factor eIF4AIII modulates synaptic strength and neuronal protein expression. *Cell* 130:179–191.
29. Crozier RA, Wang Y, Liu CH, Bear MF (2007) Deprivation-induced synaptic depression by distinct mechanisms in different layers of mouse visual cortex. *Proc Natl Acad Sci USA* 104:1383–1388.
30. Huber KM, Kayser MS, Bear MF (2000) Role for rapid dendritic protein synthesis in hippocampal mGluR-dependent long-term depression. *Science* 288:1254–1257.
31. Pham TA, et al. (2004) A semi-persistent adult ocular dominance plasticity in visual cortex is stabilized by activated CREB. *Learn Mem* 11:738–747.
32. Li Y, et al. (2015) Reversal of age-associated cognitive deficits is accompanied by increased plasticity-related gene expression after chronic antidepressant administration in middle-aged mice. *Pharmacol Biochem Behav* 135:70–82.
33. Kaplan ES, et al. (2016) Contrasting roles for parvalbumin-expressing inhibitory neurons in two forms of adult visual cortical plasticity. *Elife* 5:e11450.

Supporting Information

Jenks et al. 10.1073/pnas.1700866114

SI Materials and Methods

Animals. Plasmid construction of pGL4.11-Arc7000-mCherry-Arc-UTRs was described previously (18). The plasmid was linearized and purified after removal of vector sequences. Tg mouse lines harboring the Arc promoter mCherry-Arc transgene (Arc-mCherry/Arc) were generated by microinjection of the purified DNA fragment into the pronucleus of fertilized C57BL/6 mouse eggs. Genomic integration of the transgene and reporter expression were analyzed by PCR, Southern blotting, Western blotting, and histological assays. Among several lines that showed activity-dependent expression of mCherry-Arc, one line that exhibited high reporter expression in the neocortex was selected and used for this study. Genotypes were identified by PCR with the following specific primers: arcpromoter3 (5′-GAGCCTGCCACACTCGCTAA-3′) and mcherry-tg3-2 (5′-TCAAGTAGTCGGGGATGTCG-3′). Requests for mice should be addressed directly to H.B. or H.O. Arc KO mice were obtained from Kuan Wang, NIH, Bethesda, and were previously described (22). Male C57BL/6 mice and female mCherry-Arc-Tg mice were bred together, yielding WT and Arc-Tg hemizygous (one allele of the transgene) littermates. Heterozygous Arc KO mice were bred together to yield WT and KO offspring. Both male and female mice were used, and the experimenter was blinded to genotype in all experiments. Male C57BL/6 mice (Charles River Laboratories) at the age of P22–25 were used for the Alzet pump implantation experiments. Male C57BL/6 mice (The Jackson Laboratory) at the age of P180 were used for lentiviral VEP experiments. All procedures were approved by the Institutional Animal Care and Use Committees of the Massachusetts Institute of Technology, the University of Utah, and The University of Tokyo Graduate School of Medicine, in conjunction with NIH guidelines.

IHC. WT and Arc-Tg mice at P30 and P180 were dark-housed for 24 h and either killed in the dark ("dark" condition) or exposed to light for 2 h and then killed ("light" condition). Brains were dissected out and fixed in 4% paraformaldehyde for 24 h, and then cryoprotected in 30% sucrose. Brains were sectioned on a cryostat at 30 μm and stored in cryoprotectant at −20 °C until needed. Sections containing visual cortex were blocked in 2% fish gelatin (Sigma–Aldrich)/5% normal donkey serum (Jackson ImmunoResearch)/0.1% Triton X-100 (Amresco) for 2 h, stained for Arc (custom-made antibody; ProteinTech) overnight at room temperature, and washed three times for 10 min each time in 1× PBS plus 2% fish gelatin. Slides were then incubated in secondary antibody (donkey anti-rabbit Alexa Fluor 488; Jackson ImmunoResearch) for 4 h and washed three times for 10 min each time in 1× PBS before being mounted on slides and coverslipped in Fluoromount mounting media (Sigma–Aldrich). A 10-section (1,272 × 1,272-μm) z-stack (each plane 2 μm apart) of binocular V1 for each mouse was acquired using a 10× objective on a confocal microscope (FV1000; Olympus). Sections used from each mouse had the same coordinates relative to bregma (−3.39 mm) to control for location of binocular V1 and cortical thickness. A maximum intensity projection of the z-stack was created in ImageJ (NIH). Every maximum intensity projection image was thresholded to the same level, and the integrated density of Arc-positive cells in layer IV was measured. Layer IV was determined by measuring 250 μm down from the dorsal cortical surface and then applying a 200-μm-tall × 900-μm-wide region of interest to measure the integrated density of only layer IV neurons.

qRT-PCR. P30 and P180 WT and Arc-Tg mice were dark-housed for 24 h and then either killed in the dark (dark condition) or exposed to 2 h of light (light condition) before euthanasia. Brains were removed, visual cortices were isolated and homogenized in TRIzol Reagent (Thermo Fisher Scientific), and RNA was isolated following the manufacturer's guidelines. Reverse transcription was performed using a High Capacity cDNA Reverse Transcription Kit (Thermo Fisher Scientific). qPCR was then performed using PowerUP SYBR Green Master Mix (Thermo Fisher Scientific). Analysis was performed by fitting the average of duplicate cycle threshold (Ct) values to a linear curve obtained from a serial dilution series for each primer set. Ct values for Arc from each cDNA sample, corresponding to RNA extracted from the visual cortex of one mouse, were normalized to GAPDH values run in parallel. Primers for amplification of murine Arc and GAPDH are listed below (5′ → 3′): Arc forward: GGA GGG AGG TCT TCT ACC GTC, Arc reverse: CCC CCA CAC CTA CAG AGA CA, GAPDH forward: CAT GGC CTT CCG TGT TCC TA, and GAPDH reverse: GCC TGC TTC ACC ACC TTC TT.

VEP Recordings.

Electrode implantation. Mice were anesthetized with an i.p. injection of ketamine (50 mg/kg) and xylazine (10 mg/kg), and a local anesthetic of 1% lidocaine hydrochloride (0.1 mL) was injected over the scalp. Petrolatum ophthalmic ointment (Dechra Pharmaceuticals) was applied to protect the eyes. The scalp was sterilized by alternately applying Betadine and 70% alcohol. For purposes of head fixation, a post was fixed to the skull just anterior to bregma using cyanoacrylate and a further application of dental cement. Two small (<0.5 mm) burr holes were made in the skull overlying the binocular visual cortex (3 mm lateral to lambda), and tungsten microelectrodes (FHC) were inserted ∼450 μm below the cortical surface along the dorsal-ventral stereotaxic axis, positioning the electrode tip in cortical layer IV. Reference electrodes were placed bilaterally in prefrontal cortex. Electrodes were secured in place using cyanoacrylate, and the entire exposed area of skull was covered with dental cement. Animals were maintained at ∼37 °C throughout the procedure and recovery, and general condition and reflex signs were monitored closely. Mice were monitored postoperatively for signs of infection or discomfort, and were allowed at least 24 h for recovery before habituation to the restraint apparatus. All animals were killed after the last recording session and processed for histology to determine the precise location of the recording electrode and virus expression (if injected).

Recording procedure. VEP recordings were conducted in awake mice. Mice were habituated to the restraint apparatus before the first recording session. The mice were alert and still during recording. Visual stimuli were presented to left and right eyes randomly. A total of 200 stimuli were presented per condition.

Visual stimuli. Visual stimuli consisted of full-field sine wave gratings (0.05 cycles per degree) of varying contrast (0–100%) generated by a VSG2/2 card (Cambridge Research Systems) and presented on a computer monitor suitably linearized by γ-correction. VEPs were elicited by horizontal, vertical, or oblique (45° or 135°) bars. The display was positioned 20 cm in front of the mouse and centered on the midline, thereby occupying 92° × 66° of the visual field. Mean luminance, determined by a photodiode placed in front of the computer screen, was 27 cd/m^2.

Analysis. VEP amplitude was quantified by measuring the trough-to-peak response amplitude of the average VEP waveform, as described previously (14). The fractional change in contra and ipsi

eye VEP amplitude was calculated as the VEP amplitude following MD divided by the VEP amplitude before MD, as described previously (20).

Virus Production/Injection.

Virus production. Kimberly Huber, University of Texas Southwestern Medical Center, Dallas, generously donated FUGW lentiviral plasmids for Ubq-GFP and Ubq-GFP-Arc. Lentiviral and packaging plasmids were transfected into HEK293 cells using FuGENE transfection reagent (Promega Corporation). Supernatant was collected 48–72 h posttransfection, spun at 3,000 × *g* at 4 °C, and then passed through a 0.45 μm filter. Filtered supernatant was then centrifuged at 75,000 × *g* to pellet the virus. After drying the pellet, virus was resuspended in ice-cold PBS and stored at −80 °C. The viral titer for each virus ranged from 8 to 9 * 10^7 genome copies per milliliter.

Virus injection. The experimenter was blinded to the viruses being injected before surgery. P180 WT mice (C57BL/6J) were used for these experiments. Virus injection was carried out during electrode implantation surgery (discussed above), after drilling of the burr hole over binocular visual cortex and before lowering the electrode. Injection was done using a Nanoject II Auto-Nanoliter Injector (Drummond Scientific). A pulled glass pipette was backfilled with mineral oil before being attached to the Nanoject II. Virus was then loaded through the tip of the pipette. The pipette tip was lowered ∼450 μm below the cortical surface and allowed to rest for 5 min. One microliter of virus was injected over 25 min. The pipette was left in place for 5 min before being withdrawn, and electrode implantation was completed as described above. To quantify relative Arc expression in GFP- and GFP-Arc–injected mice, a subset of mice did not receive electrodes and were killed 11 d following viral injection (corresponding to the end of the MD experiments). Brains were prepared for Arc IHC as described above, using a donkey anti-rabbit Alexa Fluor 555 (Jackson ImmunoResearch) secondary antibody. The integrated density of Arc-positive cells in layer IV was measured in binocular visual cortex as described above.

Slice Electrophysiology.

Slice preparation. WT or Arc KO mouse slices were prepared from juvenile P25–40 animals. For WT or Arc-Tg slice experiments, both P26-41 and P180-200 WT and Arc-Tg mice were exposed for 30 min to a 45 × 24-cm arena with toys and walls covered with stripes to ensure Arc expression (23) before receiving isoflurane anesthesia, followed by acute decapitation. Three hundred fifty-micrometer slices of visual cortex were made in high-sucrose dissection buffer containing 87 mM NaCl, 2.5 mM KCl, 1.25 mM NaH_2PO_4, 25 mM $NaHCO_3$, 0.5 mM $CaCl_2$, 7 mM $MgCl_2$, 75 mM sucrose, 10 mM dextrose, and 1.3 mM ascorbic acid. Slices recovered for 15 min at 32 °C, and then for at least 1 h at room temperature, in carbogenated artificial cerebrospinal fluid containing 124 mM NaCl, 5 mM KCl, 1.23 mM NaH_2PO_4, 26 mM $NaHCO_3$, 10 mM dextrose, 1 mM $MgCl_2$, and 2 mM $CaCl_2$ before recordings began.

Recordings. Extracellular field potential recordings were conducted using an interface chamber for Arc KO experiments and a submersion chamber for Arc-Tg slice experiments. A two-contact cluster microelectrode (FHC) was placed in white matter, a glass recording pipette was placed in cortical layer IV, and extracellular field potentials (40–50% of maximal response amplitude) were recorded. Baseline was collected at 0.03 Hz, and recordings were included only when the baseline drift was less than 5% over 30 min. LTD was induced by applying 900 pulses at 1 Hz for 15 min. The last 5 min of baseline and post-LFS recordings were averaged, and statistical comparisons were performed to determine the magnitude of LTD using two-tailed *t* tests.

Alzet pump implantation. P22–25 mice were anesthetized with ketamine (50 mg/kg) and xylazine (10 mg/kg,) i.p. and placed in a stereotaxic holder. Petrolatum ophthalmic ointment was applied to protect the eyes. Alzet micro-osmotic pumps (0.25 $\mu L \cdot h^{-1}$, no. 1002; Durect Corp) were filled with either saline or CHX (10 mg/mL; Sigma–Aldrich) and connected to brain infusion cannulae (Alzet brain infusion kit 3). The scalp was sterilized by alternately applying Betadine and 70% alcohol, and 0.1 mL of lidocaine (2%) was applied under the scalp before scalp incision. A midline incision (1–1.5 cm) was made in the scalp, and the skin and connective tissue were retracted. Following incision, a lidocaine (2%) and epinephrine (1:50,000) solution was applied to the periosteum to avoid excessive bleeding or discomfort. A small burr hole was made in the skull (0.1 mm anterior, 2.7 mm lateral to lambda) with a dental drill through which an infusion cannula was lowered (450 μm below the dura mater). Cannulae were fixed to the skull by applying instant adhesive (Loctite 454). The attached minipump was placed in an s.c. pocket at the nape of the neck. The rest of the exposed scalp was covered with dental cement to hold the cannula in place and prevent inflammation. Animals were maintained at ∼37 °C throughout the procedure and recovery, and general condition and reflex signs were monitored closely. Chemical infusion through the implanted pump continued for 5 d following surgery.

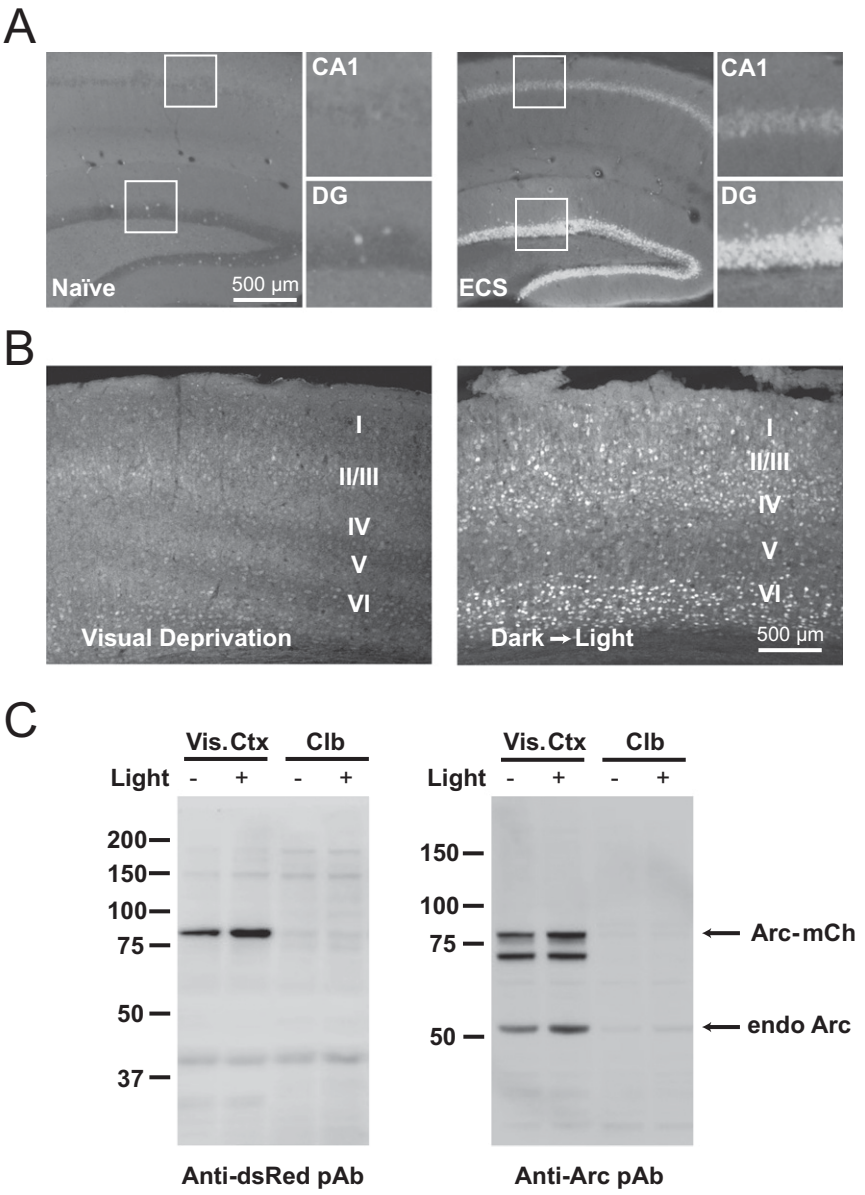

Fig. S1. Characterization of Arc-Tg mouse line. (*A*, *Left*) Arc-mCherry transgene mirrors endogenous Arc expression. In the hippocampus, basal expression of Arc-mCherry is low in both area CA1 and the dentate gyrus (DG). (*Insets*) Magnified CA1 and DG. (*A*, *Right*) Following electroconvulsive shock (ECS), levels of Arc-mCherry expression are dramatically increased in CA1 and DG, consistent with previous findings of ECS-induced induction of endogenous Arc. (Scale bar: 500 μm.) (*B*) Arc-mCherry transgene in the primary visual cortex reliably reports visual experience. (*Left*) P30 mouse dark-housed for 24 h (visual deprivation) has low levels of Arc-mCherry expression in all layers of visual cortex. (*Right*) P30 mouse dark-housed and then exposed to light for 2 h before euthanasia has increased levels of Arc-mCherry expression in the input layers of the visual cortex (layers II/III, IV, and VI). (*C*) Visually driven Arc-mCherry (mCh) expression is specific to visual areas and recapitulates endogenous (endo) Arc expression. Dark-housed mice (Light –) had little Arc-mCherry and endogenous Arc expression in visual cortex (Vis. Ctx) compared with light-exposed mice (Light +), as assessed by antibodies against mCherry (Anti-DsRed pAb) and Arc. This effect of light exposure was specific to the visual system, as both basal and light-induced Arc-mCherry and native Arc expression was equally low in the cerebellum (Clb).

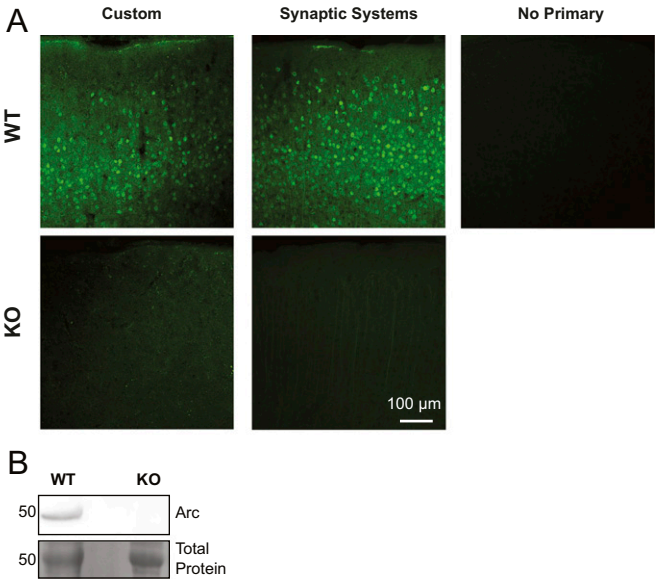

Fig. S2. Validation of custom Arc antibody. (*A*) Side-by-side comparison of custom Arc antibody and commercially available Arc antibody (catalog no.156-003; Synaptic Systems). Custom and commercial Arc antibodies show comparable levels of staining in WT P30 mouse visual cortex (*Upper Left* and *Center*) and comparable levels of background in Arc KO P30 mouse visual cortex (*Lower Left* and *Center*). (*Upper Right*) WT tissue not stained with a primary antibody for comparison. (*B*) Western blot of visual cortex lysates from a P30 WT and Arc KO mouse stained with the custom Arc antibody. Arc is detected in WT, but not Arc KO, lysate.

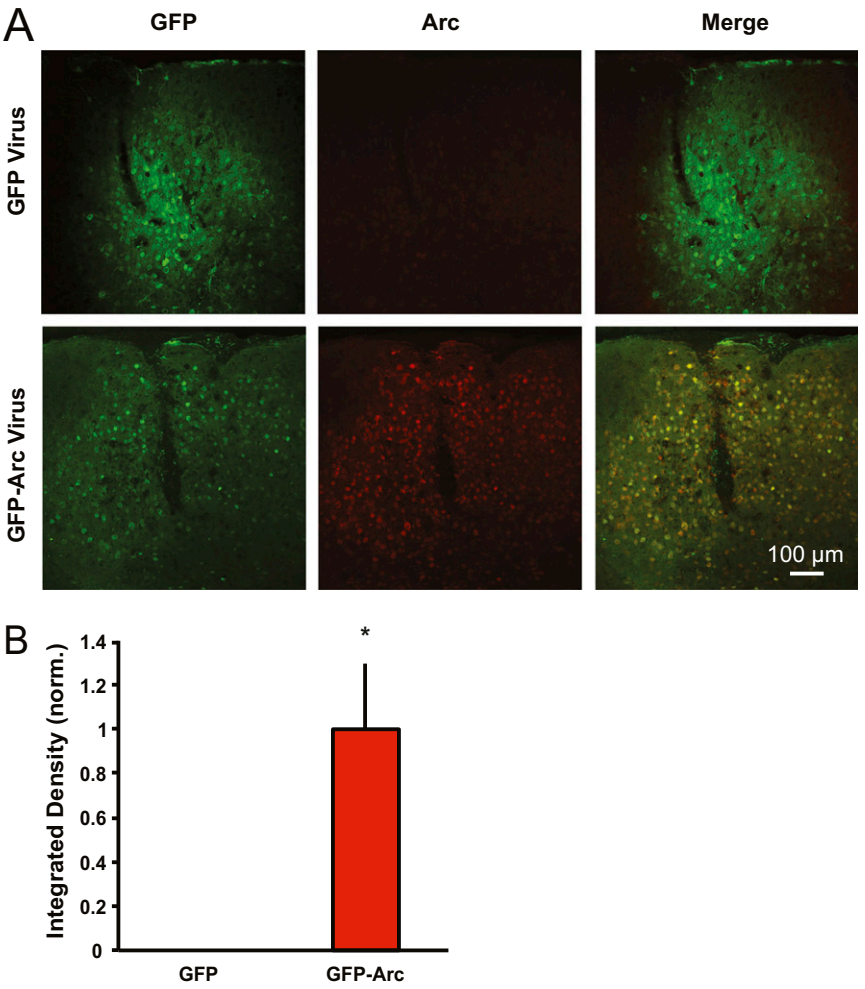

Fig. S3. GFP-Arc lentivirus increases Arc expression in P180 WT visual cortex. P180 WT mice were injected unilaterally in the visual cortex with lentivirus expressing either GFP alone or GFP-Arc. (*A*) Representative images from visual cortex of a mouse injected with GFP lentivirus (*Upper*) and a mouse injected with GFP-Arc lentivirus (*Lower*). (*Left* and *Middle*) GFP expression from GFP and GFP-Arc lentiviruses (no antibody staining) is shown. (*Right*) IHC for Arc expression is shown. (*B*) Quantification of Arc expression from GFP- and GFP-Arc–injected mice (four GFP-injected, four GFP-Arc–injected). When images were set to a threshold determined by the maximum Arc expression in GFP-Arc–injected mice, there was no detectable Arc expression in layer IV of GFP-injected mice above background staining, as seen in noninjected P180 WT (Fig. 2). However, there was a significant increase in Arc expression in GFP-Arc–injected mice ($P = 0.02$, Student t test). Data are normalized (norm.) to GFP and displayed as mean ± SEM.

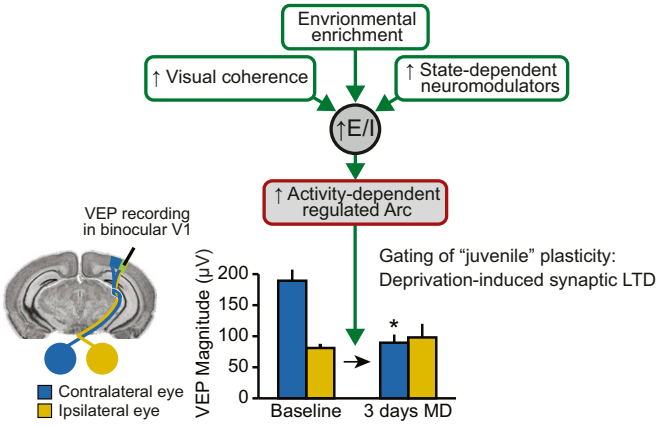

Fig. S4. Model of Arc's role in controlling the "juvenile" quality of OD plasticity. Various genetic, environmental, and pharmacological manipulations have been shown to promote juvenile-like plasticity in adult visual cortex. It has been proposed that these manipulations cause a general increase in the ratio of excitation (E) to inhibition (I). Here, we propose that the increase in E/I restores juvenile plasticity specifically by allowing the induction of activity-regulated genes such as Arc. Increased Arc expression promotes activity-dependent synaptic depression that underlies juvenile OD plasticity. *Significantly lower than contralateral eye at baseline.

Cell

The Neuronal Gene *Arc* Encodes a Repurposed Retrotransposon Gag Protein that Mediates Intercellular RNA Transfer

Elissa D. Pastuzyn,[1] Cameron E. Day,[1] Rachel B. Kearns,[1] Madeleine Kyrke-Smith,[1] Andrew V. Taibi,[1] John McCormick,[2] Nathan Yoder,[1] David M. Belnap,[3,4] Simon Erlendsson,[5,6] Dustin R. Morado,[6] John A.G. Briggs,[6] Cédric Feschotte,[2,7] and Jason D. Shepherd[1,3,8,*]

[1]Department of Neurobiology and Anatomy
[2]Department of Human Genetics
[3]Department of Biochemistry
[4]Department of Biology
The University of Utah, Salt Lake City, UT, USA
[5]Department of Biology, University of Copenhagen, Copenhagen, Denmark
[6]MRC Laboratory of Molecular Biology, Cambridge, UK
[7]Present address: Department of Molecular Biology and Genetics, Cornell University, Ithaca, NY, USA
[8]Lead Contact
*Correspondence: jason.shepherd@neuro.utah.edu
https://doi.org/10.1016/j.cell.2017.12.024

SUMMARY

The neuronal gene *Arc* is essential for long-lasting information storage in the mammalian brain, mediates various forms of synaptic plasticity, and has been implicated in neurodevelopmental disorders. However, little is known about Arc's molecular function and evolutionary origins. Here, we show that Arc self-assembles into virus-like capsids that encapsulate RNA. Endogenous Arc protein is released from neurons in extracellular vesicles that mediate the transfer of *Arc* mRNA into new target cells, where it can undergo activity-dependent translation. Purified Arc capsids are endocytosed and are able to transfer *Arc* mRNA into the cytoplasm of neurons. These results show that Arc exhibits similar molecular properties to retroviral Gag proteins. Evolutionary analysis indicates that Arc is derived from a vertebrate lineage of Ty3/*gypsy* retrotransposons, which are also ancestors to retroviruses. These findings suggest that Gag retroelements have been repurposed during evolution to mediate intercellular communication in the nervous system.

INTRODUCTION

Brains have evolved to process and store information from the outside world through synaptic connections between interconnected networks of neurons. Despite the fundamental importance of information storage in the brain, we still lack a detailed molecular and cellular understanding of the processes involved and their evolutionary origins. Eukaryotic genomes are littered with DNA of viral or transposon origin, which compose about half of most mammalian genomes (Smit, 1999). A growing body of evidence indicates the sequences encoded by these elements can provide raw material for the emergence of new functions and regulatory elements (Chuong et al., 2017). In vertebrates, these include dozens of protein-coding genes derived from sequences previously encoded by transposons (Feschotte and Pritham, 2007) or retroviruses (Kaneko-Ishino and Ishino, 2012). Interestingly, many of these transposon-derived genes are expressed in the brain, but their molecular functions remain to be elucidated.

The neuronal gene *Arc* contains structural elements found within viral Group-specific antigen (Gag) polyproteins that may have originated from the Ty3/*gypsy* retrotransposon family (Campillos et al., 2006; Shepherd, 2017; Zhang et al., 2015), although the role these Gag elements play in Arc function has not been explored. Arc is a master regulator of synaptic plasticity in mammals and is required for protein synthesis-dependent forms of long-term potentiation (LTP) and depression (LTD) (Bramham et al., 2010; Shepherd and Bear, 2011). Arc can regulate synaptic plasticity through the trafficking of AMPA-type glutamate receptors (AMPARs) via the endocytic machinery (Chowdhury et al., 2006). This endocytic pathway maintains levels of surface AMPARs in response to chronic changes in neuronal activity through synaptic scaling, thus contributing to neuronal homeostasis (Shepherd et al., 2006). Arc's expression in the brain is highly dynamic; its transcription is tightly coupled to encoding of information in neuronal circuits *in vivo* (Guzowski et al., 1999). *Arc* mRNA is transported to dendrites and becomes enriched at sites of local synaptic activity where it is locally translated into protein (Steward et al., 1998; Waung et al., 2008). Intriguingly, aspects of *Arc* mRNA regulation resemble some viral RNAs, as *Arc* contains an internal ribosomal entry site (IRES) that allows cap-independent translation (Pinkstaff et al., 2001). Arc is required *in vivo* to transduce experience into long-lasting changes in visual cortex plasticity (McCurry et al., 2010) and for long-term memory (Guzowski et al., 2000; Plath et al., 2006). In addition, Arc has been implicated in various neurological disorders that include Alzheimer's disease (AD)

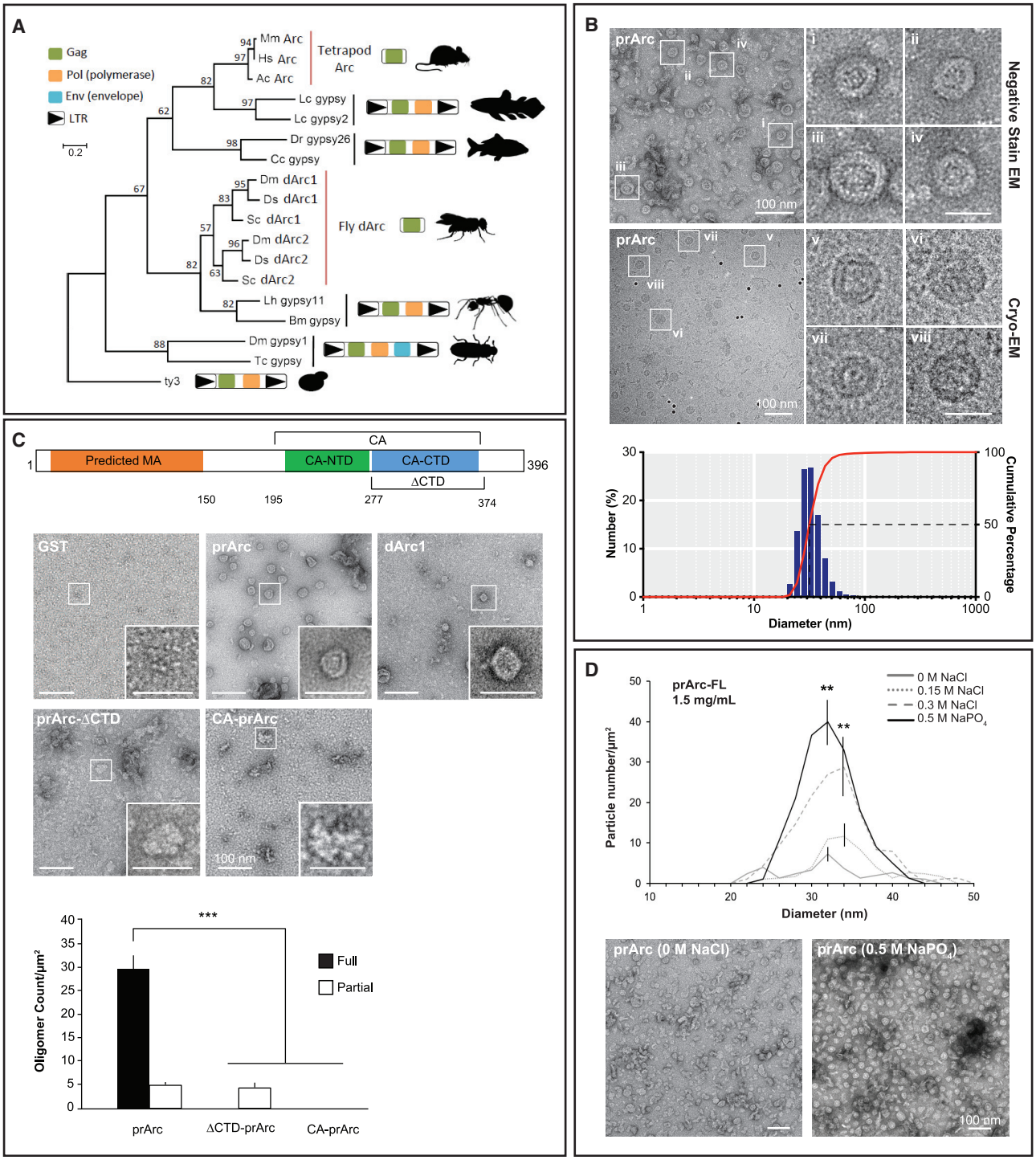

Figure 1. Arc Forms Virus-like Capsids via a Conserved Retroviral Gag CA Domain

(A) Maximum likelihood phylogeny based on an amino acid alignment of tetrapod Arc, fly dArc1, and Gag sequences from related Ty3/*gypsy* retrotransposons. Schematics of Gag-only *Arc* genes and Ty3/*gypsy* elements are included to the right of the tree. In lineages without Arc genes, the most closely related sequences to Arc are Gag-pol polyproteins flanked by long terminal repeats (LTRs) as expected in bona fide Ty3/*gypsy* retrotransposons.

(B) (Top) Representative negative-stain EM images of full-length purified rat Arc (prArc) protein (1 mg/mL, 42,000×). (i–iv) Magnified view of boxed particles. Scale bars, 30 nm. Representative cryo-EM images of prArc (2 mg/mL, 62,000×). (v–vii) Magnified images of Arc capsids showing the double-layered capsid shell. Scale bars, 30 nm. (Bottom) Dynamic light-scattering analysis of prArc capsids. The weighted size distribution profile is represented as a histogram of the number of particles.

(legend continued on next page)

(Wu et al., 2011), neurodevelopmental disorders, such as Angelman (Greer et al., 2010; Pastuzyn and Shepherd, 2017) and Fragile X syndrome (Park et al., 2008), and schizophrenia (Fromer et al., 2014; Managò et al., 2016; Purcell et al., 2014). Thus, precise regulation of Arc expression and activity in the nervous system seems essential for normal cognition.

Despite its importance, little is known about Arc protein biochemistry and molecular function. Here, we uncover a potential role for Arc in mediating intercellular communication via extracellular vesicles (EVs). Synaptic communication is modulated by many other communication pathways that include glia-neuron interactions, and emerging evidence suggests that EVs mediate intercellular signaling in the nervous system (Budnik et al., 2016; Zappulli et al., 2016). EVs can be broadly divided into two groups, microvesicles and exosomes, which are defined both by size and subcellular origin. Microvesicles pinch off from the plasma membrane directly and are usually 100–300 nm in diameter, whereas exosomes are derived from intraluminal vesicles that originate from multivesicular bodies (MVBs) and are usually <100 nm in size. EVs can transport cargo that do not readily cross the plasma membrane, such as membrane proteins and various forms of RNA. The observation that EVs can function in the intercellular transport of these molecules within the nervous system opens an entirely new perspective on intercellular communication in the brain.

Here, we find that Arc protein self-assembles into oligomers that resemble virus capsids and exhibit several other biochemical properties seen in retroviral Gag proteins such as RNA binding. Moreover, Arc is released from neurons in EVs and is able to transfer its own mRNA into neurons. The *Drosophila* Arc homolog, dArc1, also forms capsids and mediates intercellular transfer of its own mRNA at the fly neuromuscular junction (Ashley et al., 2018, this issue of *Cell*), despite originating from a distinct retrotransposon lineage. These data suggest that co-option of retroviral-like Gag elements may have provided an evolutionary pathway for novel mechanisms that mediate intercellular signaling and have been intricately involved in the evolution of synaptic plasticity and animal cognition.

RESULTS

Fly and Tetrapod *Arc* Genes Independently Originated from Distinct Lineages of Ty3/*gypsy* Retrotransposons

To shed light onto *Arc*'s evolutionary origins, we performed phylogenomic analyses (Figures 1A and S1A). Highly conserved, unique orthologs of the murine *Arc* genes were identified throughout the tetrapods (mammals, birds, reptiles, amphibians), but were conspicuously absent from all fish lineages and other deuterostomes examined (94 species). The closest relatives of *Arc* in the coelacanth, zebrafish, and carp genomes were encoded by prototypical Ty3/*gypsy* retrotransposons, with indications of recent transposition activity. Similarly, orthologs and paralogs of *Drosophila Arc* (*darc1*, *darc2*) were identified in all schizophoran (true) flies represented in the database but were not detected in any other dipteran (e.g., mosquitoes) or protostome species (286 species; Figure S1B). The closest retrotransposon relatives of the fly *Arc* genes were found in the genomes of the silkworm and Argentine ant. Interestingly, while *Arc* appears to be a single-copy gene in all tetrapods examined, the gene has experienced multiple rounds of duplication during schizophoran evolution (Figure S1B). Phylogenetically, tetrapod *Arc* genes cluster with Ty3/*gypsy* retrotransposons from fish, whereas the fly *Arc* homologs group with a separate lineage of Ty3/*gypsy* retrotransposons from insects (Figure 1A). These results indicate that the tetrapod and fly *Arc* genes originated independently from distinct lineages of Ty3/*gypsy* retrotransposons, as conjectured previously (Abrusán et al., 2013), but still share significant homology in the retroviral Gag domain.

Arc Proteins Self-Assemble into Virus-like Capsids

Ty3 retrotransposons can form oligomeric particles that resemble retroviral capsids (Hansen et al., 1992), and Arc also has a propensity to oligomerize (Myrum et al., 2015). Retroviral capsid formation is essential for infectivity and is primarily mediated by the Gag polyprotein, which in HIV contains four main functional domains: matrix/MA, capsid/CA, nucleocapsid/NC, and p6 (Freed, 2015). Arc has both primary sequence (Campillos et al., 2006) and structural similarity to CA of HIV and Foamy Virus Gag polyproteins (Taylor et al., 2017; Zhang et al., 2015), suggesting that Arc may share functional similarities to Gag proteins. To characterize the biochemical properties of Arc protein, we expressed rat Arc in bacteria as a glutathione S-transferase (GST) fusion protein. The expressed protein was purified by affinity and size exclusion chromatography, and the GST tag was removed by proteolysis (Figures S2A and S2B). Purified preparations of rat Arc (prArc) were analyzed using negative-stain electron microscopy (EM) and cryoelectron microscopy (cryo-EM). These experiments revealed that prArc spontaneously forms oligomeric structures that resemble virus-like capsids (Figure 1B). prArc capsids exhibited a double-shell structure with a mean diameter of 32 ± 0.2 nm. Similarly, bacterially expressed and purified dArc1 (Figure S2C), the *Drosophila* Arc homolog, also self-assembled into capsid-like structures (Figure 1C). Purified Arc protein that was expressed in an insect cell expression system also assembled into similar virus-like capsids (data not shown), indicating that oligomerization was not an artifact of

(C) Schematic of Arc protein with the predicted matrix (MA) (orange), CA-NTD (green), and CA-CTD (blue) domains. Also depicted are the ΔCTD deletion mutant and the CA domain constructs. Representative negative-stain EM images of purified GST, prArc, the *Drosophila* Arc homolog dArc1, prArc-ΔCTD, and CA-prArc (all 1 mg/mL, 20,000×). Inset scale bars, 50 nm. (Bottom) Quantification of capsid formation. Fully formed capsids include spherical particles that are between 20–60 nm and have clear double shells, while partially formed capsids do not have clear double shells (scale bars, 100 nm). Data are the average of 3 independent experiments ± SEM using 3 different prArc preparations. ***$p < 0.001$, two-way ANOVA with *post hoc t*-tests.

(D) (Top) To determine properties of Arc capsid stability, we exchanged prArc into buffers with increasing molar concentrations of salt and examined by negative-stain EM. Arc capsids were counted manually and quantified in each buffer condition at a protein concentration of 1.5 mg/mL. Data are the average of 3 independent experiments ± SEM using different prArc preparations. **$p < 0.01$, Student's *t*-test. (Bottom) Representative EM images of prArc under 0 M NaCl and 0.5 M $NaPO_4$ conditions.

See also Figure S1.

bacterial expression. Immature retroviral capsids are formed by the uncleaved Gag polyprotein, and the major stabilizing interactions are made by the C-terminal domain (CTD) of the CA region (Mattei et al., 2016). To test whether the putative Arc CA CTD is also required for self-assembly, we expressed and purified a rat Arc mutant protein that lacked this domain (prArc-ΔCTD, missing amino acids [aa] 277–374, Figures 1C, S2A, and S2B) (Zhang et al., 2015). EM analyses revealed that prArc-ΔCTD was unable to form double-shelled capsids, although intermediate irregular structures were occasionally observed (Figure 1C). To test whether the Arc CA domain was sufficient for capsid assembly we created a mutant Arc protein that contained aa195–364 (CA-prArc; Figures 1C and S2A). CA-prArc was not sufficient to form capsid-like structures. Arc capsids exhibit other properties similar to HIV capsids, including sensitivity to salt and phosphate levels (Purdy et al., 2008); increasing concentrations of NaCl from 0 to 300 mM resulted in stable prArc capsids and high $NaPO_4$ further stabilized capsid formation (Figure 1D).

To test whether Arc forms oligomers in cells, we expressed Arc in HEK293 cells, which lack endogenous Arc, and performed chemical crosslinking to test for the presence of oligomeric species. Arc proteins crosslinked *in situ* formed higher molecular weight species with the SDS-PAGE mobility expected for dimer and trimer subunits (Figure S2D), which is reminiscent of HIV Gag subunits using a similar crosslinking assay (Campbell and Rein, 1999). In contrast, transfected GFP did not form higher molecular weight crosslinks under the same conditions.

Arc Binds and Encapsulates RNA

Retroviral encapsulation of viral genomic RNA is a complex process mediated by a network of interactions between Gag, RNA and lipid membranes (Mailler et al., 2016). HIV Gag contains zinc-finger knuckle motifs in the NC domain that mediate viral RNA binding and selection (Carlson et al., 2016), but in the absence of viral RNA, Gag can also bind cellular mRNAs, which may reflect nonspecific RNA interactions with the basic MA and NC domains (Comas-Garcia et al., 2016). Interestingly, Foamy Virus Gags do not contain zinc-finger domains and bind RNA through C-terminal glycine-arginine-rich patches (Hamann and Lindemann, 2016), indicating that distinct Gag domains from different viral families have evolved to perform similar biochemical processes. Like Foamy Virus Gag, Arc does not appear to contain zinc-finger domains but may bind RNA through ionic interactions in its N terminus. We observed that prArc appeared to co-purify with RNA or other nucleic acids, as the preparations had a higher $A_{260/280}$ spectrophotometric ratio than would be expected for a pure recombinant protein (prArc 1.04 ± 0.024; Endophilin3A 0.55 ± 0.006; $n = 3$, $p < 0.01$; Figure S2B). We therefore hypothesized that Arc might bind and encapsulate RNA. To ascertain whether prArc capsids contain mRNA, we determined levels of *Arc* mRNA and a highly abundant bacterial mRNA, *asnA* (Zhou et al., 2011), using qRT-PCR. We detected both *Arc* and *asnA* mRNA (Figure 2A). However, *Arc* mRNA levels were ~10-fold higher than *asnA*. Bacterial cell lysate contained ~15-fold higher *Arc* mRNA levels than *asnA* (Figure 2A), suggesting that prArc capsids show little specificity for a particular mRNA, but encapsulate abundant RNA according to stoichiometry. If mRNA is encapsulated in capsids, it should be resistant to ribonuclease (RNase) treatment. RNase did not degrade *Arc* or *asnA* mRNA, but significantly degraded exogenous free *GFP* mRNA (Figure 2B), indicating that *Arc* and *asnA* mRNA were protected from RNase degradation.

We tested whether Arc protein associates with *Arc* mRNA *in vivo* by immunoprecipitating Arc protein from mouse cortical lysate, followed by qRT-PCR (Figure 2C). *Arc* mRNA was found to selectively immunoprecipitate (IP) with Arc protein, while *GAPDH* was not enriched in Arc IPs. These results suggest that Arc protein and its mRNA form a complex in neurons *in vivo*.

Arc Capsid Assembly Requires RNA

To form the immature viral capsid, HIV Gag must bind RNA (Mailler et al., 2016). To test whether Arc capsid formation requires RNA, we purified full-length Arc protein as above and then stripped bound nucleic acids ("prArc(RNA−)," Figure S3A) as previously performed on HIV Gag (Ganser et al., 1999). This procedure reduced the $A_{260/280}$ ratio significantly (prArc(RNA−) 0.68 ± 0.03, prArc 1.04 ± 0.024; $n = 3$, $p < 0.05$) and we were unable to detect *Arc* mRNA association by qRT-PCR (Figure 2D). Stripping RNA resulted in significantly fewer fully formed capsids (Figure 2E), suggesting that Arc capsids require RNA for normal assembly. To show directly that RNA facilitated Arc capsid assembly, we exogenously added *GFP* mRNA to prArc(RNA−) (7.3% w/w), which resulted in significantly more fully formed Arc capsids.

Arc Protein and *Arc* mRNA Are Released by Neurons in Extracellular Vesicles

Retroviral capsids and EVs are released from cells using similar cellular machinery, such as the MVB pathway (Nolte-'t Hoen et al., 2016). Since Arc exhibits many of the biochemical properties of a viral Gag protein, we tested whether Arc protein might also be released from cells. We harvested media from Arc-transfected HEK293 cells and purified the EV fraction. This fraction contained vesicular structures that were < 100nm and resembled exosomes (Figure S3B). Arc protein was detected in the EV fraction, which was also positive for the EV marker ALIX, but lacked actin (Figure 3A). Conversely, Arc-ΔCTD-transfected HEK cells exhibited little expression in the EV fraction (Figure 3B), suggesting that proper Arc capsid assembly may be required for Arc release via EVs. We performed qRT-PCR on the EV fraction from HEK cell media and detected *Arc* mRNA that was resistant to RNase treatment (Figure 3C).

Native Arc protein was also found in the EV fraction prepared from media harvested from DIV15 cultured cortical mouse neurons (Figure 3D). Since *Arc* mRNA associates with Arc protein in brain lysate, we used RT-PCR to show that *Arc* mRNA is also present in EVs purified from neurons (Figure 3E). Arc protein in EVs was resistant to trypsin digestion (Figure S3C), indicating that Arc protein and RNA were protected or bound in a complex within EVs. To directly determine whether Arc protein is present in EVs, we conducted immunogold-labeling of endogenous Arc in the EV fraction from cultured neurons and found that Arc is present in a subpopulation of EVs (Figure 3F). To test whether Arc release in EVs is activity dependent, we purified the EV fraction from media collected from untreated or KCl-treated wild-type (WT) cultured cortical neurons (Figure S3D). KCl treatment, which increases neuronal activity, resulted in significantly more Arc released into the media.

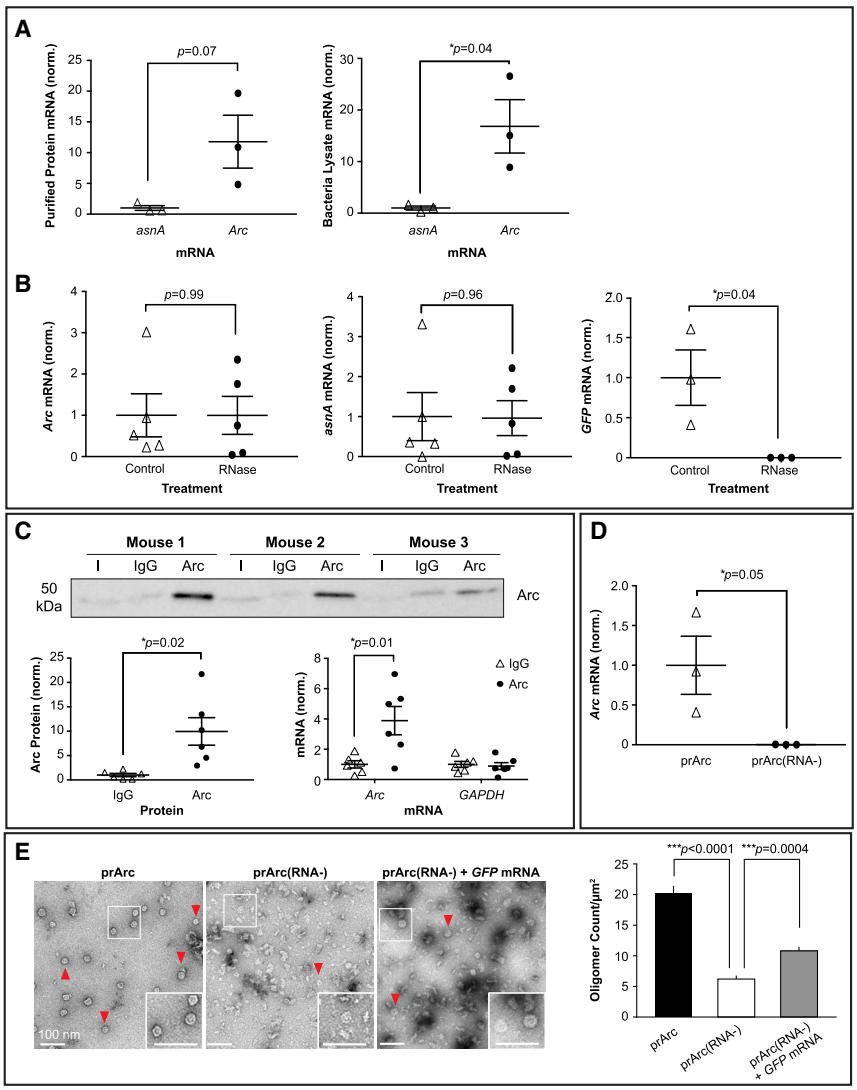

Figure 2. Arc Protein Interacts with mRNA

(A) (Left) qRT-PCR of *Arc* mRNA and the bacterial mRNA *asnA* from prArc. (Right) qRT-PCR of *Arc* and *asnA* mRNA from total bacteria lysate. Data presented as the mean ± SEM normalized to the average of the *asnA* group (Student's *t*-test, n = 3 independent protein preparations, *p < 0.05).

(B) Protein preparations were treated with or without RNase A for 15 min, and qRT-PCR was performed. RNase treatment did not affect *Arc* and *asnA* mRNA levels (paired *t*-test, n = 5 independent protein samples), but significantly degraded exogenous/free *GFP* mRNA (paired *t*-test, n = 3 independent samples, *p < 0.05). Data are presented as ± SEM normalized to the average of the untreated group.

(C) (Top) Representative western blot of Arc protein that was immunoprecipitated (IP) from WT mouse cortical tissue using an Arc or immunoglobulin G (IgG) antibody. Input (I) = 10% total lysate. (Bottom, left) Quantification of Arc protein IP showing significant enrichment of Arc protein using an Arc antibody. (Bottom, right) qRT-PCR was performed on the eluted fractions from the IP. *Arc* mRNA was specifically pulled down in the IP (two-way ANOVA with repeated-measures and Sidak's multiple comparisons: Arc+Arc versus Arc+IgG, p = 0.01; Arc+Arc versus GAPDH+Arc, p = 0.013; Arc+Arc versus GAPDH+IgG, p = 0.011). Data are presented as the mean ± SEM normalized to the average of the IgG group.

(D) qRT-PCR of *Arc* mRNA from prArc and prArc(RNA−). There was significantly less *Arc* mRNA in the prArc(RNA−) preparations. Presented as the mean ± SEM normalized to the average of the prArc group (Student's *t*-test, n = 3 independent samples, *p = 0.05).

(E) (Left) Representative negative-stain EM images of prArc, prArc(RNA−), and prArc(RNA−) incubated with 7.3% (w/w) *GFP* mRNA at RT for 2 hr (0.25 mg/mL, 15,000×). Fully formed capsids are indicated by red arrows (scale bars, 100 nm). (Right) Capsids were quantified as in Figure 1C. Data are presented as the average of 6 images from each condition ± SEM. ***p < 0.001, unpaired *t*-test.

See also Figure S2.

Arc Mediates Intercellular Transfer of mRNA in Extracellular Vesicles

Virus particles are able to infect cells through complex interactions of the viral envelope and host cell membrane, while EVs can also transfer cargo such as RNAs cell-to-cell (Valadi et al., 2007). We predicted that Arc might be able to transfer mRNA, either directly via mRNA encapsulated in prArc or in *Arc*-containing EVs. We transfected GFP/myc-Arc or nuclear-GFP into HEK (donor) cells and collected media from these cells after 18 hr, which was then incubated with untransfected, naive HEK (recipient/"transferred") cells for 24 hr. We observed high Arc expression in a sparse population of naive HEK cells (Figure 4A), while cells incubated with media from cells transfected with nuclear-GFP alone did not express nuclear-GFP. Fluorescent *in situ* hybridization (FISH) for *Arc* mRNA revealed high levels of *Arc* mRNA in recipient cells. Uptake of Arc protein and mRNA was endocytosis-dependent, as application of Dynasore (a potent inhibitor of clathrin-dependent endocytosis [Macia et al., 2006]) significantly blocked transfer of Arc protein (Figure S4A). Since encapsulation of RNA by Arc capsids is nonspecific *in vitro*, we tested whether Arc could co-transfer highly abundant mRNAs. Donor HEK cells were transfected with myc-Arc and/or a membrane-bound GFP (mGFP), and media were collected after 24 hr. Recipient HEK cells showed clear transfer of both GFP protein and mRNA when donor cells contained Arc (Figure 4B). No transfer was observed from cells transfected only with mGFP. These data suggest that Arc EVs released from HEK cells are capable of transferring highly abundant mRNAs cell-to-cell.

To test whether Arc capsids can transfer *Arc* mRNA into neurons, we incubated cultured hippocampal neurons from Arc knockout (KO) mice with prArc. Since the Arc KO line contains GFP knocked into the Arc locus (Wang et al., 2006), we imaged Arc in the red channel and were unable to detect GFP

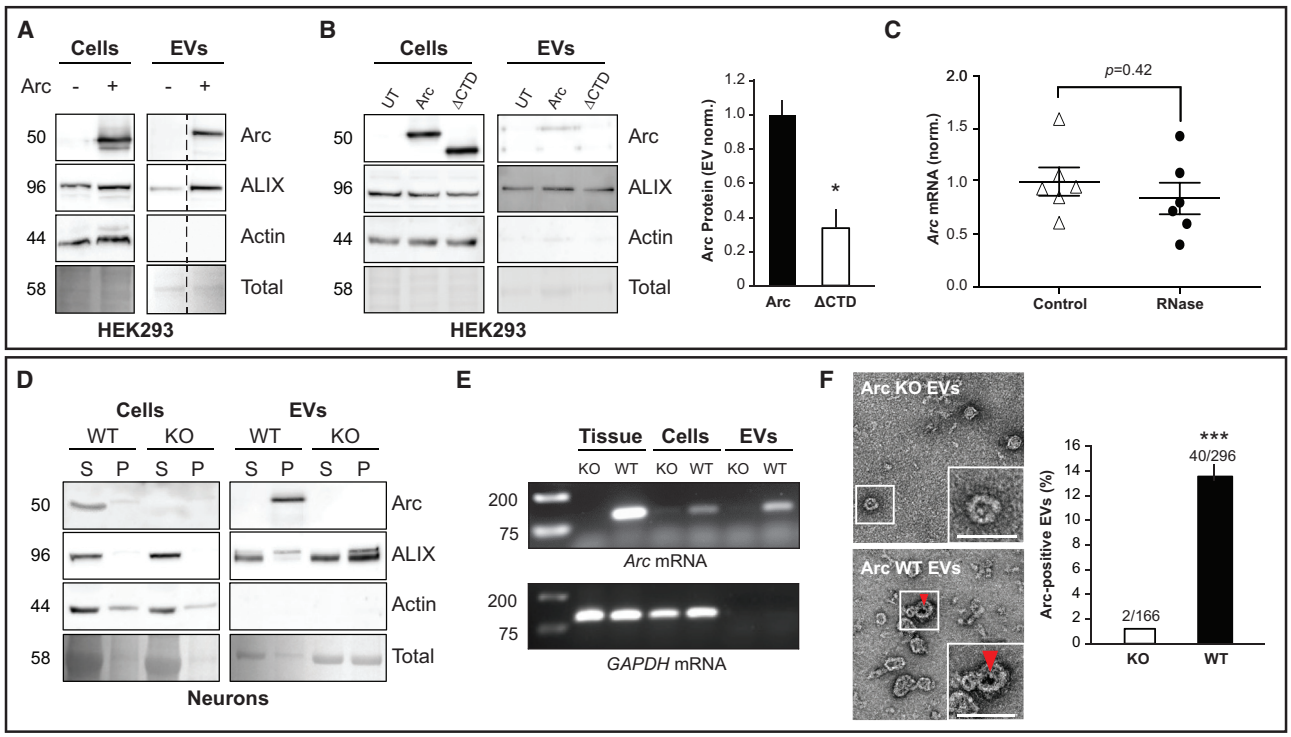

Figure 3. Arc Is Released from Cells in Extracellular Vesicles

(A) HEK cells in 10-cm dishes were transfected with full-length rat WT myc-Arc and media collected 24 hr later. Representative western blots (n = 3 independent experiments) show Arc protein in total cell lysates (cells) and the EV fraction purified from cell media in Arc transfected (+) and untransfected (−) cells. ALIX was used as an EV fraction marker. Ponceau stain was used to visualize the total amount of protein in each lane. The dashed line indicates splicing marks in the blot to compare the (−) and (+) EV lanes. All data are from the same blot, and experiments were performed at the same time.

(B) HEK293 cells were transfected with myc-Arc-WT or myc-Arc-ΔCTD, and media was collected 24 hr later. Representative western blots (n = 3 independent experiments) show Arc protein in total cell lysates (cells) and the EV fraction from cell media. Arc levels in the EV fraction were normalized to Arc protein levels in the cell lysate for each experiment, and data are presented normalized to WT levels (n = 3). *p < 0.05, Student's *t*-test.

(C) HEK EV fractions were untreated (control) or treated with RNase (n = 6 independent cultures) prior to RNA extraction. qRT-PCR was used to measure *Arc* mRNA levels, and data are presented as the mean ± SEM normalized to the average of the untreated group. Paired *t*-test.

(D) Media were harvested from DIV15 cultured cortical neurons obtained from WT and Arc KO mice after 24 hr incubation, and the EV fraction was purified from collected media. Blots indicate levels of Arc, ALIX, and actin from supernatant (S)/soluble fraction and pellet (P)/insoluble fraction for total cellular lysate (cells). (S)/last wash of the ultracentrifugation purification protocol and final pellet (P)/EV fraction for purified EV fraction (EVs). 2.5% of S and P were loaded for cellular lysates. 5% of S and P were loaded for the EV fraction.

(E) RT-PCR using Arc and GAPDH primers was performed on WT or KO mouse cortical tissue, mouse cortical DIV15 WT or KO neurons (cells), and EVs purified from media collected from WT or KO cultured neurons. *Arc* mRNA was present in all three preparations, whereas *GAPDH* mRNA was absent from EVs.

(F) (Top) Immunogold labeling for Arc in EVs obtained from the same Arc KO or WT cultured neuronal media in (D). Red arrow indicates a 10 nm immunogold particle (20,000x). (Bottom) Quantification of EVs (vesicular structures < 100 nm) that were Arc-positive ± SEM using immunogold labeling (n = 3 independent experiments/EV preparations). ***p < 0.001, Student's *t*-test.

See also Figure S3.

fluorescence in the green channel (Figure S4B). We observed uptake of Arc protein into KO neurons above antibody background levels (see Figure S4C for antibody specificity) within 1h of protein incubation, which peaked around 4h of incubation (Figure 5A). To directly determine whether Arc capsids can transfer *Arc* mRNA into neurons, we measured *Arc* mRNA levels in Arc KO neurons incubated with prArc. *Arc* FISH showed robust and high levels of transferred *Arc* mRNA after 4h of incubation with prArc (Figure 5B). RNase treatment of prArc prior to incubation had no effect on mRNA transfer (Figure S5A), further suggesting that Arc capsids are able to protect and encapsulate *Arc* mRNA. Blocking endocytosis using Dynasore prevented uptake of both prArc protein and *Arc* mRNA (Figure S5B). Transferred mRNA and protein were evident both in early endosomes (marked by Rab5) and non-endosome compartments in dendrites (Figure S5C). Both uptake and transfer of purified prArc-ΔCTD and CA-prArc protein and mRNA was significantly less than the full-length protein, indicating that capsid formation is required for uptake into neurons (Figures 5C and 5D). Lack of protein uptake was not due to poor detection by the custom-made Arc polyclonal antibody (Figure S5D). Strikingly, prArc(RNA−) was unable to be taken up but instead coated the outside of neurons (Figure S6), further suggesting that intact Arc capsids are required for uptake and transfer.

To test whether endogenous Arc can transfer mRNA, we incubated Arc KO cultured hippocampal neurons with purified EVs

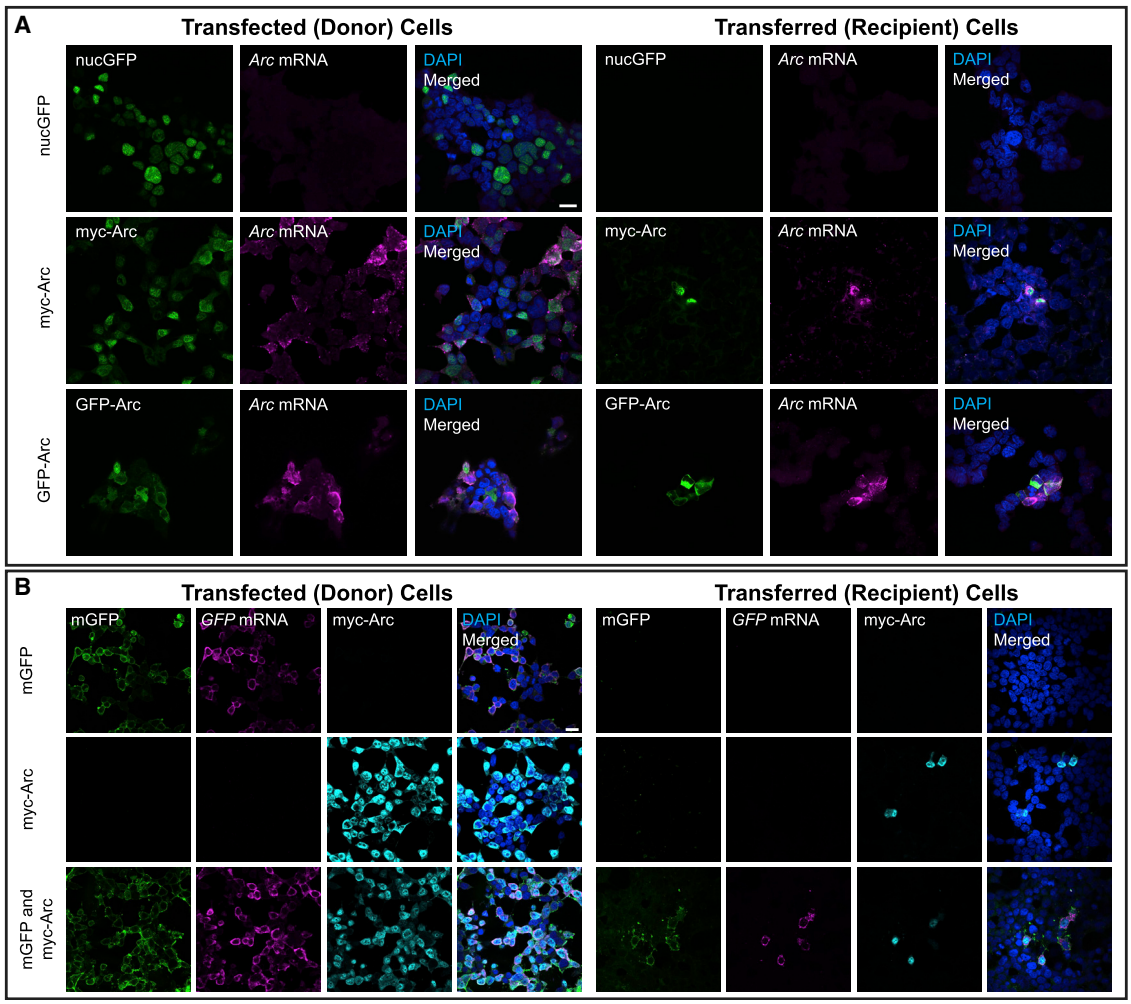

Figure 4. Arc Extracellular Vesicles Mediate Intercellular Transfer of Protein and mRNA in HEK293 Cells

(A) Donor HEK cells in 10-cm dishes were transfected with GFP-Arc, myc-Arc, or nuclear GFP (nucGFP) for 6 hr. Culture media containing plasmid DNA and transfection reagents was then removed and replaced with fresh culture media. 18 hr later, this media was removed and used to replace media on naive recipient HEK cells on coverslips in 12-well plates. 24 hr later, these cells were fixed, and combined FISH for *Arc* mRNA and immunocytochemistry (ICC) for Arc protein was performed. (Left) Representative images of HEK cells grown on coverslips and transfected with the same protocol used for the 10-cm dishes, showing Arc protein (ICC) and *Arc* mRNA (FISH). (Right) Representative images of recipient HEK cells showing *Arc* mRNA and protein were present in cells that received media from GFP-Arc- and myc-Arc-transfected cells, but not nucGFP-transfected cells. Scale bar, 20 μm. Representative of 7 independent experiments and cultures.

(B) Donor HEK cells in 10-cm dishes were transfected like in (A) with membrane GFP (mGFP), myc-Arc, or both constructs together. The media was replaced after 6 hr, and 18 hr later, transferred to naive recipient HEK cells in 12-well plates. 24 hr later, cells were fixed, and combined FISH/ICC for *GFP* mRNA and Arc protein was performed. (Left) Representative images of transfected HEK cells grown on coverslips, showing mGFP fluorescence, Arc protein, and *GFP* mRNA. (Right) Representative images of recipient HEK cells that show co-transfer of GFP protein and mRNA with Arc protein. No GFP transfer was observed in the mGFP only group. Scale bar, 20 μm. Representative of 3 independent experiments and cultures.

See also Figure S4.

prepared from media from WT or KO cortical neurons. Arc KO neurons incubated with WT EVs showed a clear increase in dendritic Arc levels, while KO neurons incubated with EVs derived from KO cells exhibited no increase in dendritic Arc levels (Figure 6A). In addition, FISH showed that *Arc* mRNA in WT EVs was transferred into KO neurons (Figure 6B). Uptake of *Arc* mRNA was not significantly affected by prior treatment of EVs with RNase (Figure S7A), indicating that uptake was not due to free or unbound *Arc* mRNA in the EV fraction. Blocking endocytosis with Dynasore prevented the uptake of Arc protein and mRNA from EVs (Figure S7B). Notably, transferred *Arc* mRNA expression exhibited cell-wide localization in both early endosomes and non-endosome compartments (Figure S7C) and was virtually indistinguishable from *Arc* mRNA distribution in WT neurons. These data indicate that endogenous Arc released via EVs is able to transfer *Arc* mRNA neuron-to-neuron.

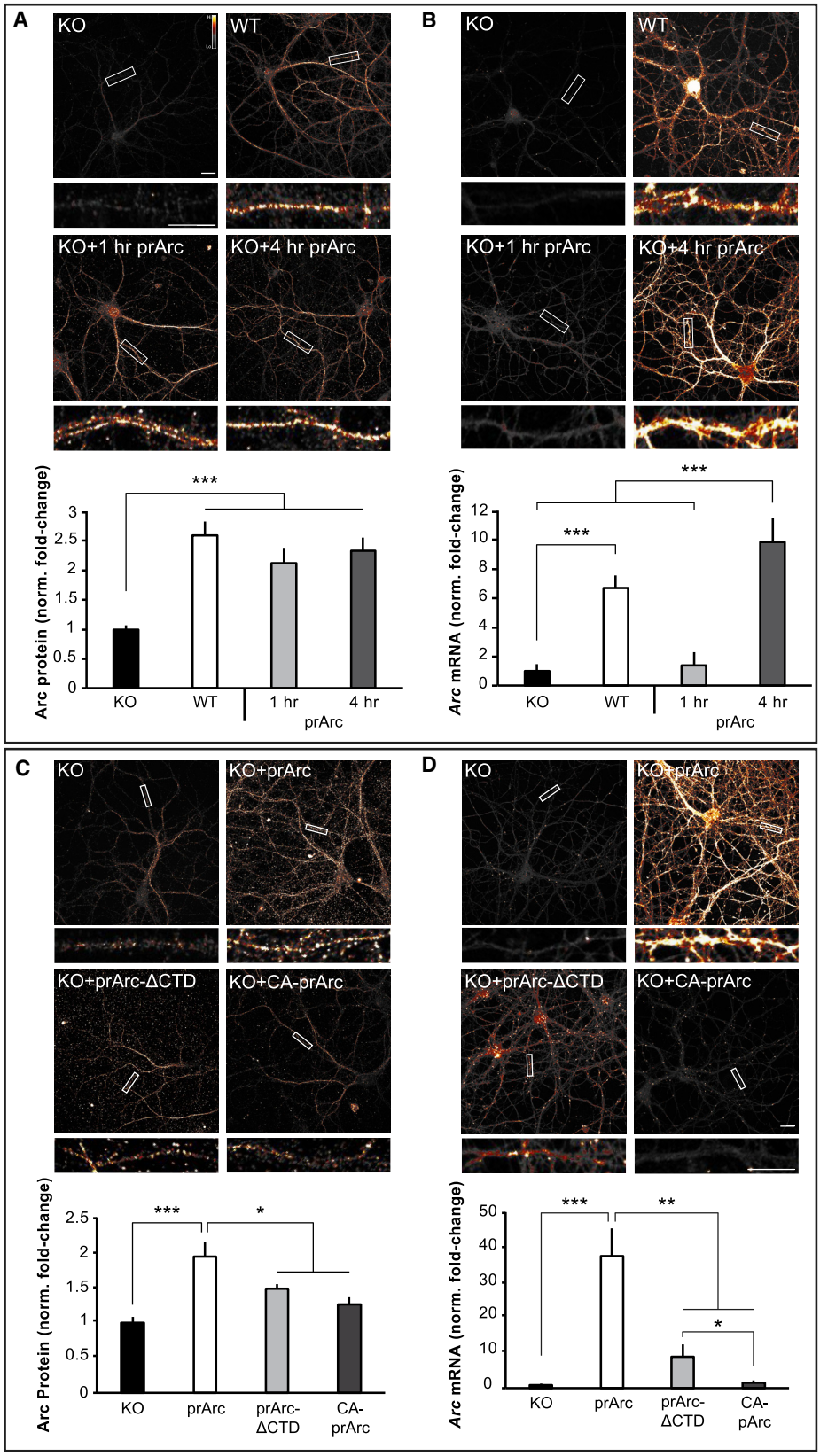

(legend on next page)

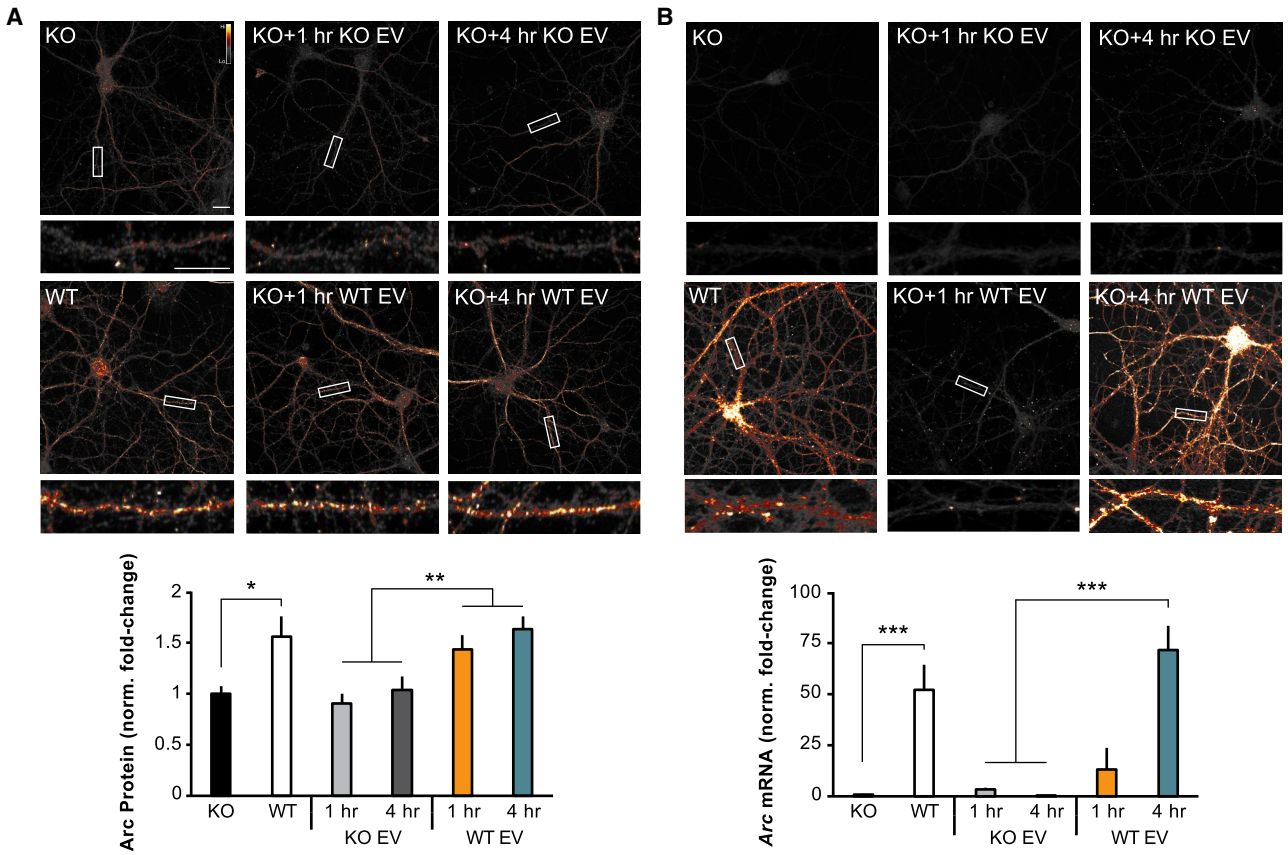

Figure 6. Endogenous Arc Transfers *Arc* mRNA into Neurons via Extracellular Vesicles

(A) Representative images of Arc ICC from DIV15 cultured hippocampal Arc KO neurons treated for 1 or 4 hr with 10 μg of the EV fraction prepared from 10-cm dishes of DIV15 high-density cortical WT or Arc KO neurons. 1 and 4 hr treatment with KO EVs did not increase dendritic Arc levels, whereas 1 and 4 hr of treatment with WT EVs significantly increased dendritic Arc protein levels.

(B) Neurons were treated like in (A); representative images of *Arc* mRNA (FISH) are shown. 1 and 4 hr treatment with KO EV did not increase dendritic *Arc* mRNA levels. 1 hr treatment with WT EV did not significantly increase dendritic *Arc* levels, whereas 4 hr treatment increased dendritic *Arc* mRNA levels. 30-μm segments of two dendrites/neuron were analyzed for integrated density measurements in all groups (n = 10 neurons). *Arc* mRNA and Arc protein levels were normalized to untreated KO neurons and displayed as fold change ± SEM. Student's *t*-test: *p < 0.05. **p < 0.01. ***p < 0.001. Scale bars, 10 μm. Representative of 6 independent experiments using different EV preparations and cultures.

See also Figure S7.

Transferred *Arc* mRNA Can Undergo Activity-Dependent Translation

If *Arc* mRNA associated with Arc capsids is transferred into the cytoplasm of neurons, we predicted that we would observe an increase in dendritic Arc protein by inducing translation of *Arc* mRNA through activation of the group 1 metabotropic glutamate receptor (mGluR1/5) by the agonist DHPG, as previously shown for endogenous Arc (Waung et al., 2008). As predicted, Arc

Figure 5. Arc Capsids Transfer *Arc* mRNA into Neurons

(A) Representative images of Arc ICC from DIV15 cultured hippocampal Arc KO neurons treated for 1 or 4 hr with 4 μg prArc, or WT control neurons. prArc-treated neurons show increased dendritic Arc levels relative to untreated KO neurons.

(B) Neurons were treated like in (A); representative images of *Arc* mRNA (FISH) are shown. 4 hr of prArc treatment significantly increased dendritic *Arc* mRNA levels in KO neurons.

(C) Representative images of Arc ICC from DIV15 cultured hippocampal KO neurons treated with 4 μg prArc, prArc-ΔCTD, or CA-prArc for 4 hr. KO neurons treated with prArc-ΔCTD and CA-prArc showed lower levels of Arc protein than prArc-treated neurons.

(D) Neurons were treated like in (C); representative images of *Arc* mRNA are shown. Neurons treated with prArc-ΔCTD and CA-prArc showed lower levels of *Arc* mRNA than prArc-treated neurons. Dendritic segments boxed in white are magnified beneath each corresponding image. 30-μm segments of two dendrites/neuron were analyzed for integrated density measurements in all groups (n = 10 neurons). *Arc* mRNA and Arc protein levels were normalized to untreated KO neurons and displayed as fold change ± SEM. Student's *t*-test: *p < 0.05, **p < 0.01, and ***p < 0.001. Scale bars, 10 μm. Images are false-colored with the Smart LUT from ImageJ. All data are representative of 3–7 independent experiments using different protein preparations and cultures.

See also Figure S5.

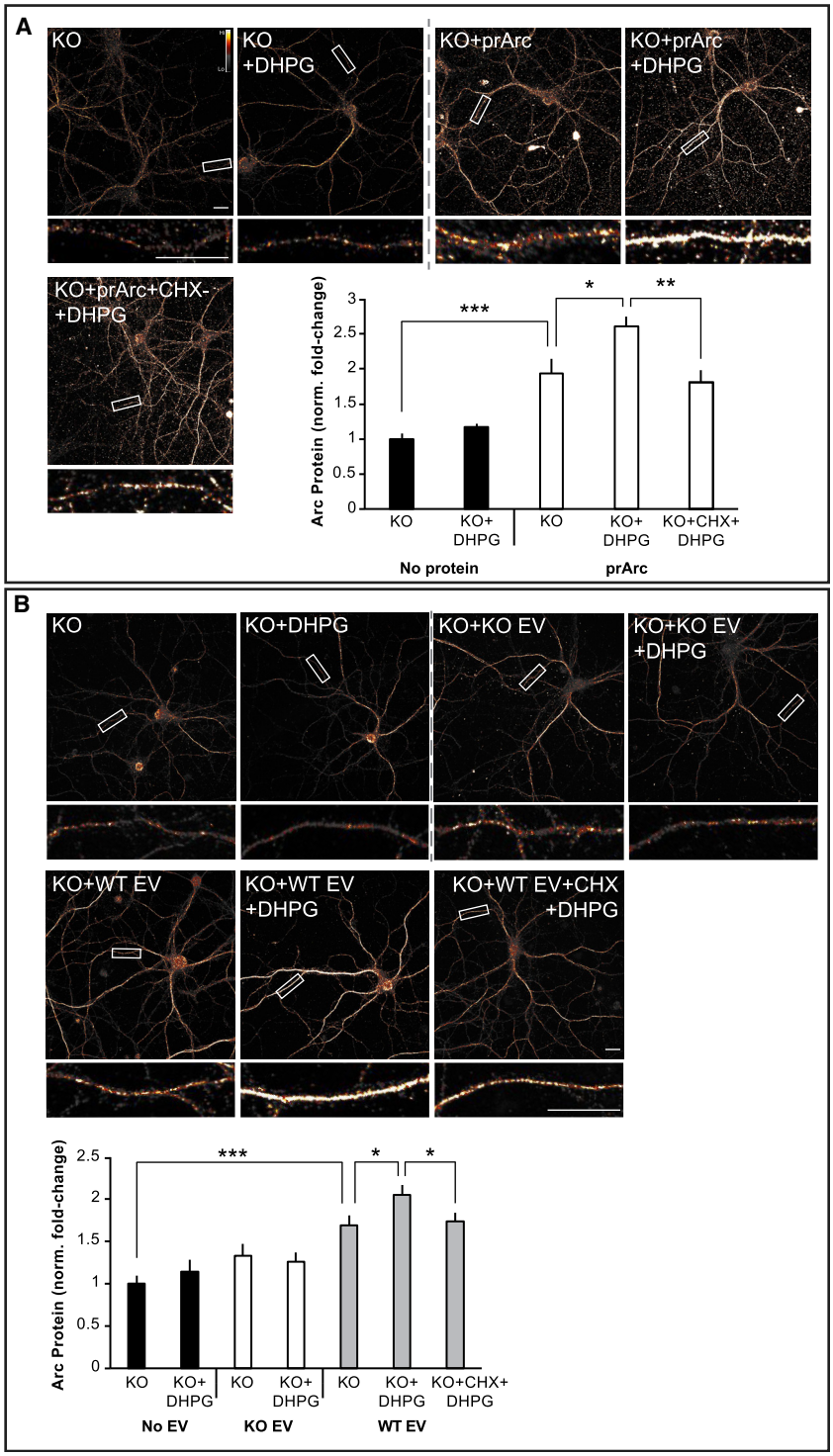

Figure 7. Arc Capsid- and EV-Transferred *Arc* mRNA Is Accessible for Activity-Dependent Translation

(A) Representative images of Arc ICC from DIV15 cultured hippocampal Arc KO neurons treated for 4 hr with 4 μg prArc. To induce translation of *Arc* mRNA, 30 min prior to fixation, neurons were treated with the mGluR1/5 agonist DHPG (100 μM) for 5 min, and then drugs were washed out. 1 hr prior to fixation, a subset of neurons were pretreated with cycloheximide (CHX; 180 μM) to block protein translation. prArc significantly increased dendritic Arc expression in KO neurons, and DHPG treatment further increased dendritic Arc levels, which was blocked by pretreatment with CHX. DHPG had no effect on untreated KO neurons.

(B) Representative images of Arc ICC from DIV15 hippocampal Arc KO neurons treated for 4 hr with 10 μg of the EV fraction prepared from 10-cm dishes of DIV15 high-density cortical WT or Arc KO neurons. A subset of neurons was treated with DHPG and CHX like in (A). WT EVs significantly increased dendritic Arc expression in KO neurons, whereas KO EVs had no effect. DHPG treatment had no effect on dendritic Arc expression in untreated KO neurons or KO EV-treated KO neurons. However, DHPG treatment significantly increased dendritic Arc levels in WT EV-treated KO neurons, which was blocked by pretreatment with CHX. 30-μm segments of two dendrites/neuron were analyzed for integrated density measurements in all groups (n = 10 neurons). *Arc* mRNA and Arc protein levels were normalized to untreated KO neurons and displayed as fold change ± SEM. Student's t test: $^{*}p < 0.05$, $^{**}p < 0.01$, and $^{***}p < 0.001$. Scale bars, 10 μm. Representative of 3 independent experiments using different EV/protein preparations and cultures.

protein levels were significantly increased in dendrites of Arc KO neurons after DHPG (5 min; 100 μM) application in cells incubated with prArc (Figure 7A). This increase was not evident if a protein synthesis inhibitor (cycloheximide; 180 μM) was applied prior to DHPG application. KO neurons incubated with WT EVs for 4 hr and then treated with DHPG exhibited an increase in dendritic Arc levels that was also dependent on protein synthesis (Figure 7B). Although these experiments cannot definitively distinguish *de novo* translated Arc from protein that was taken up, these data suggest that Arc capsids or EVs are capable of transferring *Arc* mRNA between neurons and that this mRNA is available in the cytoplasm of dendrites for activity-dependent translation.

DISCUSSION

Here, we show that mammalian Arc protein exhibits many hallmarks of Gag proteins encoded by retroviruses and retrotransposons: self-assembly into capsids, RNA encapsulation, release in EVs, and intercellular transmission of RNA. These data suggest that Arc can mediate intercellular trafficking of mRNA via Arc EVs (which we term "ACBARs" for "Arc Capsids Bearing Any RNA"), revealing a novel molecular mechanism by which genetic information may be transferred between neurons.

Arc Functions as a Repurposed Gag Protein

Our data show a remarkable conservation of viral Gag properties in Arc. Since Arc shows structural homology to the Gag CA domain (Zhang et al., 2015), the capability of self-assembly into oligomeric capsids is perhaps not too surprising. However, Arc seems to retain other important biochemical properties of Gag that are not intuitive from its sequence. Despite lacking clear zinc-finger RNA binding domains such as in HIV Gag, Arc encapsulates RNA, and RNA binding seems critical for capsid formation. This is reminiscent of Foamy Virus Gags, which have evolved different RNA-binding motifs to HIV Gag (Hamann and Lindemann, 2016) and also structurally resemble Arc (Taylor et al., 2017). HIV Gag-RNA interactions are complex and involve multiple components of Gag, including the MA domain, and are regulated by host cellular factors (Mailler et al., 2016). Gag MA-RNA interactions are also critical for virus particle formation at membranes (Kutluay et al., 2014). Moreover, if viral RNA is not present, Gag encapsulates host RNA, and any single-stranded nucleic acid longer than ~20–30 nt can support capsid assembly (Campbell and Rein, 1999), indicating a general propensity to bind abundant RNA. Indeed, precisely how viral RNA is preferentially packaged into Gag capsids in cells remains an intensive area of investigation (Comas-Garcia et al., 2016).

The uptake and transfer of RNA by purified Arc protein is surprising as this occurs in the absence of an "envelope" or lipid bilayer. Uptake of both purified Arc capsids and endogenous EVs occurs through endocytosis. While EVs and exosomes are easily taken up through the endosomal pathway, it remains unclear how RNA can cross the endosomal membrane without membrane fusion proteins (Tkach and Théry, 2016). Our data suggest that, like non-enveloped viruses, Arc protein itself contains the ability to transfer RNA across the endosomal membrane. While it remains unclear how non-enveloped capsids transfer RNA into the cytoplasm, some studies suggest this could occur through specific receptor-capsid interactions, or via a pH-dependent conformational change of the capsid that allows either pore formation or lytic degradation of membranes (Tsai, 2007). We speculate that Arc protein may interact with the endosomal membrane to allow transfer of mRNA into the cytoplasm as the capsid is disassembled. This is reflected in the lag between protein uptake and mRNA expression seen in our experiments, which may be a result of the time it takes for mRNA to become accessible to our FISH probes. The lipid membrane around ACBARs *in vivo* may dictate targeting and uptake, whereas the Arc capsid within protects and allows transfer of RNA. Intriguingly, prArc that lacks RNA is unable to form capsids and cannot be taken up, suggesting uptake may be a regulated process that requires properly formed capsids. Since Arc seems to regulate a naturally occurring mechanism of RNA transfer, we believe that harnessing this pathway may allow new means of genetic engineering or RNA delivery into cells, using ACBARs, that may avoid the hurdle of immune activation.

Arc's Gag Homology Reveals a New Signaling Pathway in Neurons

Exosome and EV signaling has emerged as a critical mechanism of intercellular communication, especially in the immune system and in cancer biology (Becker et al., 2016). However, the role of intercellular signaling through EVs in the nervous system has only recently been investigated, with studies suggesting that these pathways may play important roles in synaptic plasticity (Budnik et al., 2016; Zappulli et al., 2016). Canonical exosomes are formed in MVBs, which are derived from the endosomal pathway and usually require the ESCRT complex to be released (Raposo and Stoorvogel, 2013), although the biogenesis of EVs in general is more varied. HIV Gag is able to form virions independent of the MVB pathway, although the ESCRT machinery is still required for particle release; thus, Arc may form ACBARs independent of the canonical exosome pathway. These pathways are not mutually exclusive, and elucidating the biogenesis of ACBARs within neurons will require further investigation.

Since Arc is rapidly synthesized locally in dendrites (Park et al., 2008; Waung et al., 2008), it is conceivable that high local concentrations of Arc protein promote capsid assembly in dendrites where encapsulation of dendritically localized mRNAs could occur. Since Arc capsids do not seem to show specificity in RNA binding *in vitro* and Arc EVs can transfer highly abundant mRNAs, we speculate that the specificity of ACBAR cargo is conferred by the precise spatial and temporal expression of Arc protein in neurons (Figure S7D). Consistent with the identification of *Arc* mRNA associated with Arc protein from brain, *Arc* mRNA levels are highly and uniquely abundant in dendrites *in vivo* after bouts of neuronal activity or experience (de Solis et al., 2017). Gag-RNA interactions are regulated by host cellular proteins such as Staufen (Mouland et al., 2000), a protein that is also a critical regulator of dendritic mRNA trafficking in neurons, including *Arc* mRNA (Heraud-Farlow and Kiebler, 2014). The parallels between dendritic mRNA regulation and virus-RNA interactions are striking, suggesting that cellular factors may play an important role in ACBAR biogenesis and RNA packing. Many questions remain: What other cargo do ACBARs contain? What are the docking mechanisms for ACBARs? Is there spatial/temporal specificity of intercellular signaling in the brain?

Our data also indicate that Arc may mediate intercellular signaling to control synaptic function and plasticity in a non-cell-autonomous manner. Although there is a paucity of data on neuronal EVs, previous studies have shown that EVs can be secreted in an activity-dependent manner and include AMPARs as cargo (Fauré et al., 2006). Since Arc has previously been implicated in AMPAR trafficking at synapses and spine elimination (Chowdhury et al., 2006; Mikuni et al., 2013) at weak synapses (Okuno et al., 2012), a potential role for ACBARs may be to eliminate synaptic material. Arc also regulates homeostatic forms of plasticity, such as AMPAR scaling (Shepherd et al., 2006) and cross-modal plasticity across different brain regions (Kraft et al., 2017), which could be regulated at the circuit level in a non-cell autonomous manner. We favor the idea that released Arc functions to carry intercellular cargo that alters the state of neighboring cells required for cellular consolidation of information.

Previous studies have shown that *Drosophila* neuromuscular junction plasticity requires trans-synaptic signaling mediated through the Wnt pathway in exosomes (Korkut et al., 2009). Interestingly, the *Drosophila* Arc homolog dArc1 exhibits similar properties of intercellular transfer of mRNA in the fly nervous system and is one of the most abundant proteins in *Drosophila* EVs

(Ashley et al., 2018; Lefebvre et al., 2016), suggesting a remarkable convergence of biology despite a large evolutionary divergence of these species. A recent study has also implicated Arc in the mammalian immune system (Ufer et al., 2016), where it controls dendritic cell-dependent T cell activation, expanding the potential repertoire and importance of Arc-dependent intercellular signaling beyond the nervous system. Moreover, EVs have been implicated in the pathology of various neurodegenerative disorders, as several pathogenic proteins, such as prions, β-amyloid peptide, and α-synuclein, are released from cells in association with EVs (Zappulli et al., 2016). In AD, immunohistochemical analysis in brain sections from patients with AD showed enrichment of the exosomal marker ALIX around neuritic plaques (Rajendran et al., 2006). This suggests that EVs may provide a significant source of extracellular Aβ peptide. Arc regulates the activity-dependent cleavage of APP and β-amyloid production through interactions with presenilin (Wu et al., 2011), suggesting that ACBARs may also be involved in AD pathogenesis.

Evolution of Synaptic Plasticity and Cognition

Ty3/*gypsy* retrotransposons are ancient mobile elements that are widely distributed and often abundant in eukaryotic genomes and are considered ancestral to modern retroviruses (Malik et al., 2000). There is evidence that coding sequences derived from Ty3/*gypsy* and other retroviral-like elements have been repurposed for cellular functions repeatedly during evolution (Feschotte and Gilbert, 2012). For instance, multiple envelope genes of retroviral origins have been co-opted during mammalian evolution to promote cell-cell fusion and syncytiotrophoblast formation in the developing placenta (Cornelis et al., 2015). There are more than one hundred Gag-derived genes in the human genome alone (Campillos et al., 2006), and genetic KOs of their murine orthologs have revealed that some, like *Arc*, are essential for cognition (Irie et al., 2015). However, the molecular function of these Gag-derived proteins has been poorly characterized, and whether they were co-opted to serve similar cellular processes remains an open question. This study and the accompanying article from Ashley et al. (2018) now reveal that two distantly related Gag-derived genes have been independently co-opted in fly and tetrapod ancestors to participate in a similar process of EV-dependent intercellular trafficking of RNA in the nervous system. Given the plethora of retroelements populating eukaryotic genomes, we speculate that many other Gag proteins have been repurposed for cellular processes that await discovery in a variety of organisms.

STAR★METHODS

Detailed methods are provided in the online version of this paper and include the following:

- KEY RESOURCES TABLE
- CONTACT FOR REAGENT AND RESOURCE SHARING
- EXPERIMENTAL MODEL AND SUBJECT DETAILS
  - Cell lines
  - Mouse models
  - Primary neuron culture
- METHOD DETAILS
  - Plasmids
  - Protein purification
  - Electron microscopy
  - Dynamic light scattering
  - Phylogenetic reconstruction
  - HEK cell experiments
  - Neuron transfer experiments
  - Immunocytochemistry
  - Combined FISH/ICC in neurons and HEK cells
  - Cell imaging and analysis
  - Western blots
  - Coomassie gels
  - Immunoprecipitation
  - Chemical crosslinking of Arc proteins *in situ*
  - RNA extraction
  - RT-PCR
  - qRT-PCR
  - Extracellular vesicle purification
  - Trypsin digestion and RNase assays
  - Immunogold labeling
- QUANTIFICATION AND STATISTICAL ANALYSES

SUPPLEMENTAL INFORMATION

Supplemental Information includes seven figures and one table and can be found with this article online at https://doi.org/10.1016/j.cell.2017.12.024.

ACKNOWLEDGMENTS

We thank Adam Frost and Raghav Kalia for technical assistance in the initial stages of this project. We thank Wesley Sundquist for helpful discussions and the Sundquist/Bass labs for experimental help and support. We thank Vivian Budnik for helpful discussions and sharing of unpublished data. We thank Kristen Keefe for experimental help with the FISH assay. We thank Jenifer Einstein and all members of the Shepherd lab for technical help and support. This work was supported by the NIH (R00 NS076364 and R01 MH112766 to J.D.S.; R01 GM77582 and R01 GM112972 to C.F.) and startup funds from the University of Utah (to J.D.S.).

AUTHOR CONTRIBUTIONS

E.D.P. performed immunoprecipitation, cultured neuron, immunocytochemistry, and the fluorescent *in situ* hybridization experiments. C.E.D. and R.B.K. performed the biochemistry and the electron microscopy experiments. A.V.T. and M.K.-S. performed the qPCR experiments. D.B. assisted with the electron microscopy experiments. J.M. and C.F. performed the phylogenomic analysis. S.E., D.R.M., and J.A.G.B. conducted the cryo-EM and the DLS experiments. N.Y. performed the initial biochemical and the electron microscopy experiments. E.D.P., C.E.D., and J.D.S. conceived and designed experiments. J.D.S. wrote the manuscript; all authors discussed results and edited the manuscript.

DECLARATION OF INTERESTS

The authors declare no competing interests.

Received: January 19, 2017
Revised: August 15, 2017
Accepted: December 18, 2017
Published: January 11, 2018; corrected online February 8, 2018

REFERENCES

Abrusán, G., Szilágyi, A., Zhang, Y., and Papp, B. (2013). Turning gold into 'junk': transposable elements utilize central proteins of cellular networks. Nucleic Acids Res. *41*, 3190–3200.

Ashley, J., Cordy, B., Lucia, D., Fradkin, L.G., Budnik, V., and Thomson, T. (2018). Retrovirus-like Gag protein Arc1 binds RNA and traffics across synaptic boutons. Cell *172*, this issue, 262–274.

Becker, A., Thakur, B.K., Weiss, J.M., Kim, H.S., Peinado, H., and Lyden, D. (2016). Extracellular vesicles in cancer: cell-to-cell mediators of metastasis. Cancer Cell *30*, 836–848.

Bramham, C.R., Alme, M.N., Bittins, M., Kuipers, S.D., Nair, R.R., Pai, B., Panja, D., Schubert, M., Soule, J., Tiron, A., and Wibrand, K. (2010). The Arc of synaptic memory. Exp. Brain Res. *200*, 125–140.

Budnik, V., Ruiz-Cañada, C., and Wendler, F. (2016). Extracellular vesicles round off communication in the nervous system. Nat. Rev. Neurosci. *17*, 160–172.

Campbell, S., and Rein, A. (1999). In vitro assembly properties of human immunodeficiency virus type 1 Gag protein lacking the p6 domain. J. Virol. *73*, 2270–2279.

Campillos, M., Doerks, T., Shah, P.K., and Bork, P. (2006). Computational characterization of multiple Gag-like human proteins. Trends Genet. *22*, 585–589.

Carlson, L.A., Bai, Y., Keane, S.C., Doudna, J.A., and Hurley, J.H. (2016). Reconstitution of selective HIV-1 RNA packaging in vitro by membrane-bound Gag assemblies. eLife *5*, 5.

Chowdhury, S., Shepherd, J.D., Okuno, H., Lyford, G., Petralia, R.S., Plath, N., Kuhl, D., Huganir, R.L., and Worley, P.F. (2006). Arc/Arg3.1 interacts with the endocytic machinery to regulate AMPA receptor trafficking. Neuron *52*, 445–459.

Chuong, E.B., Elde, N.C., and Feschotte, C. (2017). Regulatory activities of transposable elements: from conflicts to benefits. Nat. Rev. Genet. *18*, 71–86.

Comas-Garcia, M., Davis, S.R., and Rein, A. (2016). On the selective packaging of genomic RNA by HIV-1. Viruses *8*, 8.

Cornelis, G., Vernochet, C., Carradec, Q., Souquere, S., Mulot, B., Catzeflis, F., Nilsson, M.A., Menzies, B.R., Renfree, M.B., Pierron, G., et al. (2015). Retroviral envelope gene captures and syncytin exaptation for placentation in marsupials. Proc. Natl. Acad. Sci. USA *112*, E487–E496.

Daberkow, D.P., Riedy, M.D., Kesner, R.P., and Keefe, K.A. (2007). Arc mRNA induction in striatal efferent neurons associated with response learning. Eur. J. Neurosci. *26*, 228–241.

de Solis, C.A., Morales, A.A., Hosek, M.P., Partin, A.C., and Ploski, J.E. (2017). Is Arc mRNA unique: a search for mRNAs that localize to the distal dendrites of dentate gyrus granule cells following neural activity. Front. Mol. Neurosci. *10*, 314.

Fauré, J., Lachenal, G., Court, M., Hirrlinger, J., Chatellard-Causse, C., Blot, B., Grange, J., Schoehn, G., Goldberg, Y., Boyer, V., et al. (2006). Exosomes are released by cultured cortical neurones. Mol. Cell. Neurosci. *31*, 642–648.

Feschotte, C., and Gilbert, C. (2012). Endogenous viruses: insights into viral evolution and impact on host biology. Nat. Rev. Genet. *13*, 283–296.

Feschotte, C., and Pritham, E.J. (2007). DNA transposons and the evolution of eukaryotic genomes. Annu. Rev. Genet. *41*, 331–368.

Freed, E.O. (2015). HIV-1 assembly, release and maturation. Nat. Rev. Microbiol. *13*, 484–496.

Fromer, M., Pocklington, A.J., Kavanagh, D.H., Williams, H.J., Dwyer, S., Gormley, P., Georgieva, L., Rees, E., Palta, P., Ruderfer, D.M., et al. (2014). De novo mutations in schizophrenia implicate synaptic networks. Nature *506*, 179–184.

Ganser, B.K., Li, S., Klishko, V.Y., Finch, J.T., and Sundquist, W.I. (1999). Assembly and analysis of conical models for the HIV-1 core. Science *283*, 80–83.

Greer, P.L., Hanayama, R., Bloodgood, B.L., Mardinly, A.R., Lipton, D.M., Flavell, S.W., Kim, T.K., Griffith, E.C., Waldon, Z., Maehr, R., et al. (2010). The Angelman syndrome protein Ube3A regulates synapse development by ubiquitinating arc. Cell *140*, 704–716.

Guzowski, J.F., McNaughton, B.L., Barnes, C.A., and Worley, P.F. (1999). Environment-specific expression of the immediate-early gene Arc in hippocampal neuronal ensembles. Nat. Neurosci. *2*, 1120–1124.

Guzowski, J.F., Lyford, G.L., Stevenson, G.D., Houston, F.P., McGaugh, J.L., Worley, P.F., and Barnes, C.A. (2000). Inhibition of activity-dependent arc protein expression in the rat hippocampus impairs the maintenance of long-term potentiation and the consolidation of long-term memory. J. Neurosci. *20*, 3993–4001.

Hamann, M.V., and Lindemann, D. (2016). Foamy virus protein-nucleic acid interactions during particle morphogenesis. Viruses *8*, 8.

Hansen, L.J., Chalker, D.L., Orlinsky, K.J., and Sandmeyer, S.B. (1992). Ty3 GAG3 and POL3 genes encode the components of intracellular particles. J. Virol. *66*, 1414–1424.

Heraud-Farlow, J.E., and Kiebler, M.A. (2014). The multifunctional Staufen proteins: conserved roles from neurogenesis to synaptic plasticity. Trends Neurosci. *37*, 470–479.

Irie, M., Yoshikawa, M., Ono, R., Iwafune, H., Furuse, T., Yamada, I., Wakana, S., Yamashita, Y., Abe, T., Ishino, F., and Kaneko-Ishino, T. (2015). Cognitive Function Related to the Sirh11/Zcchc16 Gene Acquired from an LTR Retrotransposon in Eutherians. PLoS Genet. *11*, e1005521.

Kaneko-Ishino, T., and Ishino, F. (2012). The role of genes domesticated from LTR retrotransposons and retroviruses in mammals. Front. Microbiol. *3*, 262.

Korkut, C., Ataman, B., Ramachandran, P., Ashley, J., Barria, R., Gherbesi, N., and Budnik, V. (2009). Trans-synaptic transmission of vesicular Wnt signals through Evi/Wntless. Cell *139*, 393–404.

Korkut, C., Li, Y., Koles, K., Brewer, C., Ashley, J., Yoshihara, M., and Budnik, V. (2013). Regulation of postsynaptic retrograde signaling by presynaptic exosome release. Neuron *77*, 1039–1046.

Kraft, A.W., Mitra, A., Bauer, A.Q., Snyder, A.Z., Raichle, M.E., Culver, J.P., and Lee, J.M. (2017). Visual experience sculpts whole-cortex spontaneous infraslow activity patterns through an Arc-dependent mechanism. Proc. Natl. Acad. Sci. USA *114*, E9952–E9961.

Kutluay, S.B., Zang, T., Blanco-Melo, D., Powell, C., Jannain, D., Errando, M., and Bieniasz, P.D. (2014). Global changes in the RNA binding specificity of HIV-1 gag regulate virion genesis. Cell *159*, 1096–1109.

Lachenal, G., Pernet-Gallay, K., Chivet, M., Hemming, F.J., Belly, A., Bodon, G., Blot, B., Haase, G., Goldberg, Y., and Sadoul, R. (2011). Release of exosomes from differentiated neurons and its regulation by synaptic glutamatergic activity. Mol. Cell. Neurosci. *46*, 409–418.

Lefebvre, F.A., Benoit Bouvrette, L.P., Perras, L., Blanchet-Cohen, A., Garnier, D., Rak, J., and Lécuyer, É. (2016). Comparative transcriptomic analysis of human and Drosophila extracellular vesicles. Sci. Rep. *6*, 27680.

Macia, E., Ehrlich, M., Massol, R., Boucrot, E., Brunner, C., and Kirchhausen, T. (2006). Dynasore, a cell-permeable inhibitor of dynamin. Dev. Cell *10*, 839–850.

Mailler, E., Bernacchi, S., Marquet, R., Paillart, J.C., Vivet-Boudou, V., and Smyth, R.P. (2016). The life-cycle of the HIV-1 Gag-RNA complex. Viruses *8*, 8.

Malik, H.S., Henikoff, S., and Eickbush, T.H. (2000). Poised for contagion: evolutionary origins of the infectious abilities of invertebrate retroviruses. Genome Res. *10*, 1307–1318.

Managò, F., Mereu, M., Mastwal, S., Mastrogiacomo, R., Scheggia, D., Emanuele, M., De Luca, M.A., Weinberger, D.R., Wang, K.H., and Papaleo, F. (2016). Genetic disruption of Arc/Arg3.1 in mice causes alterations in dopamine and neurobehavioral phenotypes related to schizophrenia. Cell Rep. *16*, 2116–2128.

Mattei, S., Schur, F.K., and Briggs, J.A. (2016). Retrovirus maturation-an extraordinary structural transformation. Curr. Opin. Virol. *18*, 27–35.

McCurry, C.L., Shepherd, J.D., Tropea, D., Wang, K.H., Bear, M.F., and Sur, M. (2010). Loss of Arc renders the visual cortex impervious to the effects of sensory experience or deprivation. Nat. Neurosci. *13*, 450–457.

Mikuni, T., Uesaka, N., Okuno, H., Hirai, H., Deisseroth, K., Bito, H., and Kano, M. (2013). Arc/Arg3.1 is a postsynaptic mediator of activity-dependent synapse elimination in the developing cerebellum. Neuron *78*, 1024–1035.

Mouland, A.J., Mercier, J., Luo, M., Bernier, L., DesGroseillers, L., and Cohen, E.A. (2000). The double-stranded RNA-binding protein Staufen is incorporated in human immunodeficiency virus type 1: evidence for a role in genomic RNA encapsidation. J. Virol. *74*, 5441–5451.

Myrum, C., Baumann, A., Bustad, H.J., Flydal, M.I., Mariaule, V., Alvira, S., Cuéllar, J., Haavik, J., Soulé, J., Valpuesta, J.M., et al. (2015). Arc is a flexible modular protein capable of reversible self-oligomerization. Biochem. J. *468*, 145–158.

Nolte-'t Hoen, E., Cremer, T., Gallo, R.C., and Margolis, L.B. (2016). Extracellular vesicles and viruses: Are they close relatives? Proc. Natl. Acad. Sci. USA *113*, 9155–9161.

Okuno, H., Akashi, K., Ishii, Y., Yagishita-Kyo, N., Suzuki, K., Nonaka, M., Kawashima, T., Fujii, H., Takemoto-Kimura, S., Abe, M., et al. (2012). Inverse synaptic tagging of inactive synapses via dynamic interaction of Arc/Arg3.1 with CaMKIIβ. Cell *149*, 886–898.

Park, S., Park, J.M., Kim, S., Kim, J.A., Shepherd, J.D., Smith-Hicks, C.L., Chowdhury, S., Kaufmann, W., Kuhl, D., Ryazanov, A.G., et al. (2008). Elongation factor 2 and fragile X mental retardation protein control the dynamic translation of Arc/Arg3.1 essential for mGluR-LTD. Neuron *59*, 70–83.

Pastuzyn, E.D., and Shepherd, J.D. (2017). Activity-dependent Arc expression and homeostatic synaptic plasticity are altered in neurons from a mouse model of Angelman syndrome. Front. Mol. Neurosci. *10*, 234.

Pinkstaff, J.K., Chappell, S.A., Mauro, V.P., Edelman, G.M., and Krushel, L.A. (2001). Internal initiation of translation of five dendritically localized neuronal mRNAs. Proc. Natl. Acad. Sci. USA *98*, 2770–2775.

Plath, N., Ohana, O., Dammermann, B., Errington, M.L., Schmitz, D., Gross, C., Mao, X., Engelsberg, A., Mahlke, C., Welzl, H., et al. (2006). Arc/Arg3.1 is essential for the consolidation of synaptic plasticity and memories. Neuron *52*, 437–444.

Purcell, S.M., Moran, J.L., Fromer, M., Ruderfer, D., Solovieff, N., Roussos, P., O'Dushlaine, C., Chambert, K., Bergen, S.E., Kähler, A., et al. (2014). A polygenic burden of rare disruptive mutations in schizophrenia. Nature *506*, 185–190.

Purdy, J.G., Flanagan, J.M., Ropson, I.J., Rennoll-Bankert, K.E., and Craven, R.C. (2008). Critical role of conserved hydrophobic residues within the major homology region in mature retroviral capsid assembly. J. Virol. *82*, 5951–5961.

Rajendran, L., Honsho, M., Zahn, T.R., Keller, P., Geiger, K.D., Verkade, P., and Simons, K. (2006). Alzheimer's disease beta-amyloid peptides are released in association with exosomes. Proc. Natl. Acad. Sci. USA *103*, 11172–11177.

Raposo, G., and Stoorvogel, W. (2013). Extracellular vesicles: exosomes, microvesicles, and friends. J. Cell Biol. *200*, 373–383.

Shepherd, J.D. (2017). Arc - an endogenous neuronal retrovirus? Semin. Cell Dev. Biol. Published online September 24, 2017. https://doi.org/10.1016/j.semcdb.2017.09.029.

Shepherd, J.D., and Bear, M.F. (2011). New views of Arc, a master regulator of synaptic plasticity. Nat. Neurosci. *14*, 279–284.

Shepherd, J.D., Rumbaugh, G., Wu, J., Chowdhury, S., Plath, N., Kuhl, D., Huganir, R.L., and Worley, P.F. (2006). Arc/Arg3.1 mediates homeostatic synaptic scaling of AMPA receptors. Neuron *52*, 475–484.

Smit, A.F. (1999). Interspersed repeats and other mementos of transposable elements in mammalian genomes. Curr. Opin. Genet. Dev. *9*, 657–663.

Steward, O., Wallace, C.S., Lyford, G.L., and Worley, P.F. (1998). Synaptic activation causes the mRNA for the IEG Arc to localize selectively near activated postsynaptic sites on dendrites. Neuron *21*, 741–751.

Taylor, W.R., Stoye, J.P., and Taylor, I.A. (2017). A comparative analysis of the foamy and ortho virus capsid structures reveals an ancient domain duplication. BMC Struct. Biol. *17*, 3.

Tkach, M., and Théry, C. (2016). Communication by extracellular vesicles: where we are and where we need to go. Cell *164*, 1226–1232.

Tsai, B. (2007). Penetration of nonenveloped viruses into the cytoplasm. Annu. Rev. Cell Dev. Biol. *23*, 23–43.

Ufer, F., Vargas, P., Engler, J.B., Tintelnot, J., Schattling, B., Winkler, H., Bauer, S., Kursawe, N., Willing, A., Keminer, O., et al. (2016). Arc/Arg3.1 governs inflammatory dendritic cell migration from the skin and thereby controls T cell activation. Sci. Immunol. *1*, eaaf8665.

Valadi, H., Ekström, K., Bossios, A., Sjöstrand, M., Lee, J.J., and Lötvall, J.O. (2007). Exosome-mediated transfer of mRNAs and microRNAs is a novel mechanism of genetic exchange between cells. Nat. Cell Biol. *9*, 654–659.

Wang, K.H., Majewska, A., Schummers, J., Farley, B., Hu, C., Sur, M., and Tonegawa, S. (2006). In vivo two-photon imaging reveals a role of arc in enhancing orientation specificity in visual cortex. Cell *126*, 389–402.

Waung, M.W., Pfeiffer, B.E., Nosyreva, E.D., Ronesi, J.A., and Huber, K.M. (2008). Rapid translation of Arc/Arg3.1 selectively mediates mGluR-dependent LTD through persistent increases in AMPAR endocytosis rate. Neuron *59*, 84–97.

Wu, J., Petralia, R.S., Kurushima, H., Patel, H., Jung, M.Y., Volk, L., Chowdhury, S., Shepherd, J.D., Dehoff, M., Li, Y., et al. (2011). Arc/Arg3.1 regulates an endosomal pathway essential for activity-dependent β-amyloid generation. Cell *147*, 615–628.

Zappulli, V., Friis, K.P., Fitzpatrick, Z., Maguire, C.A., and Breakefield, X.O. (2016). Extracellular vesicles and intercellular communication within the nervous system. J. Clin. Invest. *126*, 1198–1207.

Zhang, W., Wu, J., Ward, M.D., Yang, S., Chuang, Y.A., Xiao, M., Li, R., Leahy, D.J., and Worley, P.F. (2015). Structural basis of arc binding to synaptic proteins: implications for cognitive disease. Neuron *86*, 490–500.

Zhou, K., Zhou, L., Lim, Q., Zou, R., Stephanopoulos, G., and Too, H.P. (2011). Novel reference genes for quantifying transcriptional responses of Escherichia coli to protein overexpression by quantitative PCR. BMC Mol. Biol. *12*, 18.

STAR★METHODS

KEY RESOURCES TABLE

REAGENT or RESOURCE	SOURCE	IDENTIFIER
Antibodies		
rabbit polyclonal anti-Arc	Custom made (ProteinTech)	N/A
rabbit polyclonal anti-Arc	Synaptic Systems	Cat. #156-003
NucBlue fixed cell stain	Thermo Fisher Scientific	Cat. #R37606
chicken polyclonal anti-MAP2	Abcam	Cat. #ab5392
Alexa Fluor 405, 488, and 647 secondary antibodies (made in donkey against chicken, rabbit, or mouse)	Jackson ImmunoResearch	Cat. #703-605-155, 711-605-152, 703-545-155, 711-545-152, 715-605-151
Alexa Fluor 555 secondary antibody (made in donkey against rabbit)	Thermo Fisher Scientific	Cat. #A31572
sheep polyclonal anti-digoxigenin-POD	Sigma-Aldrich	Cat. #11207733910
mouse monoclonal anti-Arc (clone C-7)	Santa Cruz	Cat. #sc-17839
rabbit polyclonal anti-ALIX	Dr. Wesley Sundquist, U. of Utah	N/A
mouse monoclonal anti-actin (HRP-conjugated)	Abcam	Cat. #ab20272
chicken polyclonal anti-GFP	Aves	Cat. #GFP-1010
goat anti-rabbit, mouse, or chicken HRP-conjugated secondary antibodies	Jackson ImmunoResearch	Cat. #103-035-155, 111-035-003, 115-035-003
mouse monoclonal anti-Rab5	BD Biosciences	Cat. #610724
Bacterial and Virus Strains		
DH5α Competent *E. coli.*	Thermo Fisher Scientific	Cat. #18265017
BL21 Competent *E. coli.*	Thermo Fisher Scientific	Cat. #C600003
Chemicals, Peptides, and Recombinant Proteins		
polyethyleneimine "MAX"	Polysciences, Inc.	Cat. #24765
Dynasore	Abcam	Cat. #ab120192
(*S*)-3,5-DHPG	Tocris Bioscience	Cat. #0805
cycloheximide	Sigma-Aldrich	Cat. #C7698-1G
RNase A	Omega Bio-tek	Cat. #D6942-02
RNase A	Thermo Fisher Scientific	Cat. #EN0531
SUPERase-In RNase inhibitor	Thermo Fisher Scientific	Cat. #AM2694
16% formaldehyde solution	Thermo Fisher Scientific	Cat. #28906 and 28908
normal donkey serum	Jackson ImmunoResearch	Cat. #017-000-121
Fluoromount aqueous mounting medium	Sigma-Aldrich	Cat. #F4680-25ML
prehybridization solution (2X)	Sigma-Aldrich	Cat. #P1415-50ML
Denhardt's solution (50X)	Thermo Fisher Scientific	Cat. #750018
formamide	Fisher Scientific	Cat. #BP227-100
blocking reagent	Sigma-Aldrich	Cat. #11096176001
normal sheep serum	Jackson ImmunoResearch	Cat. #013-000-121
Protein A agarose	Thermo Fisher Scientific	Cat. #15918014
normal rabbit IgG	Santa Cruz	Cat. #sc-2027
deoxyribonuclease I from bovine pancreas	Sigma-Aldrich	Cat. #DN25-100MG
papain	Worthington Biochemicals	Cat. #LS003126
poly-L-lysine	Sigma-Aldrich	Cat. #P2636-100MG
cytosine β-D-arabinofuranoside	Sigma-Aldrich	Cat. #C1768-100MG
TRIzol Reagent	Thermo Fisher Scientific	Cat. #15596026

(*Continued on next page*)

Continued

REAGENT or RESOURCE	SOURCE	IDENTIFIER
Chloroform	Sigma-Aldrich	Cat. #C2432-500ML
PowerUp SYBR Green Master Mix	Thermo Fisher Scientific	Cat. #A25742
SYBR Safe DNA Gel Stain	Thermo Fisher Scientific	Cat. #S33102
protease inhibitor cOmplete ULTRA tablets, EDTA-free	Sigma-Aldrich	Cat. #95892791001
pepstatin	Roche	Cat. #11524488001
PMSF	Roche	Cat. #10837091001
leupeptin	Roche	Cat. #11034626001
sprotinin	Roche	Cat. #10981532001
lysozyme from chicken egg white	Sigma-Aldrich	Cat. #L6876
Glutathione Sepharose 4B affinity resin	GE Healthcare	Cat. #17075601
PreScission Protease	GE Healthcare	Cat. #27-0843-01
uranyl acetate	Agar Scientific	Cat. #AGR1260A
Critical Commercial Assays		
DIG RNA labeling kit (SP6/T7)	Sigma-Aldrich	Cat. #11175025910
illustra MicroSpin G-50 columns	GE Healthcare	Cat. #27-5330-01
TSA Plus Cyanine 3 kit	PerkinElmer	Cat. #NEL744001KT
RNeasy Micro Kit	QIAGEN	Cat. #74004
Direct-zol RNA Micro Kit	Zymo	Cat. #R2062
Purelink Midi Plasmid Prep Kit	Promega	Cat. #A2492
QiaQuick Gel Purification Kit	QIAGEN	Cat. #28706
EZNA Plasmid Mini Kit	Zymo	Cat. #D6942-02
HiScribe T7 High Yield RNA Synthesis Kit	New England Biolabs	Cat. #E2040S
High Capacity cDNA Synthesis Kit	Applied Biosystems	Cat. #4368814
PCR Purification Kit	QIAGEN	Cat. #28104
Deposited Data		
N/A		
Experimental Models: Cell Lines		
Human: HEK293T cells	ATCC	Cat. #CRL-11268
Experimental Models: Organisms/Strains		
Mouse: C57BL/6-*Arc*^{tm1Stl}/J	Dr. Kuan Hong Wang, NIH	Jackson Labs: stock #007662
Oligonucleotides		
See Table S1	N/A	N/A
Recombinant DNA		
pGEX-6p1-GST-ArcFL	This manuscript	N/A
pGEX-6p1-GST-ArcΔCTD	This manuscript	N/A
pET11a-ArcCA	This manuscript	N/A
pGEX-4T1-GST-dArc1	Dr. Mark Metzstein, U of Utah	N/A
pBluescript-SKII-GFP	This manuscript	N/A
pBluescript-SKII-ArcUTRs	Dr. Kristen Keefe, U of Utah	N/A
pGL4.11-arc7000-mEGFP-ArcUTRs	Dr. Haruhiko Bito, U of Tokyo	N/A
eGFP-C3-Arc	Dr. Kimberly Huber, UT Southwestern	N/A
pBOS-nuclear-GFP	Addgene	#11154
Software and Algorithms		
MUSCLE	EMBL-EBI, Hinxton, Cambridge, UK	https://www.ebi.ac.uk/Tools/msa/muscle/
Boxshade plot server	Swiss Institute of Bioinformatics, Switzerland	https://www.ch.embnet.org/software/BOX_form.html

(*Continued on next page*)

Continued

REAGENT or RESOURCE	SOURCE	IDENTIFIER
A Plasmid Editor (APE)	University of Utah	http://biologylabs.utah.edu/jorgensen/wayned/ape/
tBLASTn	NIH	https://blast.ncbi.nlm.nih.gov/Blast.cgi?PROGRAM=tblastn&PAGE_TYPE=BlastSearch
Repbase	Genetic Information Research Institute, Mountain View, CA	http://www.girinst.org/repbase/
MEGA7	Pennsylvania State University	http://www.megasoftware.net/
BLASTp	NIH	https://blast.ncbi.nlm.nih.gov/Blast.cgi?PAGE=Proteins
ImageJ	NIH	https://imagej.nih.gov/ij/

CONTACT FOR REAGENT AND RESOURCE SHARING

Further information and requests for resources and reagents should be directed to and will be fulfilled by the Lead Contact, Jason D. Shepherd (jason.shepherd@neuro.utah.edu).

EXPERIMENTAL MODEL AND SUBJECT DETAILS

Cell lines

HEK293T cells were purchased from ATCC (#CRL-11268). Cells were maintained at 37°C with 5% CO_2 in DMEM media supplemented with 10% fetal bovine serum and 1% penicillin/streptomycin (Thermo Fisher Scientific, Waltham, MA) and passaged every 3-4 days at 70% confluency. For transfections and transfer experiments, HEK cells were seeded to 10-cm dishes or collagen-coated glass coverslips in 12-well plates.

Mouse models

Wild-type and Arc knock-out mice

C57BL/6 Arc knock-out (KO) mice (C57BL/6-*Arc*^{tm1Stl}/J, a kind gift from Dr. Kuan Wang, NIH) have GFP knocked in to the Arc ORF (Wang et al., 2006). Arc KO and wild-type (WT) mice used in these studies were littermates from heterozygous (*Arc*$^{+/-}$) crosses. Both male and female mice were used. No differences between sexes in the experiments conducted in this study were noted, and data from both sexes were therefore grouped together. Mice were housed in breeding pairs, or group-housed with littermates of the same sex after weaning (2-5 mice/cage), on a 12:12 h day:night cycle, with food and water provided *ad libitum*. Hippocampal and cortical primary neuron cultures were prepared from E18 embryos, while brain lysates were taken from P30-50 mice. Mice were test- and procedure-naive before terminal experiments. All animal experiments were approved by the Institutional Animal Care and Use Committee of the University of Utah.

Primary neuron culture

Primary neuron cultures were prepared from male and female E18 Arc KO or WT mouse cortex and hippocampus as previously described (Shepherd et al., 2006). Tissue was dissociated in DNase (0.01%; Sigma-Aldrich, St. Louis, MO) and papain (0.067%; Worthington Biochemicals, Lakewood, NJ), and then triturated with a fire-polished glass pipette to obtain a single-cell suspension. Cells were pelleted at 500x*g* for 4 min, the supernatant removed, and cells resuspended and counted with a TC-20 cell counter (Bio-Rad, Hercules, CA). Neurons were plated on glass coverslips (Carolina Biological Supply, Burlington, NC) coated with poly-L-lysine (0.2 mg/mL; Sigma-Aldrich) in 12-well plates (Greiner Bio-One, Monroe, NC) at 90,000 cells/mL, or in 10-cm plastic dishes at 800,000 cells/mL. Neurons were initially plated in Neurobasal media containing 5% horse serum, 2% GlutaMAX, 2% B-27, and 1% penicillin/streptomycin (Thermo Fisher Scientific) in a 37°C incubator with 5% CO_2. On DIV4, neurons were fed via half media exchange with astrocyte-conditioned Neurobasal media containing 1% horse serum, GlutaMAX, and penicillin/streptomycin, 2% B-27, and 5 μM cytosine β-D-arabinofuranoside (AraC) (Sigma-Aldrich). Neurons were fed with astrocyte-conditioned media every three days thereafter.

METHOD DETAILS

Plasmids

The open reading frame (ORF) of full-length rat Arc (NP_062234.1) cDNA was subcloned from pRK5-myc-Arc. The insert was amplified by PCR, digested with *Bam*H1 and *Xho*1, and ligated into the pGEX-6p1 (GE Healthcare, Little Chalfont, UK) expression vector

between the *Bam*H1 and *Xho*1 restrictions sites. The GST-Arc ORF was similarly amplified and cloned into the pFastBac1 vector (Thermo Fisher Scientific) between the *Bam*H1 and *Xho*1 restriction sites. prArc-ΔCTD was generated by blunt end cloning after PCR amplification of the Arc ORF from pGEX-6p1-Arc, excluding sequence coding aas 277-374. aas 195-364 of the Arc ORF (CA-prArc) was similarly cloned into the pET11a vector, which contained a His tag. pBluescript-SKII-GFP was generated by restriction digest of mEGFP (BBA16881.1) from pGL4.11-arc7000-mEGFP-ArcUTRs (generously provided by Dr. Haruhiko Bito, University of Tokyo) and subsequent ligation into the KpnI and *Sac*I restriction sites flanking the insert in pBluescript-SKII-ArcUTRs plasmid (generously provided by Dr. Kristen Keefe, University of Utah). The pGEX-4T-1 *Drosophila* Arc1 (NP_610955.1) construct was provided by Dr. Mark Metzstein, University of Utah. EGFP-C3-Arc and pRK5-myc-Arc were generously provided by Dr. Kimberly Huber (UT Southwestern) and Dr. Paul Worley (Johns Hopkins University), respectively. All protein expression constructs were transformed into DH5α *E. coli* cells and individual colonies were screened by Sanger Sequencing (GeneWiz, South Plainfield, NJ) sequencing services, using primers synthesized by Integrated DNA Technologies (Coralville, IA). Trace files were analyzed using A Plasmid Editor (APE) freeware available from the University of Utah. Sequenced verified constructs were then transformed into BL21-DE3 bacterial cells for protein expression. See Table S1 for specific oligo primer sequences.

Protein purification

Starter bacteria cultures for protein expression were grown overnight at 37°C in LB supplemented with ampicillin and chloramphenicol. Starter cultures were used to inoculate large-scale 500 mL cultures of ZY auto-induction media. Large-scale cultures were grown to OD_{600} of 0.6-0.8 at 37°C at 150 rpm and then shifted to 19°C at 150 rpm for 16-20 h. Cultures were then pelleted at 5000x*g* for 15 min at 4°C and cell pellets were resuspended in 30 mL lysis buffer (500 mM NaCl, 50 mM Tris, 5% glycerol, 1 mM DTT, pH 8.0 at room temperature (RT) for Arc constructs and GST; 300 mM KCl, 50 mM Tris, 1% Triton X-100, 1 mM DTT, pH 7.4 at RT for Endophilin3A) and flash frozen in liquid nitrogen. Frozen pellets were thawed quickly at 37°C and brought to a final volume of 1 g pellet:10 mL lysis buffer, supplemented with DNase, lysozyme, aprotinin, leupeptin, PMSF, and pepstatin. Lysates were then sonicated for 8-10x45 s pulses at 90% duty cycle and pelleted for 45 min at 21,000x*g*. For GST-tagged constructs, cleared supernatants were then passed through a 0.45 μm filter and incubated with pre-equilibrated GST Sepharose 4B affinity resin in a gravity flow column overnight at 4°C. Bound protein was then washed twice with two column volumes (20 resin bed volumes each) of lysis buffer, re-equilibrated with 150 mM NaCl, 50 mM Tris, 1 mM EDTA, 1 mM DTT, pH 7.2 at RT, and cleaved on-resin overnight at 4°C with PreScission Protease (GE Healthcare) for the GST-tagged constructs, or thrombin (Sigma-Aldrich) for dArc1. Cleaved proteins were then buffer exchanged to 150 mM NaCl, 50 mM Tris, pH 7.4 at RT to kill protease activity, run on an S200 size exclusion column to separate the cleaved protein, and peak fractions were pooled. GST was affinity-purified as described above using Sepharose 4B resin and eluted directly using 15 mM reduced L-glutathione, 10 mM Tris, pH 7.4 at RT. His-tagged CA-prArc was affinity-purified as described above using Ni^{+} resin (Roche, Basel, Switzerland) and eluted directly using 250 mM imidazole, 10 mM Tris, pH 7.4 at RT. GST and CA-prArc were then buffer exchanged to 150 mM NaCl, 50 mM Tris, pH 7.4 at RT. To strip Arc protein of nucleic acids for prArc(RNA-) preparations, cell pellets were lysed in 20 mM NaCl, 50 mM Tris, 5% glycerol, 2 mM $MgCl_2$, 1 mM DTT, pH 8.0 at RT as described above. Nucleic acids were precipitated from cell supernatants by dropwise addition of 10% PEI, pH 8.0 to a final concentration of 0.1% followed by incubation at 4°C for 20 min and pelleting for 20 min at 27,000x*g*. The resulting supernatant was then precipitated by addition of saturated ammonium sulfate to a final concentration of 30%. Precipitated protein was pelleted at 10,000x*g* for 10 min, resuspended in 60 mL lysis buffer, and affinity purified. The cleaved affinity-purified product was then dialyzed to Q-column buffer A (Q-A; 20 mM NaCl, 50 mM Tris, pH 7.4 at RT) overnight. Dialyzed protein was then subjected to anion exchange chromatography (HiTrap Q, GE Healthcare) with a gradient of Q-A buffer to Q-B buffer (1 M NaCl, 50 mM Tris, pH 7.4). Average yields for purified proteins were 10.5 mg (8-13 mg) per liter of cell culture.

Electron microscopy

Negative stain

For all negative stain specimens, copper 200-mesh grids coated with Formvar and carbon (Electron Microscopy Sciences or Ted Pella, Redding, CA) were glow discharged for 20-45 s in a vacuum chamber at 30mA. 3.5 μL sample was then applied to the grid for 35-45 s and excess sample was wicked away using filter paper. Grids were then immediately washed 2-4x for 5 s with 30 μL water droplets, then once with 1% uranyl acetate (UA) on parafilm. Excess water/UA was wicked away and then a final droplet of UA was applied for 30 s. Excess UA was wicked away and grids were air-dried for 30-60 s. Imaging was performed using either an FEI T12, FEI Tecnai Spirit microscope operated at 120 kV equipped with a Gatan Orius SC200B CCD camera or JEOL 1400 electron microscope.

Cryo-EM

Purified Arc protein was dialysed into 300 mM NaCl, 50 mM Tris, pH 7.4 and concentrated twice using Amicon 100 MWCO centrifugal filters (Millipore, Burlington, MA) to yield a final protein concentration of ~2 mg/mL. 10 nm diameter gold beads were added to the sample. Degassed 2/2-3C C-flat grids (Electron Microscopy Sciences, Hatfield, PA) were glow discharged for 45 s at 30 mA. Sample was applied to the grid 2 times for 30 s, and the grid was plunge frozen in liquid ethane using a FEI Vitrobot Mark IV. Micrographs were acquired using a FEI Tecnai G^2 F20 microscope operated at 200 kV, equipped with a FEI Falcon II direct detector. The nominal defocus was 1.3 μm.

EM quantification

Grids were surveyed visually to check for uniformity of sample application. For each experiment, six images were taken from randomly selected grid squares. Full and partially formed particles between 20-40 nm were then counted manually using ImageJ. Counts were then divided by the image field of view (2.07 μm^2) and data presented as oligomer count/μm^2.

Arc capsid assembly assay

GFP mRNA was added to prArc(RNA-) (5 mg/mL in low salt buffer: 20 mM NaCl, 50 mM Tris, pH 7.4 at RT) at a nucleic acid:protein ratio of 7.3% (w/w) (corresponding to 1 molecule of Arc to 10 nucleotides). Reactions were then diluted to 1 mg/mL of prArc(RNA-) by dropwise addition of low salt buffer or capsid assembly buffer (500 mM $NaPO_4$, 50 mM Tris, 0.5 mM EDTA, pH 7.5 at RT) and incubated for 2 h at RT. Following incubation, negative stain EM grids were prepared of each reaction at 0.25 mg/mL and capsid formation was quantified by manual counting of 6 images. Fully formed capsids included spherical particles between 20-50 nm with clear double shells. Similar results were seen in three independent protein preparations.

Dynamic light scattering

Purified Arc protein was subjected to dynamic light scattering measurements on a Malvern Zetasizer Nano ZSP instrument. The scattering was carried out at 25°C and at a fixed angle of 173° (backward scattering). The scattered intensity is represented as number of particles under the assumption that the scattering intensity from spherical particles is proportional to the size to the sixth power.

Phylogenetic reconstruction

NCBI genome sequence databases were queried using the human or *Drosophila melanogaster* Arc protein sequence using tBLASTn. Repbase was also queried using the CENSOR program to identify known repeat families with high sequence similarity to mammalian or brachyceran *Arc* genes, respectively. The following sequence IDs were used for analysis: (GenBank locus) Mm ARC—AHBB01089569; Hs ARC—LIQK02016549; Ac ARC—AAWZ02020354; Lc gypsy2—AFYH01030203; CC gypsy—LHQP01046008; Dm ARC1—JSAE01000572; Ds ARC1—CAKG01020471; Sc ARC1—LDNW01019671; Dm ARC2—JXOZ01003752; Ds ARC2—AWUT01001000; Sc ARC2—LDNW01019670; Bm gypsy—BABH01046987; Tc gypsy—AAJJ02003810. Repbase: Lc gypsy—Gypsy2-1-I_Lch; Dr gypsy26—Gypsy-26-I_DR; Lh gypsy11—Gypsy-11_LH-I; Dm gypsy1—Gypsy1-I_DM; ty3—TY3. Protein (Arc and Gag) sequences that were found to have high similarity to Arc proteins and Gags of other related Ty3/*gypsy* elements were aligned using the MUSCLE program. Trimmed Arc/Gag alignments were uploaded to MEGA7 for subsequent maximum likelihood phylogenetic reconstruction using default parameters, and 500 bootstrap iterations were performed to generate a lineage tree. *Drosophila melanogaster* dArc1 and dArc2 protein sequences were used to query schizophoran fly protein databases using BLASTp. More hits were observed than expected if *darc1* were present in one-to-one orthologs in the species examined. Protein FASTA sequences were aligned using MUSCLE and a maximum likelihood phylogram was generated using MEGA.

HEK cell experiments

Transfections

HEK cells were transfected using polyethyleneimine (PEI) at a ratio of 3 μg PEI:1 μg DNA diluted in Opti-MEM (Thermo Fisher Scientific). Cells were transfected at approximately 60%–70% confluency. For EV isolation and media transfer experiments, culture media was exchanged 4-6 h post-transfection to remove PEI and DNA, and media was harvested 24 h later.

Transfection and transfer

Media from transfected HEK cells was harvested 24 h post-transfection and centrifuged at 500x*g* for 4 min to remove dead cells and debris. Media from untransfected, naive cells was removed and replaced with the cleared transfected media and incubated for an additional 24 h. Following incubation, cells were fixed and combined immunocytochemistry/fluorescence *in situ* hybridization (ICC/FISH) for Arc or GFP protein and RNA was performed as described below.

Endocytosis blockade

To block endocytosis, a group of naive HEK cells plated on coverslips in 12-well plates that were receiving media from GFP-Arc-transfected HEK cells were treated at the same time with 80 μM Dynasore (Abcam, Cambridge, MA) for the first 6 h, then the media was removed and replaced with fresh HEK media. 18 h later, Dynasore-treated and untreated HEK cells were fixed. The entire 18-mm coverslip was viewed with a 20x objective and the number of clusters of GFP-Arc-transferred cells was manually counted. Representative images were obtained using a 20X objective on an Olympus FV1000 confocal microscope (Tokyo, Japan).

Neuron transfer experiments

DIV15 cultured neurons were used for all neuronal experiments. For purified Arc protein incubation experiments, neurons were treated with 4 μg of purified prArc, prArc-ΔCTD, CA-prArc, or prArc(RNA-) protein in normal neuronal feeding media and incubated for 1 or 4 h. For extracellular vesicle (EV) incubation experiments, neurons were treated with 10 μg protein from the purified EV fraction obtained from eight 10-cm dishes of DIV15 cultured cortical neurons in which E18 WT cortical neurons had been plated at 800,000 cells/mL (see "Cell Culture" methods), and incubated for 1 or 4 h. A subset of neurons in the purified protein- and EV-treated experiments was treated with 100 μM of the group 1 mGluR agonist dihydroxyphenylglycine ((*S*)-3,5-DHPG; Tocris Bioscience, Bristol, UK) for 5 min, which was then washed out and replaced with previously conditioned neuronal media, and neurons were allowed to rest for 25 min before fixation. To block protein translation during DHPG treatment, a subset of neurons was pretreated

with 180 μM cycloheximide (CHX, Sigma-Aldrich) 30 min before DHPG. CHX was left in the media for 1 h total. To block endocytosis, neurons were pretreated with 80 μM Dynasore (Abcam, Cambridge, MA) for 30 min before adding purified protein. For RNase treatments, a sample of either prArc or WT EV was incubated with RNase A (1:1000; Omega Bio-tek, Norcross, GA) for 15 min, then SUPERase-In RNase Inhibitor (1 U/μL; Thermo Fisher Scientific) immediately before being added to neurons. The treated samples were then added to neurons and incubated for 4 h.

Immunocytochemistry

After treatments, neurons were washed twice with 37°C 4% sucrose/1X phosphate-buffered-saline (PBS; 10X: 1.4 M NaCl, 26.8 mM KCl, 62 mM Na_2HPO_4, 35.3 mM KH_2PO_4, pH 7.4), then fixed for 15 min with 4% sucrose/4% formaldehyde (Thermo Fisher Scientific) in 1X PBS. Neurons were washed 3 × 5 min with 1X PBS, permeabilized for 10 min with 0.2% Triton X-100 (Amresco, Solon, OH) in 1X PBS, and blocked for 30 min in 5% normal donkey serum (Jackson ImmunoResearch, West Grove, PA) in 1X PBS. Neurons were then incubated in primary antibody diluted in block for 1 h at RT, washed 3 × 5 min in 1X PBS, and incubated in secondary antibody diluted in block for 1 h at RT. Neurons on coverslips were mounted on glass slides in Fluoromount (Thermo Fisher Scientific) and dried overnight at RT. Primary antibodies used were: rabbit anti-Arc (1:1000; custom-made; ProteinTech, Rosemont, IL); rabbit anti-Arc (1:1000; Synaptic Systems, Goettingen, Germany); chicken anti-MAP2 (1:5000; ab5392; Abcam); mouse anti-Rab5 (1:1000; BD Biosciences, San Jose, CA); DAPI nuclear stain (Molecular Probes, Thermo Fisher Scientific). Secondary antibodies used were: Alexa Fluor 405, 488, 555, or 647 for the appropriate animal host (1:750; Thermo Fisher Scientific or Jackson ImmunoResearch).

Combined FISH/ICC in neurons and HEK cells

The fluorescent *in situ* hybridization (FISH) procedure for *Arc* and *GFP* was based on a previously published protocol (Daberkow et al., 2007). We used a full-length rat *Arc* ribonucleotide probe (rat and mouse Arc are 99% identical at the aa level) or *EGFP* (see cloning strategy above in "Plasmids") as in the published protocol, but modified the protocol for use in cultured neurons and HEK cells instead of brain sections. *Arc* and *GFP* plasmids were linearized with *Not*1 and purified via standard phenol/chloroform extraction. The linearized antisense *Arc* or *GFP* were used to make a ribonucleotide probe that had DIG-UTP incorporated using a T7 DIG RNA labeling kit (Sigma-Aldrich), then purified with a G-50 spin column (GE Healthcare). Cells were washed once with 37°C 4% sucrose/1X PBS, then fixed for 15 min with 4% sucrose/4% formaldehyde in 1X PBS. Cells were washed 3 × 5 min with 1X PBS, permeabilized in 0.2% Triton X-100 for 10 min, washed 2 × 5 min in 1X PBS, then 5 min with 2X saline-sodium citrate (SSC; 20X: 3 M NaCl, 300 mM citric acid trisodium salt dihydrate, pH 7). Cells were prehybridized in 1X prehybridization solution (Sigma-Aldrich) for 30 min. The DIG-labeled *Arc* or *GFP* ribonucleotide probe was diluted 1:3 with ddH_2O, denatured at 90°C for 5 min, put on wet ice for 2 min, then mixed with RNA hybridization buffer (23.75 mM Tris-HCl, 1.19 mM EDTA, 357 mM NaCl, 11.9% dextran sulfate, 1.19X Denhardt's solution (Thermo Fisher Scientific), 2.5% nuclease-free water, 60% formamide (Fisher Scientific, Hampton, NH)). The *Arc* probe (1:500) or *GFP* probe (1:750) was hybridized to the cultured cells at 56°C for 16 h. The following day, cells underwent a series of washes to decrease background signal: 3 × 5 min 2X SSC, 15 min in RNase A (1:1000; Omega Bio-tek) at 37°C, 10 min 2X SSC at RT, 10 min 0.2X SSC at RT, 15 min 0.2X SSC at 56°C, 10 min 0.2X SSC at RT, 5 min TNT (0.1 M Tris-HCl, 0.15 M NaCl, 0.05% Tween-20, pH 7.5). Cells were then blocked in TNB (0.1 M Tris-HCl, 0.15 M NaCl, 0.5% w/v blocking reagent (Sigma-Aldrich), pH 7.5) with 2.5% sheep serum (Jackson ImmunoResearch) and 2.5% donkey serum for 30 min. In the primary antibody step, a DIG-HRP (1:1000; Sigma-Aldrich) and either MAP2 (1:2500; Abcam), Arc (1:500; custom-made), or Rab5 (1:500; BD Biosciences) antibody were diluted together in TNB with 2.5% sheep serum and 2.5% donkey serum and incubated on the cells for 1 h. After 3 × 5 min washes in TNT, the DIG-HRP signal was developed using a TSA Plus Cyanine 3 kit (1:50; PerkinElmer, Waltham, MA) for 30 min. Cells were washed for 5 min in TNT and 5 min in 1X PBS, then secondary antibody was diluted 1:750 in 5% donkey serum and 1X PBS and incubated on the cells for 1 h to detect MAP2, Arc, or Rab5. Nuclei were stained with DAPI (Thermo Fisher Scientific), then coverslips were mounted on glass slides with Fluoromount and dried overnight at RT.

Cell imaging and analysis

Imaging

Coverslips were imaged using a 60X oil objective on an Olympus FV1000 confocal microscope (Tokyo, Japan) and images were analyzed using ImageJ software (National Institutes of Health, Bethesda, MD). Neurons included for analysis were selected in an unbiased manner by looking at MAP2 dendritic morphology for cell health. Coverslips were viewed blind to find the brightest immunofluorescence in each independent experiment, and this value was then used to set the image acquisition settings for that experiment. Images from all coverslips in that experiment were then acquired using the exact same settings.

Analysis of dendritic Arc protein and mRNA expression

During analysis, images were blindly thresholded (to remove background fluorescence and to ensure images were analyzed in the linear range) to the brightest immunofluorescence in an individual experiment, and the same threshold was applied to all other images in that experiment. Integrated density (average pixel intensity x area) of two 30-μm dendritic segments/neuron was measured from each coverslip. In general, thick proximal dendritic branches were avoided in our analysis to control for potential differences in dendritic volume. The KO control group in each experiment, whether ICC or FISH, was set as "1," and the integrated density values in the other groups were normalized to this and are displayed in the graphs as fold-change ± SEM. For representative images in the figures, the Smart look-up table (LUT) in ImageJ was applied to highlight differences in Arc expression between groups.

Analysis of Arc/Rab5 colocalization

Two 30-μm dendritic segments/neuron were selected for analysis of Arc protein or mRNA colocalization with Rab5 protein. The Arc channel and Rab5 channel were thresholded to the same value across all images. Using ImageJ, a mask was made of the thresholded section of dendrite for both Rab5 and Arc. The Arc mask was applied to the Rab5 mask and the number of overlapping puncta was quantified. The number of Arc particles overlapping Rab5 was divided by the total number of Arc particles in the stretch of dendrite to determine the Arc/Rab5 colocalization.

Western blots

Immunoblotting and analysis

Western blot samples were mixed with 4X Laemlli buffer (40% glycerol, 250 mM Tris, 4% SDS, 50 mM DTT, pH 6.8) and heated at 70°C for 5 min. SDS-PAGE gel electrophoresis was used to separate protein samples. Separated samples were transferred to a nitrocellulose membrane (GE Healthcare). Following transfer, membranes were briefly stained with 0.1% Ponceau stain, then destained with 1% acetic acid to remove background, for imaging of total protein. Membranes were blocked in 5% milk + 1X tris-buffered saline (TBS; 10X: 152.3 mM Tris-HCl, 46.2 mM Tris base, 1.5 M NaCl, pH 7.6) for 30 min at RT, then incubated in primary antibody in 1X TBS for either 1 h at RT or overnight at 4°C. Membranes were washed 3 × 10 min in 1X TBS, then incubated in an HRP-conjugated secondary antibody (Jackson ImmunoResearch) in block for 1 h at RT. After 3 × 10 min in 1X TBS, a chemiluminescent kit (Bio-Rad, Hercules, CA) was used to detect the protein bands, and the membranes were imaged on an Azure c300 gel dock (Azure Biosystems, Dublin, CA). Blots were analyzed and quantified using the Gel Analysis plugin in ImageJ.

Antibodies

Antibodies were used at the following concentrations: Arc (1:000; mouse monoclonal, Santa Cruz), Arc (1:000; rabbit polyclonal, custom, Protein Tech), ALIX (1:500; rabbit polyclonal, custom, provided by Dr. Wesley Sundquist), actin (1:1000; HRP-conjugated, Abcam), GFP (1:1000; chicken polyclonal, Aves). All secondary antibodies were used at a dilution of 1:10,000 (HRP-conjugated goat anti-rabbit, goat anti-mouse, goat anti-chicken, Jackson ImmunoResearch).

Coomassie gels

Samples for analysis via SDS-PAGE were mixed with 4X Laemlli buffer and heated at 70°C for 5 min. Protein samples were separated on 10% SDS gels. Gels were then stained with 0.1% Coomassie blue stain (0.1% w/v Coomassie blue, 50% methanol, 10% acetic acid, 40% water) for 30 min and destained overnight in destain solution (50% methanol, 10% acetic acid, 40% water). Gels were visualized using an Azure c300 gel dock under the auto-exposure setting on the visible channel. Gel exposures were analyzed and quantified using the Gel Analysis plugin in ImageJ.

Immunoprecipitation

WT and Arc KO cortices were dissected out and homogenized in 150 mM NaCl, 50 mM Tris, 1% Triton X-100, 0.5% sodium deoxycholate, 0.05% SDS, pH 7.4 (IP lysis buffer), with protease inhibitor added fresh (Roche). Homogenates were pelleted at 200x*g* for 5 min at 4°C to remove tissue debris. Supernatants were removed, diluted from 2 mL to 4 mL, and rocked at 4°C for 10 min before being pelleted at 17,000x*g* for 10 min at 4°C to remove insoluble material. Cleared supernatants were removed, a small aliquot was taken as the input, and the remainder used for immunoprecipitation. Supernatants were immunoprecipitated with either Arc antibody (rabbit polyclonal, custom-made; Protein Tech) or normal rabbit IgG (Santa Cruz Biotechnology, Santa Cruz, CA) at 1 μg/500 μL lysate for 2 h at 4°C with gentle rocking. Following antibody incubation, a 10% volume of washed 50/50 Protein A bead slurry (Thermo Fisher Scientific) was added to the antibody/lysate mixture and incubated for an additional hour at 4°C with rocking. Bead-antibody complexes were then pelleted briefly at low speed, supernatants were removed, and beads were washed three times with IP buffer. Washed beads were then resuspended in 200 μL IP buffer. With half of the bead slurry, protein was eluted from the beads with 17 μL 4X Laemlli buffer for 5 min at RT, then 50 μL IP buffer was added and the solution was removed from the beads into a new tube and heated at 70°C for 5 min. The input (10% lysate volume) and 30 μL each of the IgG and antibody elutions were separated by SDS-PAGE on a 10% acrylamide gel and immunoblotted as described above. The bands for the input and IgG and Arc elutions were analyzed using the Gel Analysis plugin in ImageJ, and the data were represented graphically as a ratio of the signal from each elution over the input signal from each individual mouse. With the other half of the bead slurry, the IP buffer was adjusted to 1% SDS and 0.8 mg Proteinase K (New England Biolabs, Ipswich, MA) was added. Samples were then incubated at RT for 30 min with rocking and total RNA was extracted as described below.

Chemical crosslinking of Arc proteins *in situ*

Transfected HEK cells expressing myc-Arc-WT or a GFP control were briefly trypsinized, quenched with DMEM (Thermo Fisher Scientific), and pelleted. Media was removed and pelleted cells were then crosslinked with 0.4% formaldehyde in PBS for 10 min with rocking at RT. Cell suspensions were immediately quenched with Tris to a final concentration of 50 mM and repelleted. Supernatants were removed and cell pellets were then lysed with 150 mM NaCl, 50 mM Tris, 1% Triton X-100, pH 7.4 (lysis buffer) for 20 min at 4°C with rocking. Lysates were cleared by centrifugation at 21,000x*g* for 10 min at 4°C and cleared supernatants were then run on a 4%–8% gradient gel and analyzed via western blot with antibodies for Arc (mouse monoclonal, Santa Cruz) and GFP (chicken polyclonal, Aves).

RNA extraction

For all samples, total RNA was extracted using TRIzol (Thermo Fisher Scientific). TRIzol-extracted samples were mixed 5:1 with chloroform, incubated at RT for 3 min, and pelleted at 12,000x*g* at 4°C for 10 min. The resulting aqueous phase was taken and mixed 1:1 with isopropanol, incubated at RT, and pelleted at 12,000x*g* at 4°C for 10 min. The resulting supernatant was removed and pellet washed with cold 75% ethanol. Washed pellets were then repelleted at 7500x*g* for 5 min at 4°C. The supernatant was removed and dried pellets were resuspended in ddH_2O.

RT-PCR

Total RNA concentrations were measured by $A_{260/280}$ on a Nanodrop (Thermo Scientific). Reverse transcription reactions were carried out using a High Capacity cDNA Reverse Transcription Kit (Applied Biosystems, Foster City, CA) with 100-200 ng of RNA as template. Resulting cDNAs were amplified using rat Arc, GAPDH primer sets for 35 cycles with a 60°C annealing temperature. Resulting PCR products were analyzed on 1.5% agarose gels stained with SYBR Safe (Thermo Fisher Scientific). Rat Arc primers: Fwd, ACCATATGACCACCGGCGGC; Rev, TCCAGCATCTCAGCTCGGCAC. GAPDH primers: Fwd, CATGGCCTTCCGTGTTCCTA; Rev, GCCTGCTTCACCACCTTCTT. RT-PCR gels were quantified using the ImageJ gel analyzer tool.

qRT-PCR

To determine the amount of RNA associated with Arc protein, quantitative RT-PCR was performed on mRNA prepared from 1: whole mouse cortices immunoprecipitated with Arc and IgG protein, 2: EV fractions prepared from HEK cells (see below, ''Extracellular vesicle purification''), and 3: lysate and purified protein from bacteria (BL21, Thermo Fisher Scientific) transfected with rat Arc plasmid (pGEX-GST-ArcFL). Some samples were treated with RNase (25 μg, RNase A, Thermo Fisher Scientific) to determine if the mRNA associated with Arc protein was protected from degradation relative to exogenously added GFP antisense RNA (generating using T7 RNA polymerase from linearized pBluescript-SKII-GFP). Preparation 1: Mice were sacrificed after 24 h of dark-housing and 2 h of enriched environment. Whole cortices were dissected and homogenized in IP lysis buffer as described above. After immunoprecipitation, bead slurry was incubated in guanidine thiocyanate containing RLT lysis buffer and column purification of RNA was performed using QIAGEN RNeasy Micro Kit (QIAGEN, Hilden, Germany). Total eluate was used for reverse transcription using High Capacity cDNA Reverse Transcription Kit with 50 U of Multiscribe Reverse Transcriptase and random oligo primers (Thermo Fisher Scientific). Preparations 2 and 3: total RNA was extracted using TRIzol (Thermo Fisher Scientific) as described above (''RNA extraction''). Reverse transcription reactions (25°C for 10 min, 37°C for 2 h, 85°C for 5 min) were carried out using a High Capacity cDNA Reverse Transcription Kit. Resulting cDNA was prepared for qPCR using PowerUp SYBRgreen Master Mix (Thermo Fisher Scientific) in a 96-well plate with primers against rat Arc, GAPDH and asnA (see above, ''RT-PCR''; asnA primers: Fwd, GCGTGGATGCCGACACGTTG; Rev, ATACCGCCGCCGATGGTCTG). qPCR was performed on a QuantStudio 3 Real Time PCR System (Thermo Fisher Scientific) using the following protocol: Pre-incubation: 50°C for 2 min, 95°C for 2 min. Amplification: 40 cycles of 95°C for 15 s, 60°C for 15 s, and 72°C for 1 min. Melt curve: 95°C for 1 s, 60°C for 20 s, continuous ramp at 0.15°C/s up to 95°C. Ct values of greater than 30 were considered undetectable. Differences in expression were determined using the standard curve method, where a standard DNA sample was serially diluted (10-fold), analyzed for the gene of interest, and the linear equation calculated. The resulting linear equation was used to determine where the Ct values of test samples fell within the standard curve and the result was transformed (log_{10}) to reflect the dilution of the standard sample. Differences were calculated measuring the fold-change from the average of the control values for any given group (test/average control).

Extracellular vesicle purification

Extracellular vesicles (EVs) were purified from HEK cell and primary neuronal cultures as previously described (Lachenal et al., 2011). Media was spun successively at 2,000 and 20,000x*g* to remove dead cells and debris, and then at 100,000x*g* to pellet EVs. The crude EV pellet following the initial high-speed spin was resuspended in cold PBS and repelleted at 100,000x*g* for 1 h at 4°C in an SW41 rotor. The washed EV pellet was further purified by centrifugation over a 10%–20% sucrose-PBS gradient at 100,000x*g* overnight at 4°C. The resulting pellet was washed in cold PBS to remove excess sucrose and then repelleted at 100,000x*g* for 1 h at 4°C. The final, washed pellet was resuspended in PBS and used for downstream analysis with EM, western blotting, and neuron treatments.

Trypsin digestion and RNase assays

Trypsin was added to prArc and EVs at 0.05 mg/mL for 30 min at RT followed by addition of 1 mM PMSF for 10 min to inactivate trypsin. Untreated and trypsin-treated samples were then analyzed by western blot. RNase A was added to WT neuron lysates and EVs at 50 μg/mL for 15 min at 37°C. Untreated and RNase-treated samples for RT-PCR were then directly extracted with TRIzol.

Immunogold labeling

Immunogold labeling was performed with modifications as previously described (Korkut et al., 2013). Samples were fixed overnight in 2% formaldehyde at 4°C with gentle rocking. Samples were then applied to glow discharged Formvar copper mesh grids (Ted Pella) and allowed to adhere at room temperature for 10 min. Samples were then quenched by 3 washes of 0.1 M Tris, pH 7.4. Samples

were then permeabilized for 10 min at RT, blocked, and stained for Arc (1:500; custom-made). 5 nm gold-conjugated secondary antibodies were used for staining without silver enhancement. Following antibody labeling, grids were negative stained as described above.

QUANTIFICATION AND STATISTICAL ANALYSES

Two-way ANOVA with or without repeated-measures (with *post hoc* Sidak's tests) or two-tailed unpaired *t*-tests were performed using GraphPad Prism (GraphPad Software, San Diego, CA) or JMP Pro statistical software (SAS; Cary, NC). Significance was set at $p < 0.05$. All data shown are representative of at least two experimental replicates. Details of the statistics (*N*, number of experimental replicates, description of how the data are displayed) can be found in figure legends and/or the Results section.

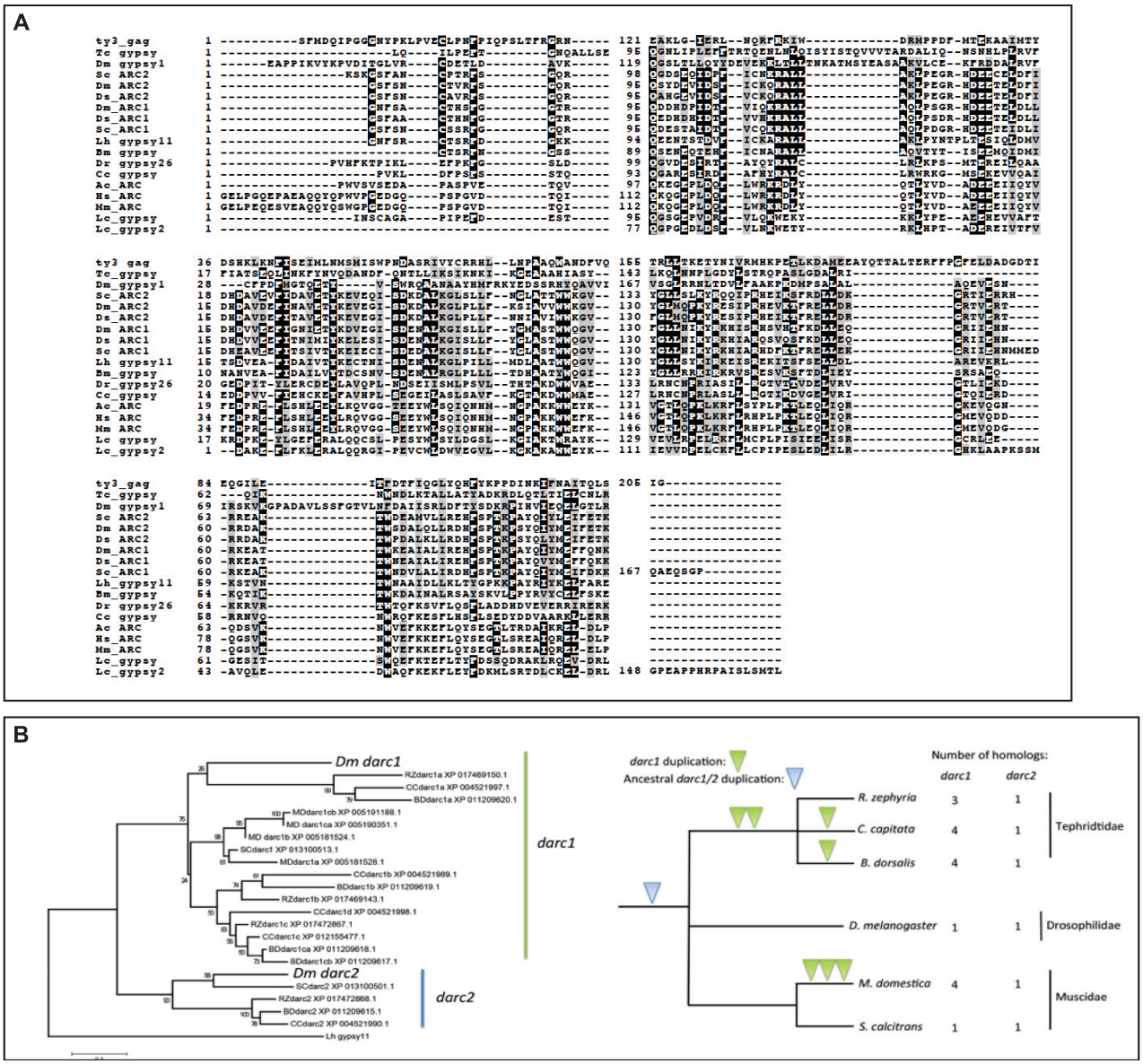

Figure S1. Alignment of Primary aa Sequences of Ty3/Gag Elements and Origin of Dipteran Arc Genes, Related to Figure 1

(A) Translated genomic DNA sequences corresponding to Arc or gypsy Gag proteins were aligned using MUSCLE (https://www.ebi.ac.uk/Tools/msa/muscle/). Aligned sequences were shaded using the boxshade plot server (https://embnet.vital-it.ch/software/BOX_form.html), using default parameters (50% sequences sharing aa identity for shading). Note: the alignments only contain fragments of Arc genes, not the full-length sequences with start sites. Species included: Mm—*Mus musculus*, house mouse; Hs—*Homo sapiens*, human; Ac—*Anolis carolinensis*, Carolina anole lizard; Lc—*Latimeria chalumnae*, West Indian Ocean coelacanth; Dr—*Danio rerio*, zebrafish; Cc—*Cyprinus carpio*, common carp; Dm—*Drosophila melanogaster*, common vinegar fly; Ds—*Drosophila suzukii*, spotted-wing fly; Sc—*Stomoxys calcitrans*, stable fly, Lh—*Linepithema humile*, Argentine ant; Bm—*Bombyx mori*, silkworm; Tc—*tribolium castaneum*, red flour beetle.

(B) (left) Maximum likelihood phylogenetic analysis of Arc homologs found in *Drosophilidae*, *Muscidae*, and *Tephritidae* flies. Multiple copies of *darc1* were observed throughout *tephritid* flies and in the house fly, *Musca domestica*. For each sequence, the GenBank accession number is given after the abbreviated species names. *Tephritidae*: RZ—*Rhagoletis zephyria*; CC—*Ceratitis capitate*; BD—*Bactrocera dorsalis*. Muscidae: MD—*Musca domestica*; SC—*Stomoxys calcitrans*. (right) Putative duplication history of dArc in *schizophoran* flies as inferred from the phylogenetic analysis in (A). Since all *schizophoran* flies examined possess a homolog of *darc1* and *darc2*, the duplication of the ancestral dArc must have occurred prior to the divergence of these species (blue triangle). This ancestral duplication event was followed by multiple rounds of duplication of *darc1* (green triangles) in some of the lineages: two duplication events in the common ancestor of the *Tephritidae*, one additional duplication in the lineage of *Ceratitis capitata*, and one additional duplication in the lineage of *Bactrocera dorsalis*. Independently, *darc1* experienced three rounds of duplication in the lineage of Musca domestica. By contrast, *darc2* has apparently remained a single copy gene in the species examined.

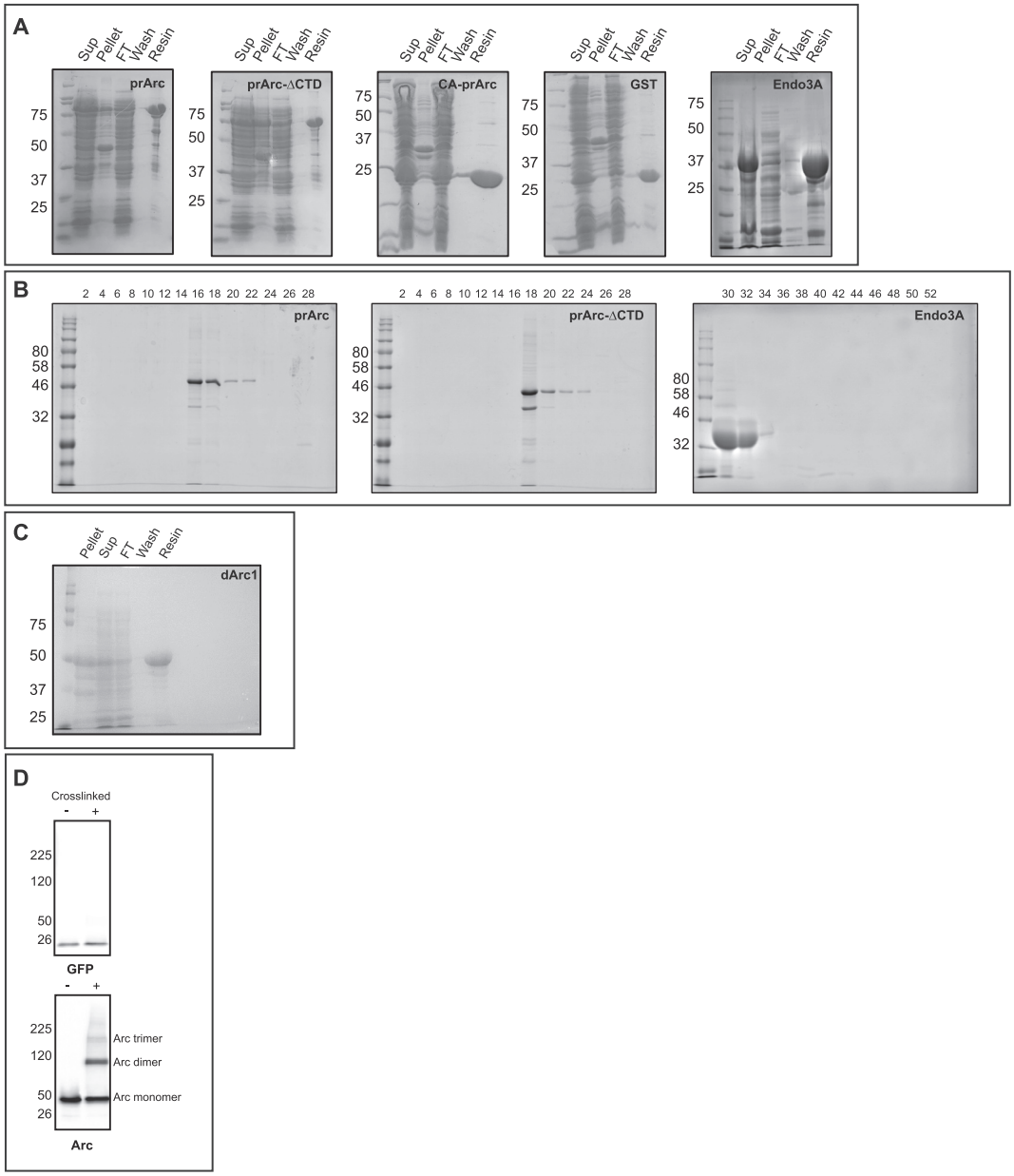

Figure S2. Recombinant Protein Purification and Experiments, Related to Figure 2

(A) (left to right) Representative Coomassie gel of affinity purifications of full-length rat Arc (prArc), prArc-ΔCTD, CA-prArc, GST, and Endo3A showing similar expression levels to that of prArc. prArc-ΔCTD and Endo3A were prepared in the same manner as prArc. GST was directly eluted from the affinity resin using 15mM L-glutathione. His-tagged CA-prArc was eluted from Ni^{2+} affinity resin using 250mM imidazole. All proteins were then buffer exchanged into 150mM NaCl, 50mM Tris, pH 7.4 following GST-tag cleavage by Precision Protease or elution. Buffer conditions were adjusted for all proteins for each experiment: 500mM $NaPO_4$, 50mM Tris, pH 7.4 for capsid stability. Analyses showing the partitioning of bacterially-expressed protein into soluble (sup) and insoluble (pellet) fractions (lanes 1, 2), capture of the protein on a GST or Ni^{2+} affinity matrices (lanes 3-5 show the flow through (FT), wash and captured protein, respectively). This panel demonstrates the protein expression levels and the efficacy and efficiency of affinity capture.

(B) Representative Coomassie gels of peak fractions of prArc, prArc-ΔCTD, and Endo3A eluted from S200 size exclusion columns. Peak fractions were pooled and concentrated to a final stock concentration of 1mg/mL. prArc was concentrated to 1mg/mL from each purification for use in all biochemistry/EM experiments, unless noted. For cell biology experiments, prArc was diluted to 0.4mg/mL and 4 μg total protein was used per condition.

(C) Representative Coomassie gel of affinity purification of *Drosophila* dArc1 from BL21 bacteria lysates demonstrating similar expression levels to rat prArc.

(D) HEK293 cells in 12-well plates were transfected with full-length rat WT Arc or GFP plasmids using Lipofectamine at equal DNA concentrations and subjected to formaldehyde crosslinking *in situ*. Cell lysates were blotted with anti-GFP or anti-Arc antibodies. Note that higher molecular species corresponding to Arc dimers and trimers can be observed in the crosslinked Arc sample, but not in the GFP sample.

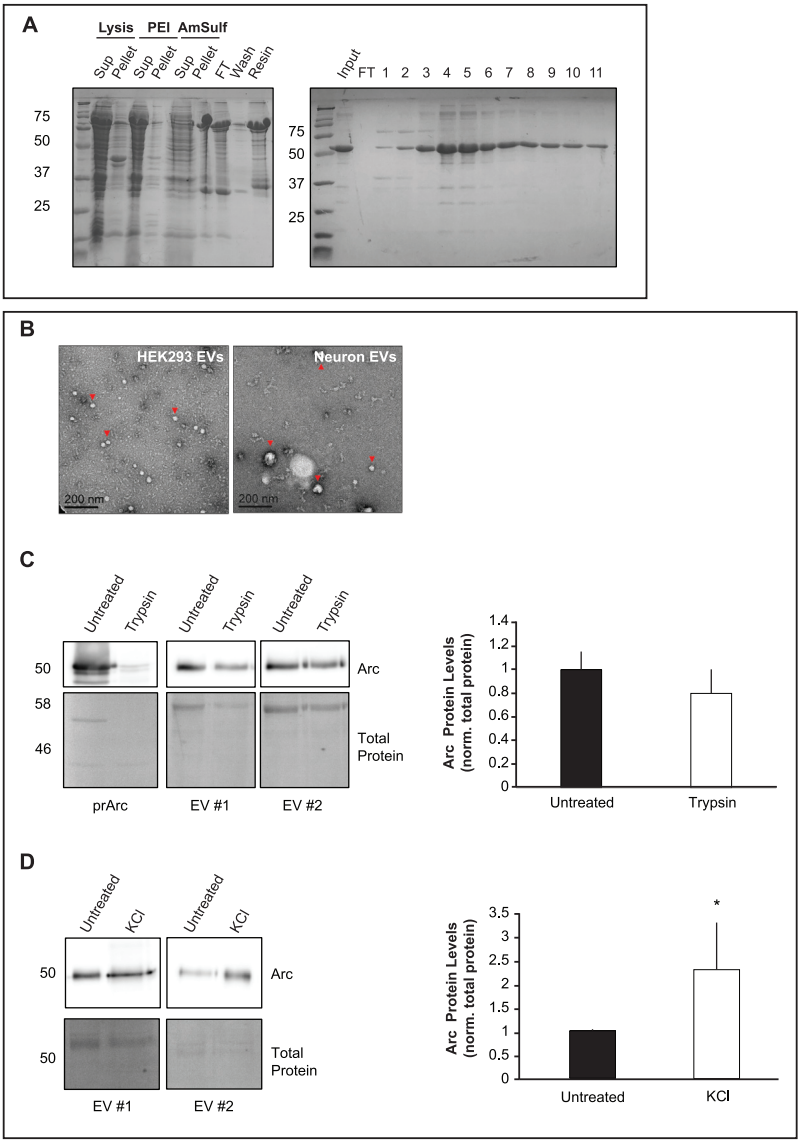

Figure S3. RNA Binding Experiments and Properties of Arc EVs, Related to Figures 2 and 3

(A) Representative Coomassie gels of nucleotide stripping of prArc. (left) Cells were lysed in 20mM NaCl, 50mM Tris, 2mM $MgCl_2$, 5% glycerol, 1mM DTT, pH 8.0. Fractions shown are supernatant and pellet fractions of cellular lysis after pelleting at 21,000x*g* for 45 min. The supernatant from this step was treated with 0.1% PEI to precipitate nucleic acids. This treatment resulted in a shift in the $A_{260/280}$ ratio from 1.71 ± 0.018 to 1.29 ± 0.023, indicating a drop in nucleic acid content. The sample was pelleted at 27,000x*g* for 20 min and the resulting supernatant was treated with ammonium sulfate (AmSulf) precipitation to concentrate Arc and pelleted at 10,000x*g* for 10 min. The AmSulf pellet containing Arc was then subjected to affinity purification as above. (right) Representative Coomassie gel of peak fractions of cleaved, affinity purified PEI treated Arc from an anion exchange column. This chromatography step further stripped bound nucleic acids from Arc. Peak fractions were concentrated to 1mg/mL and the final measured $A_{260/280}$ ratio for these fractions was 0.68 ± 0.03 (n = 3), indicating that PEI-treated prArc was largely free of nucleic acids.

(B) (left) Representative negative stain EM images of purified EVs from Arc-transfected HEK293 cell media collected for 24 h used for western blot analysis. (right) Representative negative stain EM images of purified EVs from WT cultured neuron media collected for 24 h used for western blot analysis. Red arrows indicate purified EVs.

(C) (left) Western blot of Arc in untreated EVs or EVs treated with trypsin (0.05mg/mL) for 30 min. prArc was used as a positive control for trypsin activity. (right) Quantification of Arc western blot normalized to total protein. Trypsin degraded prArc but had no effect on Arc protein present in neuronal EVs.

(D) Activity dependence of Arc secretion. Purified EV fraction from media collected from DIV15 cortical neurons in 10-cm dishes from untreated WT neurons was compared with treatment with KCl. Media was freshly exchanged with basal media or media supplemented with KCl to a final concentration of 50mM. Following media exchange, cells were incubated for 1 h and media was collected and the EV fraction was purified. (left) Western blots of Arc and total protein from the purified EV fraction from cultured neuronal media. (right) Quantification of Arc protein levels, normalized to total protein. KCl treatment resulted in significantly more Arc released into the media (n = 2; $p < 0.05$).

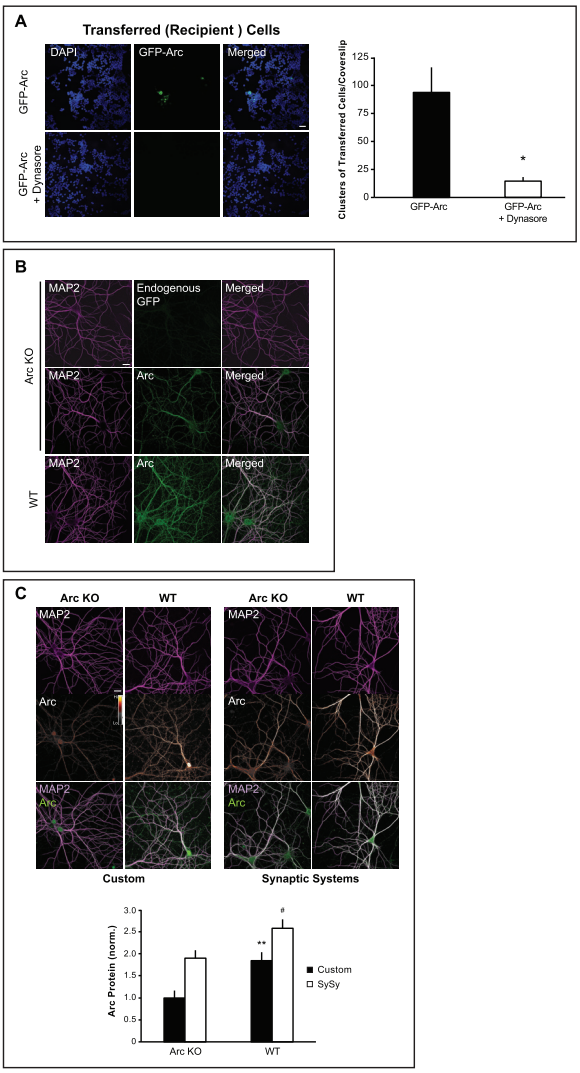

Figure S4. HEK Cell Experiments and Custom-Made Arc Antibody Control Experiments, Related to Figure 4

(A) HEK293 cells in 10-cm dishes were transfected with GFP-Arc as in Figure 4. 18 h later, media from GFP-Arc-transfected HEK cells in 10-cm dishes was transferred to naive HEK cells in 12-well plates, and 80μM Dynasore was added in one group at the same time to block endocytosis. After 6 h, the Dynasore-treated media was exchanged for fresh HEK media. 18 h later, cells were fixed and clusters of GFP-Arc-expressing cells over an entire 18mm coverslip were manually counted through a 20X objective (n = 3 coverslips/group). (left) Representative images of one 20X field of view. (right) Dynasore significantly reduced the number of clusters of GFP-Arc-positive cells over the entire coverslip. Student's *t*-test: *$p < 0.05$. Scale bar = 50 μm. Representative of three independent experiments and cultures with similar results.

(B) DIV15 cultured hippocampal Arc KO and WT neurons were immunostained for the dendritic protein MAP2 with Alexa Fluor 555 only (top row), or both MAP2 (Alexa 555) and Arc (Alexa 488; bottom two rows). Imaging settings for Arc were determined based on Arc immunostaining in WT neurons (bottom row). No GFP fluorescence from GFP knocked in to the Arc locus in the KO neurons was visible under these imaging conditions. Example of two independent experiments.

(C) DIV15 cultured hippocampal Arc KO and WT neurons were fixed and immunostained with either a custom-made rabbit polyclonal Arc antibody (ProteinTech) or the commercially available Synaptic Systems rabbit polyclonal Arc antibody, as well as the dendritic protein MAP2. All groups were imaged with the same acquisition settings. 30-μm segments of two dendrites/neuron were analyzed in all groups (n = 10 neurons) and were chosen using MAP2 staining. Both antibodies were able to detect a difference between Arc KO and WT neurons, although the signal:noise was better using the custom-made antibody. Arc in the soma/nucleus varies widely from neuron to neuron with both antibodies, under basal conditions. Student's *t*-test: **Arc KO versus WT with custom antibody, $p < 0.01$. #Arc KO versus WT with Synaptic Systems ("SySy") antibody, $p < 0.05$. Arc images are false-colored with the Smart LUT in ImageJ to better display differences in Arc expression. Example of two independent experiments.

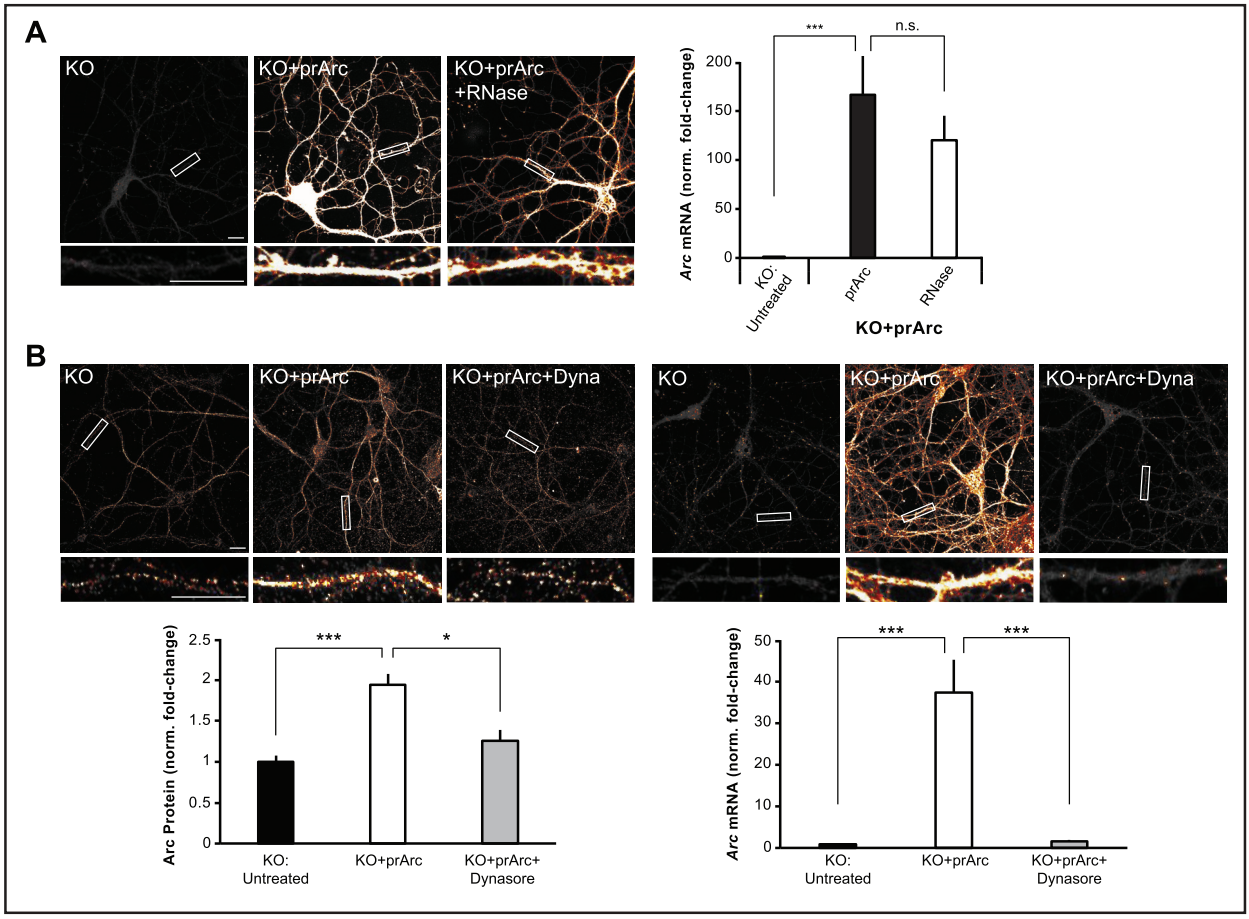

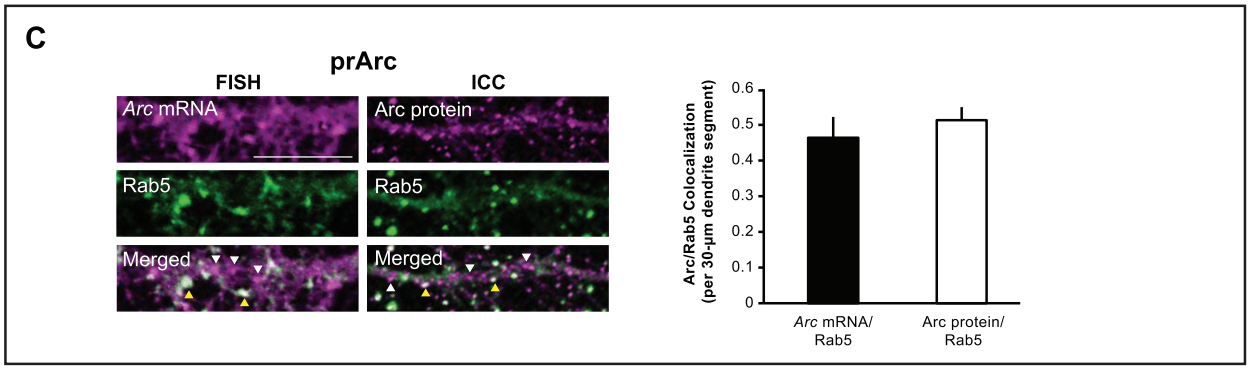

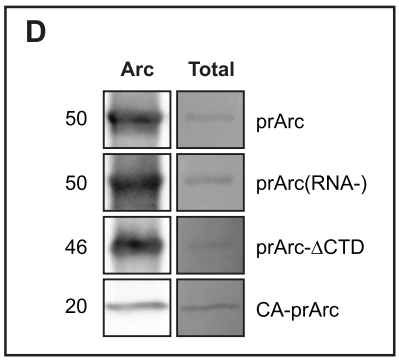

(legend on next page)

Figure S5. RNase and Uptake Experiments, Related to Figure 5

(A) To test whether *Arc* mRNA is protected in prArc capsids, samples were subjected to 15 min treatment with RNase A, then RNase inhibitor (1U/μL) to quench activity, prior to incubation with neurons. (left) Representative images of *Arc* mRNA in DIV15 cultured hippocampal Arc KO neurons incubated with the treated or untreated prArc samples for 4 h. (right) prArc treatment resulted an increase in dendritic *Arc* mRNA levels in Arc KO neurons. prArc treated with RNase did not affect *Arc* mRNA transfer.

(B) DIV15 cultured hippocampal Arc KO neurons were treated for 4 h with 4 μg prArc. In one group, 30 min before prArc was added, neurons were pretreated with 80μM Dynasore to block endocytosis. (left) Representative images of Arc protein and mRNA levels. (right) Pretreatment with Dynasore significantly blocked uptake/transfer of prArc protein and *Arc* mRNA. Student's *t*-test: *$p < 0.05$. ***$p < 0.001$. Example of three independent experiments (A, B). Scale bars in all panels = 10 μm.

(C) DIV15 cultured hippocampal Arc KO neurons were treated for 4 h with 4 μg prArc. Either combined FISH/ICC for *Arc* mRNA and Rab5 protein, or ICC for Arc and Rab5 protein, was performed. (left) Representative images of dendrites showing *Arc* mRNA plus Rab5 protein or Arc and Rab5 protein. (right) Arc protein and mRNA showed around 50% colocalization in dendrites with Rab5. White arrowheads indicate Arc alone, and yellow arrowheads indicate Arc/Rab5 colocalization. Example of two independent experiments. Scale bar = 10 μm.

(D) Purified protein samples of prArc, prArc(RNA-), prArc-ΔCTD, and CA-prArc were separated by SDS-PAGE, and the resulting western blot was immunostained for Arc using our custom-made Arc antibody. The antibody successfully detected all of the mutant constructs, suggesting that the lack of Arc immunostaining observed in transfer experiments was not a result of an inability of the antibody to detect the mutants. "Total" is Ponceau stain for total protein for each sample.

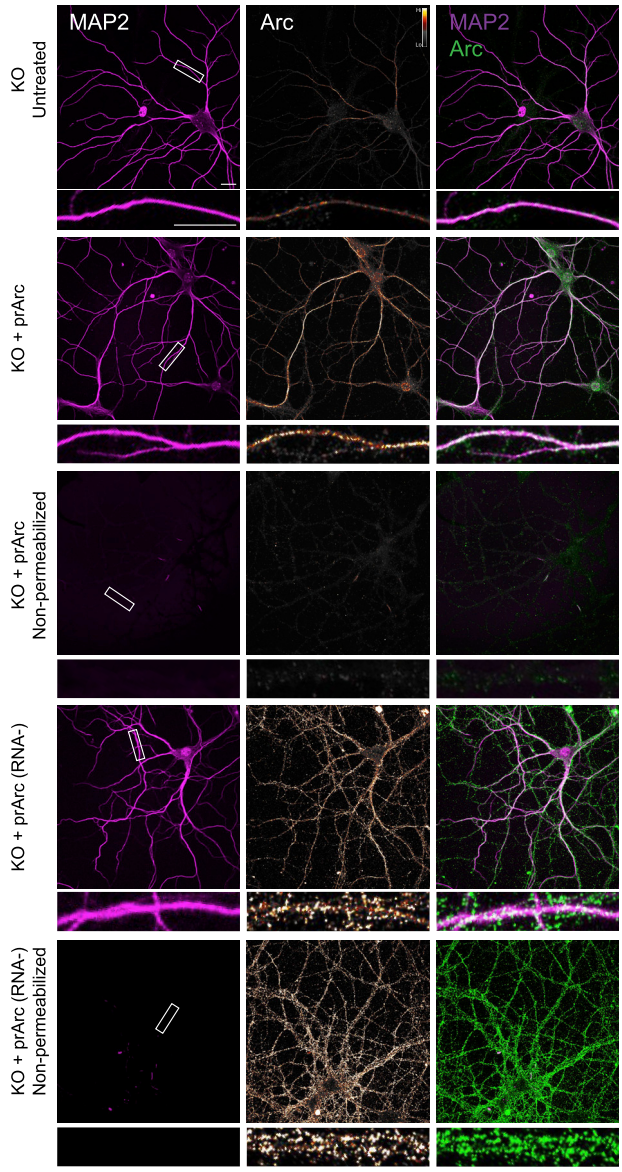

Figure S6. Purified Arc Stripped of Nucleic Acids Cannot Be Taken Up by Neurons, Related to Figure 5

DIV15 cultured hippocampal Arc KO neurons were treated with 4 μg prArc or prArc(RNA-) for 4 h before being fixed. One group from each treatment was not permeabilized during the immunocytochemistry procedure for Arc and MAP2. prArc-treated neurons that were non-permeabilized showed little to no MAP2 and Arc immunostaining. However, prArc(RNA-)-treated neurons showed no difference in Arc immunostaining between permeabilized and non-permeabilized conditions, although MAP2 immunostaining was still absent in the non-permeabilized condition, suggesting that prArc(RNA-) accumulates on the outside of the neurons. Dendritic segments boxed in white are shown magnified beneath each corresponding image. Scale bars = 10 μm. Example of three independent experiments. Arc images are false-colored with the Smart LUT from ImageJ to highlight differences in Arc expression. Merged images have MAP2 immunostaining in magenta and Arc in green.

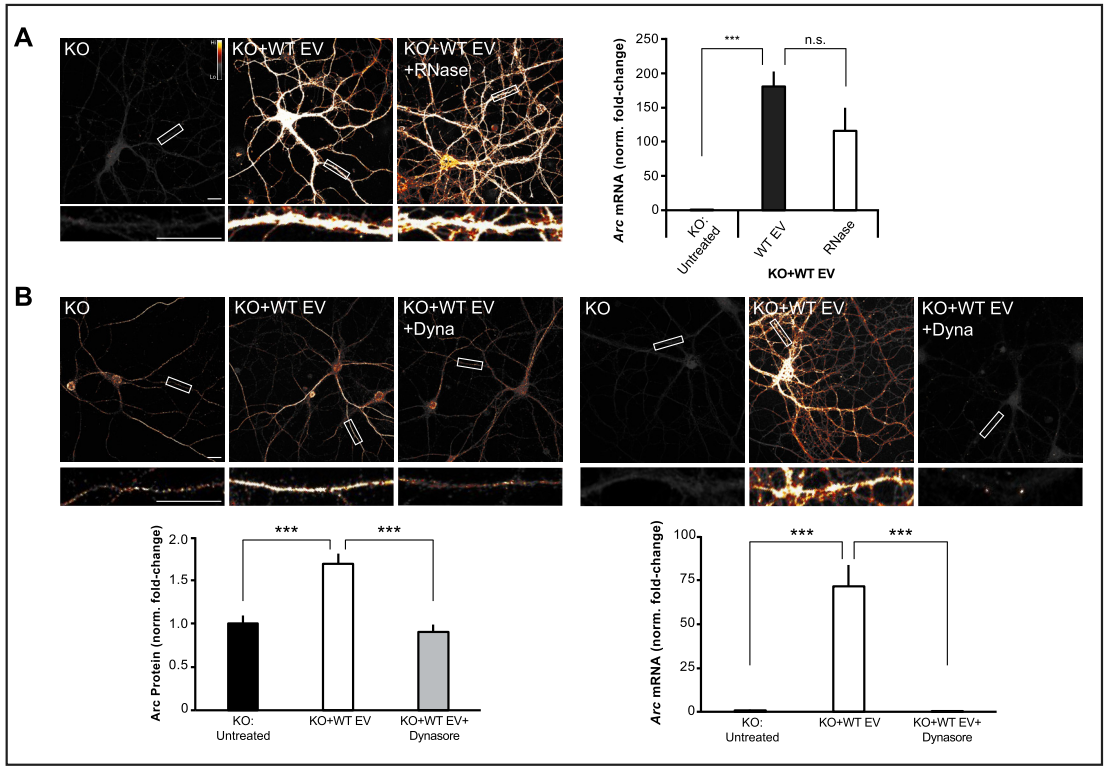

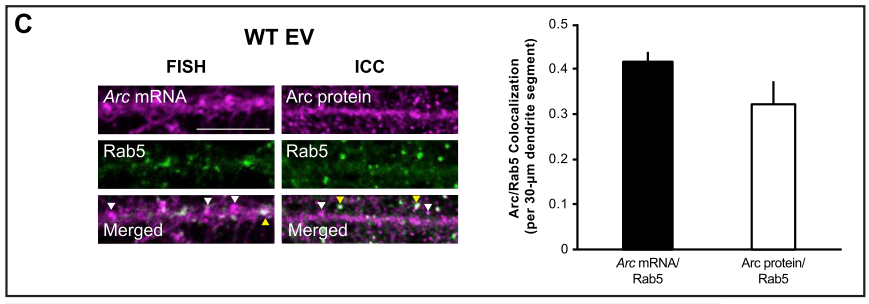

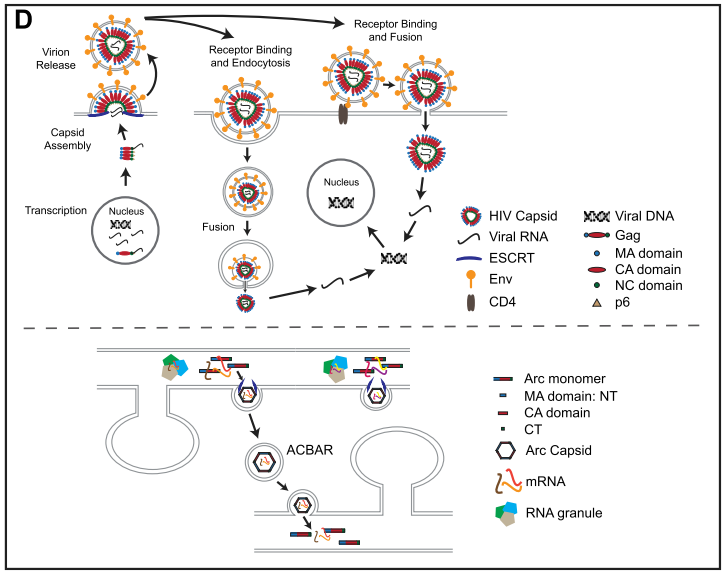

(legend on next page)

Figure S7. RNase and Uptake Experiments, Related to Figure 6

(A) To test whether *Arc* mRNA is protected in neuronal EVs, EVs prepared from 10-cm dishes of DIV15 cultured WT cortical neurons were subjected to 15 min treatment with RNase A, then RNase inhibitor (1U/μL) to quench activity, prior to incubation with neurons. DIV15 cultured hippocampal Arc KO neurons were incubated with 10 μg of the treated or untreated WT EV samples for 4 h. (left) Representative images of *Arc* mRNA levels in neurons. (right) WT EV treatment resulted an increase in dendritic *Arc* mRNA levels in Arc KO neurons. WT EV treated with RNase did not affect *Arc* mRNA transfer.

(B) DIV15 cultured hippocampal Arc KO neurons were treated for 4 h with 10 μg of the EV fraction harvested from the media of 10-cm dishes containing DIV15 high-density cultured cortical WT or Arc KO neurons. In one group, 30 min before EVs were added, neurons were pretreated with 80μM Dynasore to block endocytosis. (top) Representative images of Arc protein levels (left) or *Arc* mRNA levels (right). (bottom) Pretreatment with Dynasore significantly blocked uptake of Arc protein and mRNA from WT EVs. Arc protein and mRNA expression was normalized to Arc KO and is displayed as fold-change ± SEM. Dendritic segments boxed in white are shown magnified beneath each corresponding image. 30-μm segments of two dendrites/neuron were analyzed in all groups (n = 10 neurons) and were chosen using MAP2 staining. Student's *t*-test: ***$p < 0.001$. Scale bars = 10 μm. Example of three independent experiments. Images are false-colored with the Smart LUT from ImageJ to highlight differences in Arc expression.

(C) DIV15 cultured hippocampal Arc KO neurons were treated for 4 h with 10 μg of WT EVs, then fixed. Either combined FISH/ICC for *Arc* mRNA and Rab5 protein, or ICC for Arc and Rab5 protein, was performed. (left) Representative images of dendrites showing *Arc* mRNA plus Rab5 protein or Arc and Rab5 protein. (right) *Arc* mRNA and protein showed 30%–40% colocalization in dendrites with Rab5. White arrowheads indicate Arc alone, and yellow arrowheads indicate Arc/Rab5 colocalization. Example of two independent experiments. Scale bar = 10 μm.

(D) Model: Comparison of HIV Gag and Arc capsid life cycle. (top) HIV Gag protein self-assembles (via the CA domain) in the cytosol and at the plasma membrane (by myristoylation of the MA domain), while the capsid encapsulates viral RNA (via the NC domain). The immature HIV capsid is released from the cell in an ESCRT-dependent manner (via the p6 domain) with membrane that contains the viral envelope protein (Env). The mature virus particles bind host cells through surface receptors (such as CD4) and membrane fusion occurs. Alternatively, in some cell types virus particles are first endocytosed prior to fusion and particles released into the cell after full fusion occurs in the endosome. Viral RNA is released and then reversed transcribed into viral DNA that is integrated into the host genome. (bottom) *Arc* mRNA is trafficked out into dendrites in RNA granules that contain a selection of different mRNAs. Local translation of *Arc* mRNA takes place in dendrites in response to neuronal activity. High concentrations of Arc protein self-assemble and form Arc capsids, which encapsulate select mRNAs that are spatially proximal, including *Arc* mRNA. Arc capsids are released from dendrites in Arc Capsids Bearing Any RNA (ACBARs) and transfer of mRNA and other putative cargo takes place in neighboring dendrites.